UNIVERSITEIT
GENT

Faculteit Wetenschappen
Vakgroep Subatomaire en Stralingsfysica

Study of Nuclear Binding Energies and Shape Coexistence Using Algebraic Methods

Ruben Fossion

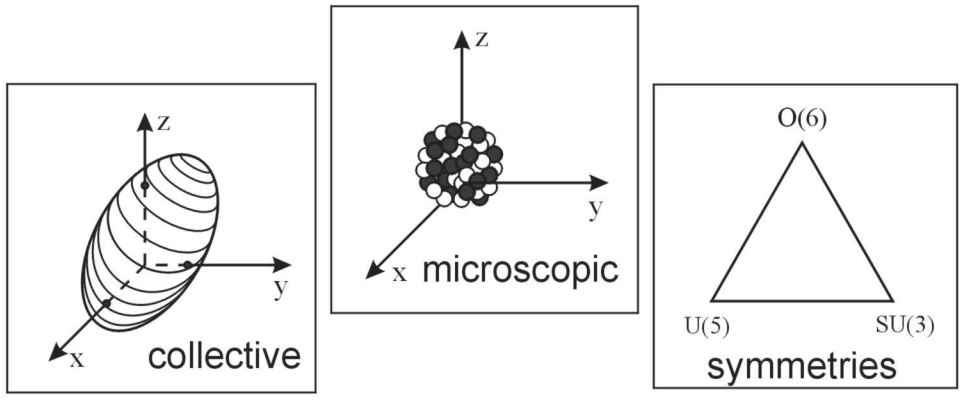

Proefschrift ingediend tot het behalen van de academische graad
van Doctor in de Wetenschappen: Natuurkunde
Academiejaar 2003-2004

Promotor: Prof. Dr. K. Heyde

Contents

List of Figures

List of Tables

Chapter 1

Introduction

1.1 Nuclear Structure

1.1.1 The Nuclear Chart

All matter is composed of atoms. Atoms, on their turn, exist out of a dense nucleus and a cloud of electrons (see fig. 1.1). The atomic nucleus is built from nucleons that exist in two types: positively charged protons and neutral neutrons. Nuclei with the same number of protons, but with different numbers of neutrons are called isotopes. The motion of the nucleons in the nucleus is governed by a repulsive Coulomb force and a strongly attractive effective nucleon-nucleon interaction. One can now study how the nucleons are organised within the nucleus under the influence of these two competing forces, and how nuclear structure evolves with mass (increasing the number of protons and/or neutrons) and with excitation and rotational energy.

Only certain combinations of numbers of protons and neutrons can be bound into a nuclear system, it is e.g. easy to understand that systems with too many protons will not be bound because of the repulsive Coulomb force. The bound nuclear systems can be represented as a narrow band in a plane spanned by proton number (Z) vs. neutron number (N), the so-called *nuclear chart* (see fig. 1.2). Over 7000 different nuclear systems are calculated to be bound. Of these, only some 270 systems are stable. Some 3000 radioactive nuclei are known at present; they have been produced at accelerator facilities or they occur naturally on earth. Most of the known radioactive nuclei are so short lived, that measuring their properties is a very difficult, if not impossible, task. As a result, only of some 500 isotopes an extensive experimental knowledge has accumulated over the years. A large part of the nuclear chart remains an unknown "Terra Incognita" up to now.

Each nucleus has a specific spectrum of excited states, that can serve as a fingerprint that partly reveals its underlying structure (a schematic nuclear energy spectrum is shown in fig. 1.3). Nuclear energy spectra also exhibit a general mass

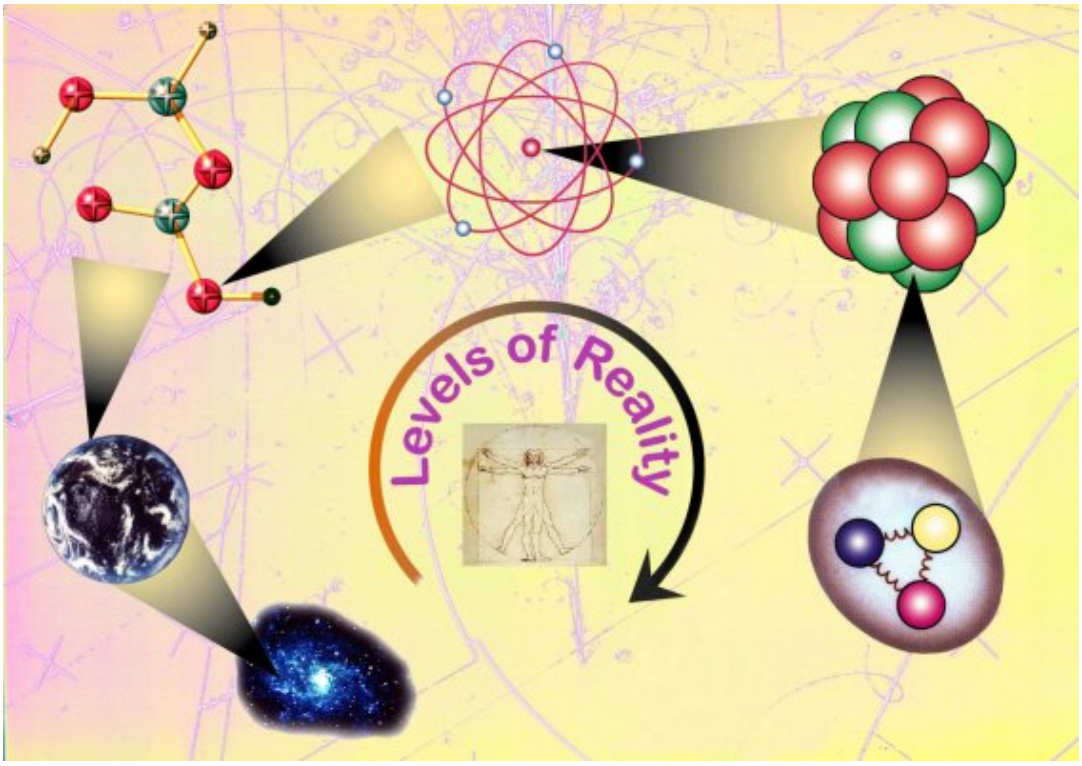

Figure 1.1 The different levels and dimensions of reality are shown, from our Universe, our Earth down to the molecules and atoms of which everything is composed. Atoms exist out of a cloud of electrons around a dense nucleus. The atomic nucleus is composed of nucleons (protons and neutrons), that are organised in a specific way, depending on the nuclear excitational and rotational energy and the nuclear mass. Nucleons themselves exist out of quarks, but quarks do not seem to play a major role in nuclear structure at lower energy scales. Taken from http://www.cyc.ucl.ac.be/npbrochure/

dependence (as e.g. through a series of isotopes, see fig. 1.4). Several theoretical models have been developed that successfully explain how nuclear energy spectra look like, and how they can be expected to evolve over the nuclear chart; often these models allow for very precise calculations of a whole range of nuclear properties. In the next section, some of the most important theoretical approaches to study nuclear structure properties are reviewed, that will put the present research work (section 1.2) in the appropriate framework.

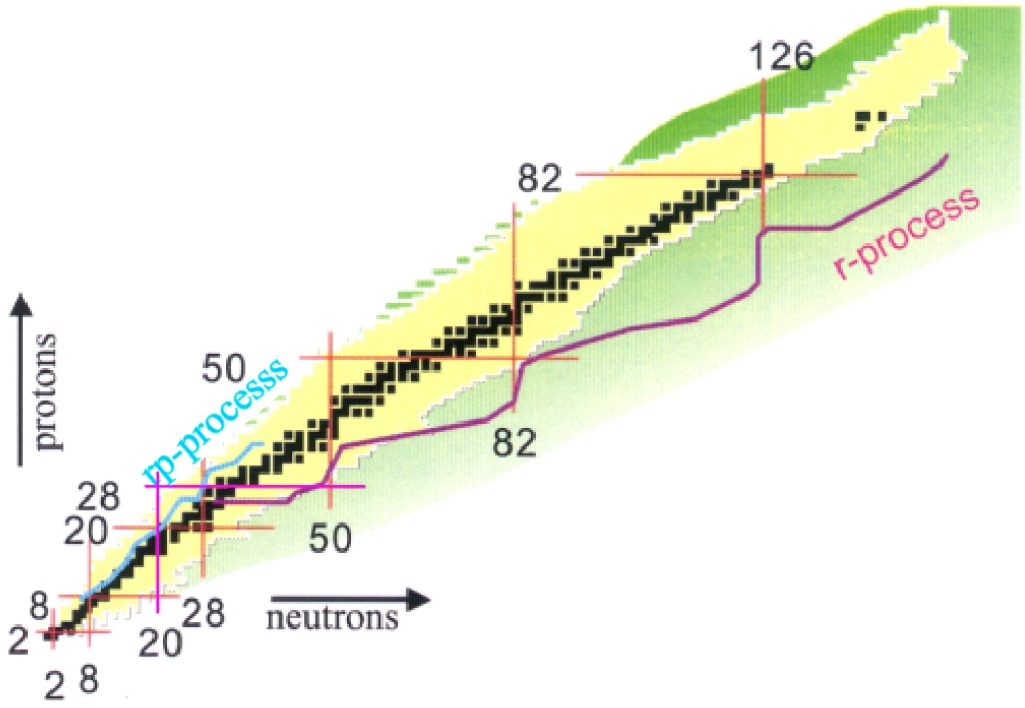

Figure 1.2 The nuclear chart shows all bound nuclei versus their number of protons (Z) and number of neutrons (N). Some 270 stable isotopes are known, the "Valley of Stability" (black squares), whereas until now more than 3000 unstable (radioactive) isotopes have been identified (yellow region). Many more unstable (exotic) isotopes are still waiting to be discovered in the "Terra Incognita" (green region). The "magic numbers" of protons and neutrons 2, 8, 20, 28, 50, 82, 126 ...are shown, that result in extra nuclear stability (see section 1.1.2). Nuclei are produced in stars during complex synthesis processes, of which the rapid *r*- and *rp*-process run exactly through the exotic regions; the slow *s*-process follows the Valley of Stability (see section 1.1.3). Taken from http://www.ornl.gov/info/ornlreview/v34_2_01/search.htm

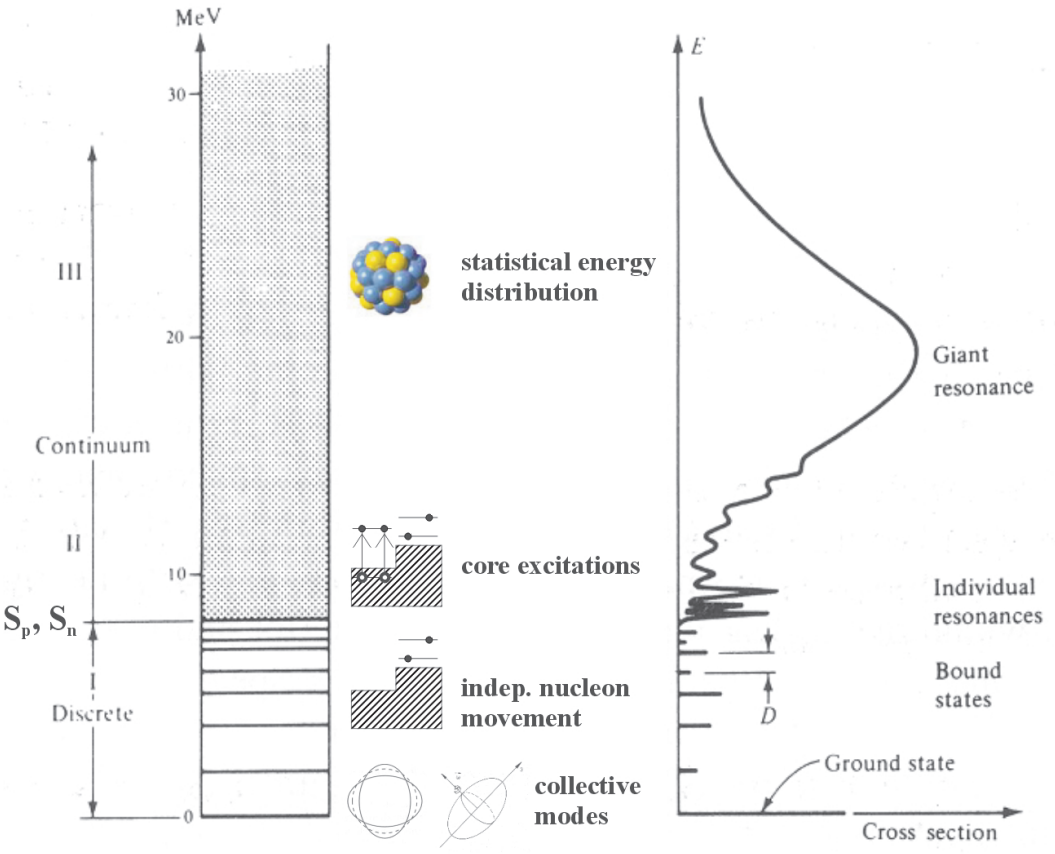

Figure 1.3 A schematic nuclear energy spectrum, indicating the presence of low-lying collective states (Geometric Model) and higher-lying few-nucleon states (Shell Model). Particle-hole excitations of the nuclear inert core (mp-mh) give rise to individual resonances, above the proton S_p or neutron S_n separation energy, in a quasi-continuum of states, governed by statistical energy distributions over the nucleons. Taken from [1].

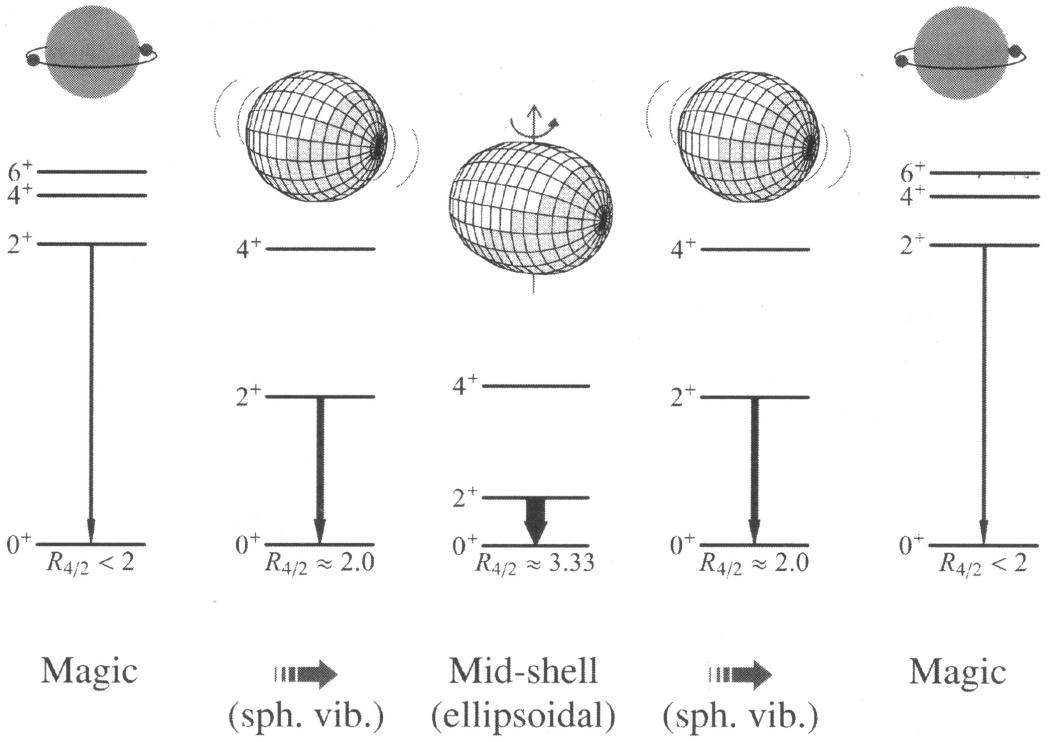

Figure 1.4 A schematic picture of how the nuclear energy spectra evolve from a closed shell towards a region with many valence nucleons (passing from few-nucleon excitations towards vibrational and rotational excitations). This is reflected in a drop in excitation energy, and in increasing E2 quadrupole transition rates from the higher-lying excited states towards the nuclear ground state. Taken from [2].

1.1.2 Nuclear Models

The atomic nucleus is a very complex system, and a theoretical study is confronted with some severe basic problems:

- The nucleon-nucleon interaction acting inside the nucleus as an effective force is not well understood as yet. Actually, the nucleon-nucleon interaction is not one of nature's basic forces, but it is the result of the strong force that acts between the quarks of which the nucleon is composed. At low nuclear excitation energies however, quarks do not seem to play an explicit role in determining the nuclear structure properties. Nucleons can thus be thought to be the basic nuclear constituent particles. Usually, the nucleon-nucleon interaction is represented by well-constructed effective interactions that approximates the attractive long-range character inside the nucleus.

- The atomic nucleus is a typical example of a *many-body system*. On the one hand, such systems have too many constituents to allow for an exact calculation of all of their properties. The most massive nuclei can count up to almost 300 nucleons. *Ab-initio* calculations start from the free nucleon-nucleon interaction in order to explain properties of the nucleus. At present, such calculations can be carried out only for the very light nuclei, up to 12 nucleons [3, 4]. On the other hand, nuclei have far too few constituents to allow for statistical methods to be used successfully.

As a result, one single theoretical model that encompasses the large diversity of nuclear excitation modes that appear all over the nuclear chart, does not exist. Several approaches have been developed over the years, that describe the nucleus from different, and often complementary, points of view:

The **Nuclear Shell Model** studies nuclear properties starting from the individual nucleons, moving idependently from each other to a first approximation, and can be called because of this a *microscopic* approach (see e.g. [5]. It incorporates a series of approximations to minimise the number of nucleon degrees of freedom (see fig. 1.5). A first approximation is to assume that the motion of each nucleon is governed by an average attractive force of all the other nucleons. Usually, a schematic Harmonic Oscillator (HO) potential is used to approximate this average spherical force field, because one can derive analytic solutions. For the rest, independently from each other, nucleons move through the nucleus along orbits that are grouped into shells. Each orbit can contain only a limited number of nucleons (because of the *Pauli principle* which dictates that identical nucleons (protons or neutrons) cannot be described by the same set of quantum numbers). In the nuclear ground state, and using the most simple shell-model considerations, nucleons will fill orbits from the bottom of the potential up to a certain level, the *Fermi level*. When a nucleus becomes excited, it rearranges some of its nucleons from below the Fermi level up to

some higher-lying free orbits. Nuclei with a "magic" number of protons or neutrons ($Z, N = 2, 8, 20, 28, 50, 82, 126 \ldots$) that fill a shell completely, are extra stable, because its nucleons have to bridge a large energy gap between the filled shell and the higher-lying unfilled orbitals in the next shell. Now a second approximation comes in. An ordinary non-magic nucleus can be thought to have an inert core of magic numbers of protons and neutrons, and only a limited number of valence nucleons over which the nucleus distributes its excitation energy. These valence nucleons have either a particle or a hole nature, depending on whether they are situated outside a closed shell, or inside (for the situation of ^{206}Pb). The nucleon-nucleon interaction was approximated by an average attractive field, but there will be some *residual interactions* that are not contained in this average mean-field. Incorporating these residual interactions between the valence nucleons produces the nuclear energy spectra as observed experimentally, and also permits the detailed calculation of a whole range of nuclear properties. Typical residual interactions exhibit a *pairing* property, that expresses the tendency of the nucleon-nucleon interaction to couple nucleons to pairs with angular momentum $J^\pi = 0^+$ (see fig. 4.2), as well as the long-range *proton-neutron quadrupole interaction* that favours nuclear deformation. The Nuclear Shell Model allows for a spectacular truncation of the number of degrees of freedom when beating the nuclear many-body problem. In the case of $^{206}_{82}Pb_{124}$ e.g., the original problem consists of 82 protons and 124 neutrons interacting through a two-body interaction, whereas in the nuclear shell model, considering the protons to form a closed proton shell, the problem is reduced to describe the residual interactions amongst 2 neutron holes, counted from the $N = 126$ neutron closed shell (see fig. 1.5. The Nuclear Shell Model can be applied to magic and near-to-magic nuclei, and predicts rather high-lying nuclear excited states that smoothly drop in energy as valence nucleons are added to the closed shell (see figs. 1.3) and 1.4). As the number of valence nucleons grows, the core can become "polarised" and collective nuclear motion comes in, in a natural way. Maria Goeppert-Mayer and Hans Jenssen were rewarded with the Nobel Prize for physics in 1963 for the development of this independent-nucleon model.

The **Liquid Drop Model** (LDM) was historically the first nuclear model that was developed. It describes very accurately the "bulk" properties of nuclei, i.e. the properties to which all the nucleons of the nucleus contribute, such as the nuclear mass, or equivalently, nuclear binding energies, or the derived nucleon-separation energies (the energy needed to separate some nucleons from the nucleus; figs. 3.1 and 3.2 show predictions of the LDM for the two-neutron separation energies through "the valley of stability" and through the Pb, Xe and Pd series of isotopes). The Liquid Drop Model describes these bulk properties "macroscopically", in terms of volume energy, surface energy, Coulomb energy, symmetry energy, ..., very much like the description of a charged liquid dropthat is suspended in space. This was the first model to successfully describe the nuclear fission process by calculat-

ing the deformation of a nucleus until it breaks up in two fragments. The **Collective** or **Geometric Model** can be viewed as an extension of the Liquid Drop Model [6]. It emphasizes the coherent behaviour in the dynamics of all of the nucleons. Among the kinds of collective motion that can occur in nuclei are rotations or vibrations that involve the entire nucleus (see fig. 1.6). In heavier nuclei, far from the magic numbers, this results in rather low-lying nuclear excited states that are connected with strong electromagnetic quadrupole transitions (see figs. 1.3 and 1.4).

The Nuclear Shell Model and the Collective Model give two extreme views on the nucleus. They are however not in contradiction: the average mean field of the Nuclear Shell Model itself, is the foremost example of a collective effect. Other theoretical models exist but are usually based on one of these two points of view. The spherical Nuclear Shell Model can be seen as a particular case of a **Mean Field** description of nuclei. In a Mean Field approach, the average one-body potential is determined in an iterative way, starting from the underlying nucleon two-body interaction (see [7] for a recent review). Depending on the number of nucleons, self-consistent Hartree-Fock or Hartree-Fock-Bogoliubov methods are used in that respect. Extensions incuding relativistic effects have been explored and lead to Relativistic Mean Field methods (see e.g. [8, 9]). The **Interacting Boson Model** (IBM) truncates the number of nucleon degrees of freedom even further than the Nuclear Shell Model. Also here, nucleons outside the closed shells are considered as active nucleons. However, one considers only pairs of these valence nucleons coupled to the lowest possible angular momentum $J^\pi = 0^+$ and 2^+ and, further on, one treats these nucleon pairs as a set of interacting s and d bosons, respectively [10]. The large truncation makes it possible to study heavy nuclei far from the magic numbers. The various collective excitations that occur in the Geometric Model can now be described starting from a microscopic picture, using algebraic (group theoretical) methods, rather than within a semi-classical and phenomenological approach. **Microscopic-Macroscopic Models** try to combine the best parts of the two extreme approaches of the Geometric Model and the Nuclear Shell Model, especially in order to describe nuclear ground-state properties, e.g. nuclear masses or binding energies. The Nuclear Shell Model accurately describes detailed nuclear structure effects, but mainly fails to reproduce nuclear properties of the nucleus in which all the nucleons contribute, the so-called "bulk" properties, that the macroscopic models like the Liquid Drop Model can adequately describe. Strutinsky was the first to construct an elegant method to reconcile both approaches [11, 12].

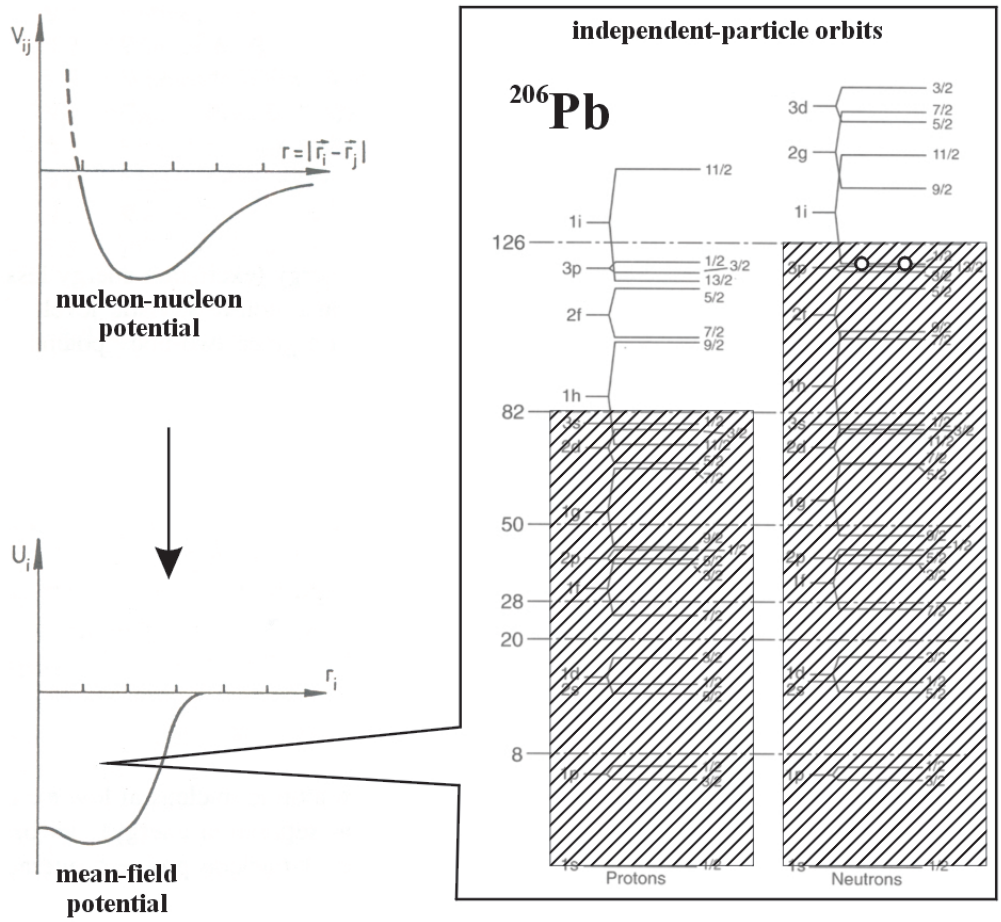

Figure 1.5 The Nuclear Shell Model approximates the $A \times (A-1)$ nucleon-nucleon interactions in the nucleus by A one-body interactions of the nucleons in a schematic mean field. In this mean field, nucleons move in orbits that are grouped into shells. In a subsequent approximation, only valence nucleons outside the closed shells are considered to contribute actively to nuclear excitations. A configuration is shown for ^{206}Pb with a closed shell of 82 protons and two neutron holes in the closed neutron shell of N = 126. Taken from [5, 13].

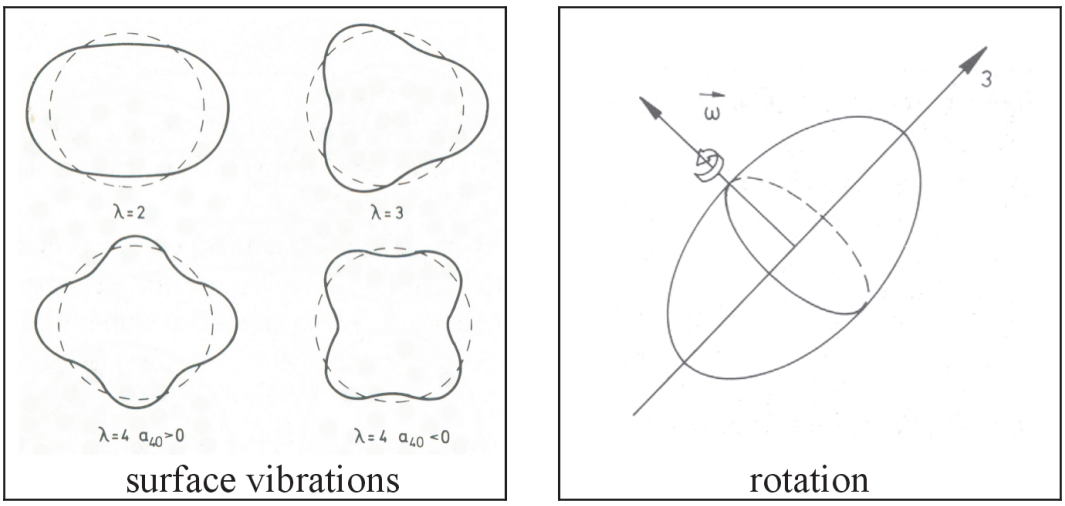

Figure 1.6 Nucleons in heavy nuclei far from the magic numbers can behave collectively, and perform small-amplitude oscillations around the spherical equilibrium shape. Nuclei with a very large number of valence nucleons can permanently be deformed and perform rotations. Taken from [1].

1.1.3 Exotic Nuclei

Using the theoretical models mentioned above, one gains an overall understanding of the general evolution of nuclear structure over large mass regions (see figs. 1.3 and 1.4). However, these models were developed and finetuned to explain the properties of the small patch of nuclei on the chart of isotopes for which experimental information was available (close to stability). Extrapolating theoretical predictions towards nuclei in the "exotic" regions of the nuclear chart (very heavy systems, or having extreme neutron-to-proton ratio's) often leads to extreme divergences and contradictions (see e.g fig. 1.7 for mass predictions in the Sn isotopes). Only recently, after the 1990's, technological breakthroughs in experimental techniques, allowing the acceleration and detection of radioactive nuclear beams (RNB), offer the opportunity to produce many short-lived "exotic" nuclei that reach far into the Terra Incognita. These radioactive nuclei play an important role in nuclear astrophysical processes. All matter in the visible universe is produced in stellar processes or during supernovae explosions. The stable or near-stable nuclei we observe on earth are the end products of complex stellar synthesis processes that run through these exotic regions of the nuclear chart (see fig. 1.2). Unclosing these exotic regions has already resulted in the discovery of new and unexpected nuclear structure phenomena. Halo nuclei and neutron-skin nuclei are probably among the most important discoveries: nuclei with such extreme high neutron-to-proton ratio, that the last barely bound neutrons form a halo or skin at large distances

from the rest of the nucleus (see fig. 1.8). This discovery came as a surprise, and lead to a wealth of theoretical publications in the years after to explain the phenomenon. This demonstrates the strong coupling that exists between epxerimental and theoretical nuclear physics. Newly discovered nuclear phenomena can point out new physics, and allow to test and to ameliorate theoretical models. Theorists on the other hand, eager to test their predictions, push experimentalists to perform measurements with higher precision, and still further into the exotic regions of the nuclear chart
Also the present research work was inspired by new experimental data for the short-lived and extremely neutron-deficient isotopes in the lead region (proton number $Z \sim 82$).

- In their recent Nature article, A. Andreyev et al. [14] reported on the presence of three nuclear shapes near Pb-186 (see fig 2.1 for the experimental excitation spectrum of the neutron-deficient lead isotopes). This shape coexistence phenomenon had been known to occur in several nuclei all over the chart of nuclei, but it was the first time that three nuclear shapes were observed to coexist in a single nucleus in an energy interval of less than 1MeV. It appears that in the neutron-deficient Pb isotopes, the excitation of a few protons across the $Z = 82$ proton closed shell can lead to the appearance of collective multi-particle multi-hole (mp-mh) excitations next to the ground-state spherical configuration. In the particular situation of ^{186}Pb, three distinct structures have been observed, and have been associated with spherical, oblate (disk-like) and prolate (cigar-like) deformed shapes.

- Another experimental impulse came from the ISOLTRAP (CERN) group, who succeeded in applying the innovative Penning-trap mass-measuring technique to the same neutron-deficient lead region of the nuclear chart. Nuclear masses give information about the binding energy and the stability of the nuclear system. The precision of the measurements at ISOLTRAP appeared to be high enough, to reveal small local variations in the otherwise smooth global behaviour of the nuclear masses. It was suggested that these local energy correlations could possibly serve as fingerprints to identify nuclear shape coexistence phenomena in the $Z \sim 82$ region, and in other mass regions of the nuclear chart [15].

In order to understand the above phenomena, we have carried out a detailed theoretical study for this three-shape coexistence in the neutron-deficient lead isotopes (chapter 2). A consistent description of the global and local properties of binding energies is presented in chapter 3. In chapter 4 we investigate the effect of some often used schematic nucleon-nucleon interactions (pairing, quadrupole and δ forces) with respect to the issue of binding energies.

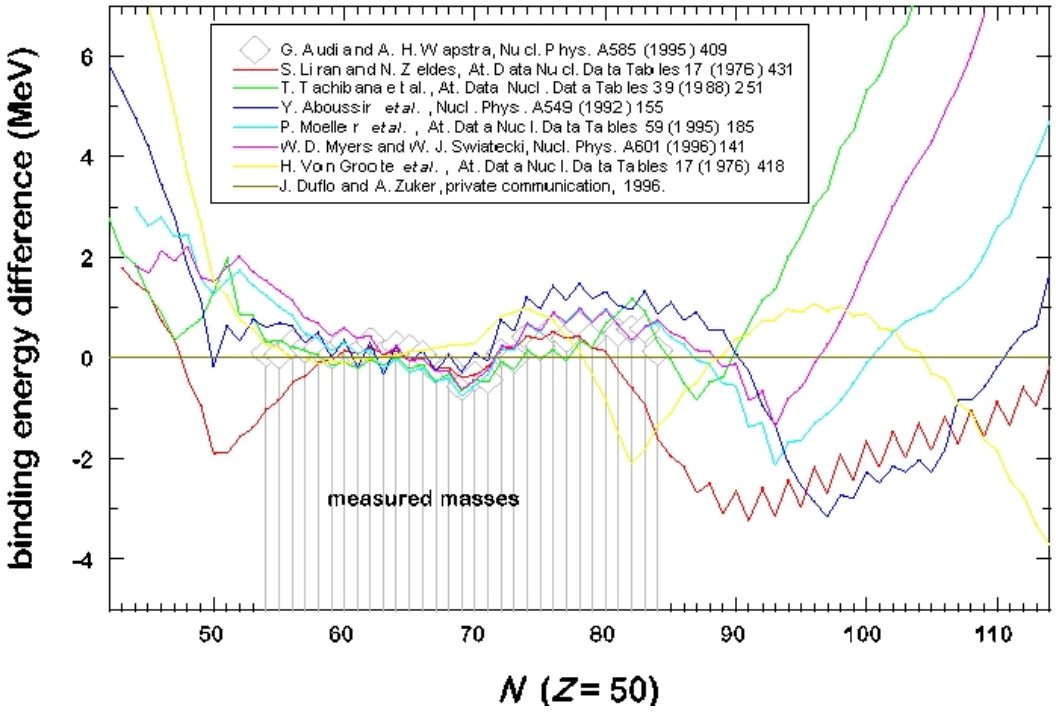

Figure 1.7 Theoretical models have been developed to explain the properties of the known isotopes near stability. Recently, acceleration techniques with radioactive nuclear beams (RNB) and state-of-the-art detection techniques allow to study extremely short-lived isotopes far into the Terra Incognita. Extrapolation of existing theoretical models outside of the known regions of stable isotopes often results into large divergencies, as demonstrated for the mass predictions of exotic Sn isotopes. Taken from http://www.nupecc.org/nupecc/report97/report97_final/node6.html

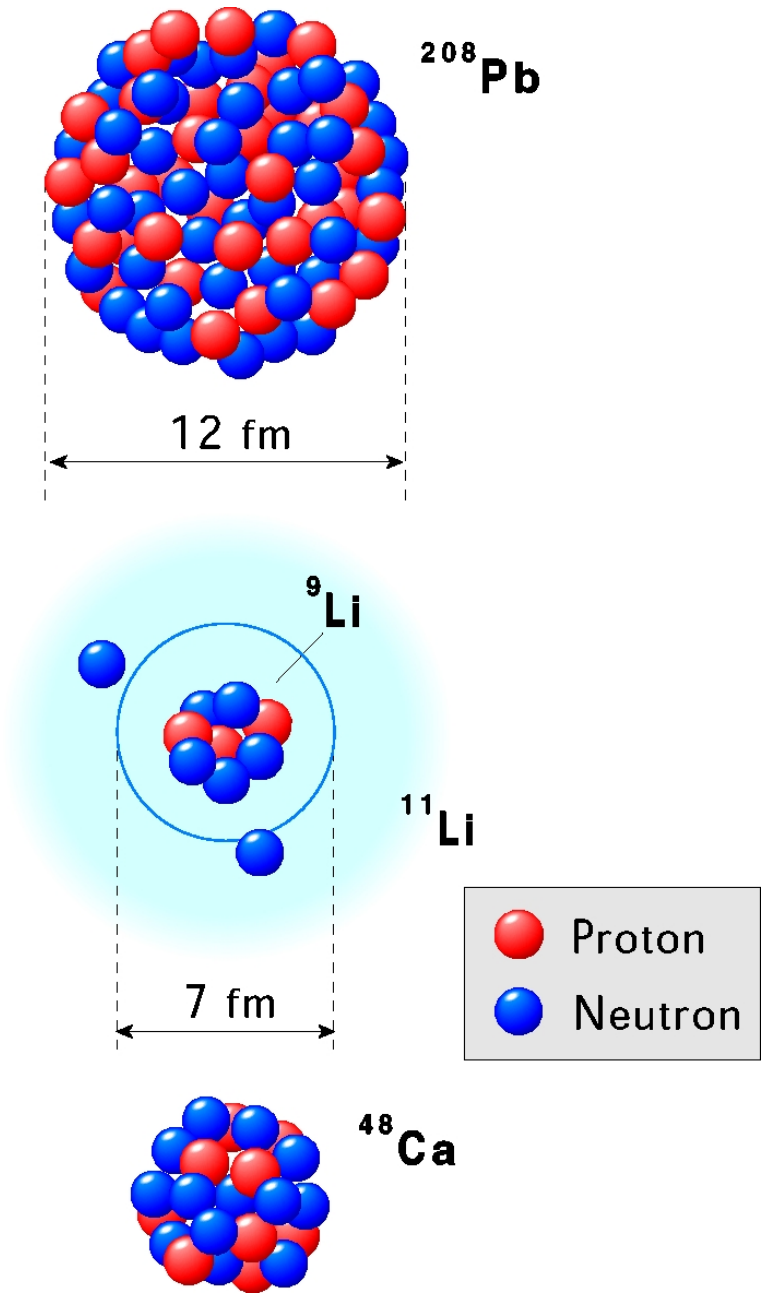

Figure 1.8 Nuclei normally are very dense objects. However, the halo nucleus ^{11}Li is so neutron rich, that the last two neutrons are barely bound, and are allowed to move at large distances from the rest of the nucleus. The effective nuclear radius of ^{11}Li is as large as the radius of the much more heavy ^{208}Pb. Taken from http://www.ph.surrey.ac.uk/~phs1wc/CD-sirius/science/scigif8.gif

1.2 Nuclear Shape Coexistence and Nuclear Ground-State properties

1.2.1 Nuclear Shape Coexistence

The concept of deformed shapes and the appearance of different shapes in a given nucleus was introduced in nuclear physics as early a 1937 by the work of Bohr and Kalckar. In those days, little did on expect how fruitful these ideas would turn out to be. The discovery of the first excited state with spin 0^+ in the doubly-magic nucleus ^{16}O [16] and its subsequent interpretation starting from rearranging four particles from the occupied orbitals into empty orbitals above the Fermi level, resulted in a cooperative strong extra binding energy effect. A subsequent highly deformed shape, coexisting with the spherical ground state opended up a new field in nuclear physics research, devoted to the investigation and understanding of shape coexistence. Soon after, it was realized that the atomic nucleus, on its way to fission, had to undergo a number of shape changes in which a specific shape could be trapped as an isomeric state in a secondary potential minimum, called fission isomers. Shape coexistence invoking multiple shapes was predicted and also observed in many spherical nuclei near magic shells [17]. These particular phases could be linked to the occupation of very specific up- and/or downsloping orbitals (using a deformed average potential like the Nilsson model), coined "intruder orbitals", which allowed for a simple understanding of the phenomenon of shape coexistence. The method put forward in those papers could be used to predict shape coexistence, e.g. in the Sn nuclei around mass number $A = 116$ and in the Pb nuclei from mass number $A = 196$ and below.

The use of deformed single-particle models is particularly transparent for incorporating the concept of shapes coexisting in a given nucleus. In a Potential Energy Surface (PES), this approach very clearly shows how the excitation energy of the nuclear ground state depends on the nuclear deformation. Calculations for the ^{186}Pb isotope show three coexisting minima at different deformations, with excitation energies that lie very close to the experimental values (see fig. 1.9). Treating residual interactions and the subsequent mixing, on the other hand, is a very difficult task in this approach and implies the implementation of techniques going beyond mean field methods.

In the present study, we have opted for a method that is essentially starting from the idea that proton particle-hole excitations across the closed shells form an essential ingredient in order to be able to accomodate the equivalent of 'shape coexistence' in a spherical shell-model approach. As discussed in subsection 1.1.2, we use a highly truncated shell-model space in which only the nucleon pairs coupled to angular momentum 0^+ and 2^+ are considered (taking advantage of the pairing and quadrupole properties present in the two-body nucleon-nucleon interaction). Moreover, we map the fermion pairs onto the corresponding s and d

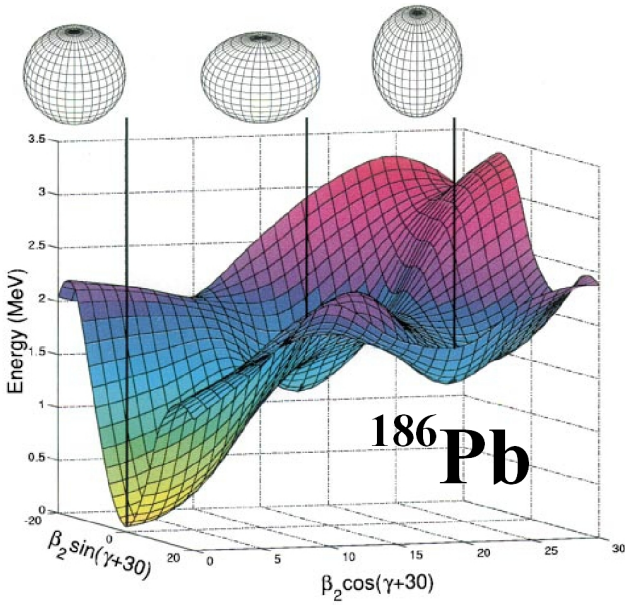

Figure 1.9 Calculated Potential Energy Surface of ^{186}Pb. Spherical, oblate (disk-shaped) and prolate (cigar-shaped) minima are indicated by thick vertical black lines. The β_2 parameter expresses the elongation of the nucleus along the symmetry axis, while the γ parameter relates to the degree of triaxiality in the deformation (that is, the relative lengths of the three principal axes of the spheroidal nucleus). The γ parameter is defined such that $\gamma = 0^\circ$ corresponds to a prolate shape and $\gamma = 60^\circ$ to an oblate shape. Taken from [14].

boson degrees of freedom. This leads to an interacting boson model (IBM) in which symmetry concepts play a particularly imporant role. This IBM has been extensively discussed in [10]. Since both particle and hole pairs adjacent to closed shells, however, play an important role, the IBM in its basic formulation cannot handle such excitations. We have extended the model, giving rise to an extended group theoretical structure with an imporant symmetry present, i.e. the symmetry that transforms particle-like bosons into hole-like bosons (and vice-versa).

In chapter 2, we use these concepts in order to construct a basis that allows for the presence of three different families that could give rise to 'shape' coexistence i.e. we treat both 0p-0h, 2p-2h and 4p-4h proton excitations across the $Z = 82$ closed shell. Together with the valence neutrons, this gives rise to a basis that consists of N, N$+2$ and N$+4$ bosons, respectively. In chapter 2, we outline the method needed to study the properties of the resulting bands and study their mixing characteristics in detail. This method is applied to the Pb mass region in which compelling experimental evidence has appeared over the years of the presence of these extra bands. Due to a number of very recent experiments [18, 19] that accessed detailed infor-

mation on both the energy of the yrast and yrare bands as well as E2 and E0 electric and monopole electromagnetic decay properties, this mass region has become a very active region of research that allows to critically study the method and results obtained in the present work and compare with calculations using deformed mean field methods [20, 21].

1.2.2 Nuclear Ground-State Properties

Local Correlations in the Global Behaviour

Nuclear ground-state properties and their variation throughout the nuclear mass chart have been addressed using the liquid drop model at first. Methods to include the shell-model effects, that modulate the global variations when crossing major and sub-shell closures or in the regions far away from closed shells where deformation in the nuclear densities result, have been worked out and implemented, resulting in so-called macroscopic-microscopic methods (Strutinsky method [11, 12]).

During the last decade, mean-field methods have been developed that allow for a consistent calculation of this variation, incorporating both the global and local variations starting from a given effective nucleon-nucleon interaction. Skyrme forces have been particularly useful in that respect and both Hartree-Fock, Hartree-Fock plus BCS and Hartree-Fock-Bogoliubov methods have been applied. Still, the best understood part of these studies lies within the global variations and subtle effects that occur in local mass regions through specific shell-model correlations can not be incorporated in a consistent way.

In chapter 3 of the present study, we make use of the symmetry-dictated truncation to the nuclear shell model, i.e. the Interacting Boson Model (IBM). The IBM has been particulary successful in describing detailed nuclear structure properties in medium-heavy and heavy nuclei using a rather general parametrization of the IBM Hamiltonian. Often, however, the binding energy of the nuclear ground state is not considered in an IBM analysis. Recently, it was pointed out by García-Ramos *et al.* that it is very important to include also the binding energies in an IBM study, or equivalently the two-neutron separation energy values, because its value is very sensitive to the Hamiltonian that is used [22]. Therefore, in the description of a given nucleus, the nuclear binding energy is a very useful observable to determine the most appropriate Hamiltonian. Fig. 1.10 shows an IBM fit to the energy spectrum of the Gd isotopes, using two different parametrisations. Both sets of parameters describe the spectrum relatively well. In fig. 1.11 it is shown that the consideration of the two-neutron separation energies can help to clear out this apparent freedom of parameters. As was shown in the latter study, and as will be recapitulated in chapter 3, in order to study the binding-energy properties, it is necessary to analyse a complete chain of isotopes and not a single nucleus, which makes the study more complicated [22]. In chapter 3, we present a description that treats both

global and local energy variations at the same time. We have set out to incorporate the overall binding energy variation over a large mass region encompassing a number of closed shells. In order to carry out such a program, we had to understand and model the global energy variation within the context of the IBM. We also needed to implement a procedure that is not restricted to a given major shell. Using the same idea as used in the macroscopic-microscopic methods, the energy is separated in a global term (related to the linear and quadratic Casimir invariant operators of the covering *U(6)* group of the IBM) and the local Hamiltonian that describes the finer details of the nuclear energy surface. To this end, we have first studied the dynamical symmetries and simple transitions between these symmetries. From the knowledge of these exploratory calculations, we have performed a detailed study in the region of rare-earth nuclei. As a general result, we come up with the conclusion that in order to have a good description, one cannot calculate the global and local energy terms in a separate way. One needs to use a single Hamiltonian that describes at the same time detailed energy spectra in all the individual nuclei but also the overall energy variation from mass $A = 110$ up to mass $A = 200$. These results are extensively presented and discussed in chapter 3.

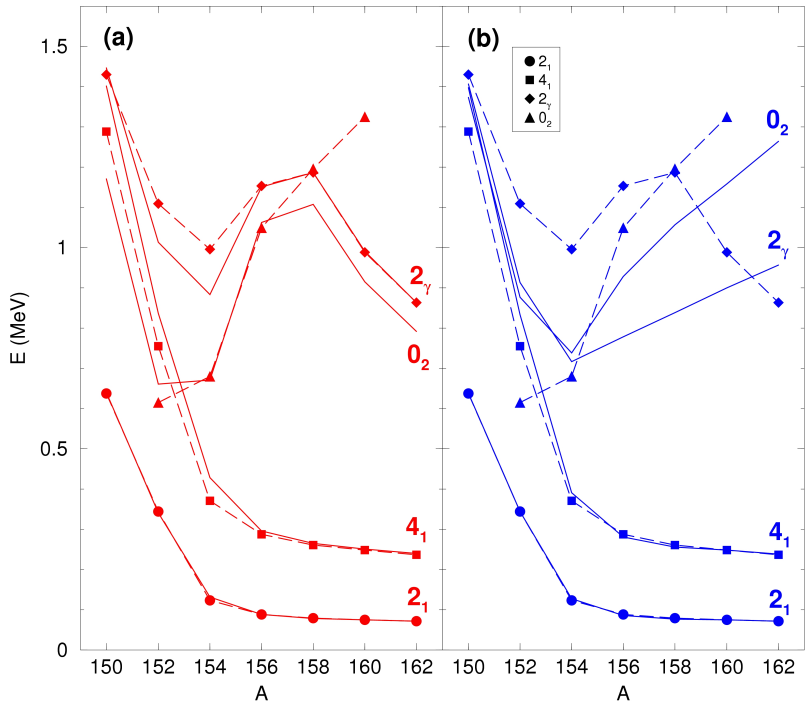

Figure 1.10 Comparison between the experimental (broken lines) and theoretical (full lines) energy spectrum for the Gd isotopes. In the left panel (a) and the right panel (b), two different IBM parameter sets are used. Taken from [22].

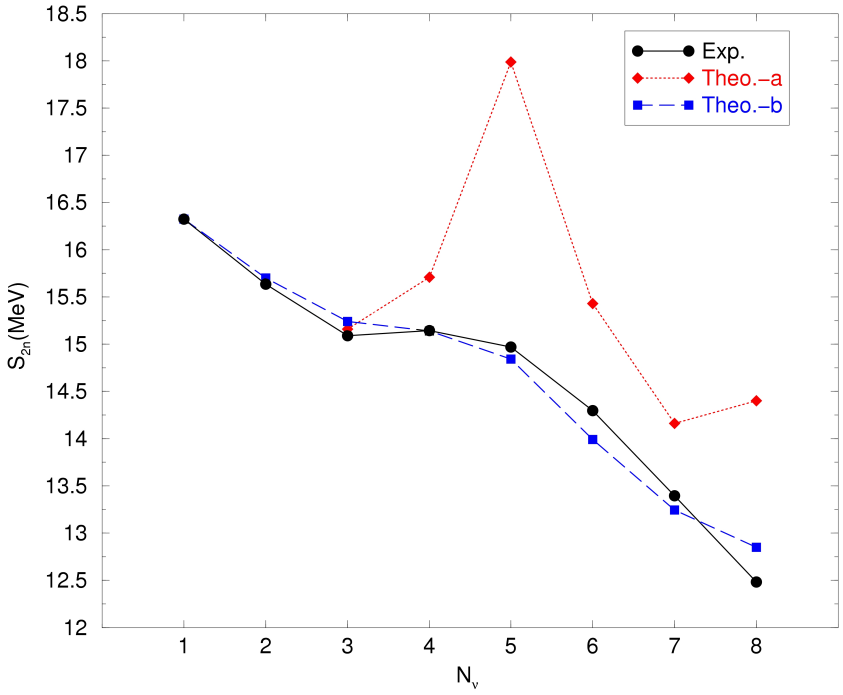

Figure 1.11 Comparison between the experimental (full line) and theoretical (broken and dotted line) two-neutron separation energy values through the series of the Gd isotopes, using the two different IBM parameter sets from fig. 1.10. Taken from [22].

Particular interest is given to the $Z = 82$ mass region in which highly precise mass measurements have been carried out at ISOLDE - CERN using the ISOLTRAP set-up [23, 24, 25, 26]. The sensitivity allows to make a detailed study of the local small energy variations that become observable on the two-neutron separation energies as the particular observable used here. We study both the effects induced by local mixing of shape coexisting configurations, as borne out by the treatment using the IBM and the mixing of various core-excited configurations (see chapter 2) as well as the results from mean-field studies using a deformed Woods-Saxon potential. Detailed comparison with the data in the Pt, Hg, Pb and Po is carried out.

Schematic Residual Interactions in the Shell Model

In principle, the shell model should be able to describe besides the detailed energy spectra over a given mass region also the variations in the nuclear binding energies of these nuclei in a consistent way. At present, calculations in the *sd* and *fp* shell-model regions give a rather good description of the binding energy although the specific variations for certain localized mass regions e.g. the Na, Mg, Al nuclei with

neutron number at $N = 20$ and adjacent isotopes, does not fit with the idea of good closed shells. Moreover, the effective nucleon-nucleon interactions used in these mass regions have mainly been fitted to energy spectra and do not have correct saturation properties at the same time.

In that respect, we study in chapter 4 a number of specific properties of nuclear simple schematic interactions, in particular the effect on nuclear binding energies and saturation properties. We compare in particular the difference between a pure pairing force and the zero-range delta interaction amongst identical nucleons (section 4.1). Whereas the energy spectra generated by both forces are essentially identical (taken aside the degeneracies of the pairing force), the correlations built by the pairing force are in angular moment space whereas the correlations of the zero-range force are in coordinate space. This then translates in the latter force, having correct saturation properties when filling a single-j shell (and also filling a number of j-shells consecutively) whereas the pure pairing force does not exhibit this saturation property (and therefore can only be used to describe a small mass region).

We moreover study the effect of the quadrupole-quadrupole ($Q \cdot Q$) force acting amongst the valence protons and neutrons as a possible correction to the pairing properties that govern a given smaller mass region near closed shells (section 4.2). We explicitely evaluate the energy contribution of the $Q \cdot Q$ force using perturbation theory. The final outcome is particularly interesting and was unexpected: it turns out that the proton-neutron quadrupole force can be incorporated in the pairing force strength to a very good approximation with a renormalisation of its strength by 5-25%. This might help to understand some of the particular variations in the nuclear binding energy near single-closed shell nuclei.

Chapter 2

Shape Coexistence and Configuration Mixing in the Neutron-Deficient Lead Isotopes

2.1 Introduction

During the last years, ample evidence for the presence of intruder excitations, in particular at and near closed-shell regions [27, 28] has been accumulated throughout the nuclear mass table. Such intruder excitations, which give rise to shape coexistence and collective band structures, are particularly well documented in the $Z = 50$ (Sn) and $Z = 82$ (Pb) mass regions. They can be associated with many-particle many-hole proton excitations across the closed shells [29] but can also be studied, in an equivalent way, using potential energy surface calculations [30].

After the discovery of 0^+ intruder excitations in the even-even Pb nuclei, down to mass $A = 192$ [31, 32, 33, 34], the development of recoil and recoil-decay-tagging (RDT) techniques and of heavy-ion induced fusion-evaporation reactions [35] have led to a wealth of new data on collective bands in the Pb isotopes that have neutron number near $N = 104$. The large number of experiments carried out over the last few years are described in a review paper by Julin *et al.* [36]. Study of the fine-structure of alpha decay of the very neutron-deficient nuclei has also proven to be an excellent tool [37] to identify excited 0^+ states and was used for the first observation of a set of three low-lying 0^+ excitations in ^{186}Pb [38, 39]. The above two major experimental techniques have been instrumental in exploring unexpected new phenomena concerning intruder states and shape coexistence.

With these methods, data have become available on ^{188}Pb [18, 40, 41, 42, 43], ^{186}Pb [38, 39, 44], ^{184}Pb [45, 46] and ^{182}Pb [47]. The experimental evidence for close-lying 0^+ excitations and for associated collective band structures (see Fig. 2.1) has brought about the need to explore and study the effects of mixing among these

structures. A first attempt using two-level mixing for the low-lying 0^+ and 2^+ excitations in $^{190-200}$Pb was carried out by Van Duppen *et al.* [48]. The importance of mixing between bands was put in a broader context by Dracoulis [49] in the Os-Pt-Hg-Pb region. More recently, detailed two-band mixing calculations [50, 51] and an attempt to perform a three-band mixing study in ^{186}Pb [52] have been reported, albeit all starting from phenomenological band-mixing assumptions. So, there is a clear need to perform a detailed study of these nuclei. We also mention that intruder 0^+ states and associated bands have been studied in the neutron-deficient Pt nuclei [53, 54, 55, 56, 57, 58, 59] down to mass $A = 168$ and in the Po nuclei [60, 61, 62, 63, 64, 65, 66, 67] in an effort to distinguish collective vibrational excitations from intruder states.

Deformed mean-field calculations [20, 30, 68, 69, 70] have indicated the possibility of obtaining oblate and prolate minima close to the spherical ground-state configuration in the total energy surface for the Pb nuclei for neutron numbers close to $N = 104$. In the Hg nuclei with a ground state corresponding to a slightly deformed oblate configuration, a second, prolate configuration is predicted with minimal energy near mid-shell ($N = 104$), while in the Pt nuclei a crossing of both minima is found and the prolate deformed minimum becomes the lowest configuration at mid-shell. In the Po nuclei the situation is more complicated [71] with an oblate minimum which approaches the spherical ground-state configuration near $N = 110$, and a prolate minimum which becomes dominant in the ground state for even lower neutron numbers. The above studies have the drawback that only the static potential energy surface properties are studied.

Many-particle many-hole (mp-nh) excitations cannot be incorporated easily in full large-scale shell-model studies because of the extremely large dimensions of the model spaces involved. These mp-nh excitations, however, can be handled within an algebraic framework of the Interacting Boson Model (IBM) [10, 72]. The inclusion in IBM of the simplest 2p-2h intruder excitations in the form of two extra nucleon pairs (two bosons) and the study of the mixing with the regular configurations was suggested by Duval and Barrett [73] and applied in the Pb region to the Hg nuclei [74, 75], the Pt nuclei [76] and the Po nuclei [71]. These IBM-mixing calculations, however, generally implied the introduction of many parameters. Calculations including up to 6p-6h excitations have been carried out, using a simplified Hamiltonian, with the aim of studying high-spin properties and backbending within the IBM configuration mixing picture by J. Jolie et al [77, 78]. In an effort to remove the obstacle of introducing many parameters when carrying out such IBM configuration mixing calculations with various mp-nh excitations, the symmetries connecting particle and hole bosons have been put forward in an algebraic framework and led to the introduction of a new label, called *intruder spin* or I spin [79] and to applications in the Pb region [80]. In this approach, explored in detail in a series of papers [81, 82, 83, 84], both the particle and hole shell-model configurations are handled as interacting particle- and hole-like s and d bosons. The method

also allows, in principle, the mixing of two dynamical symmetries.

The experimental need to explore three families each with a different intrinsic structure (spherical, oblate and prolate or, in a spherical shell-model language, the 2p-2h and 4p-4h intruder excitations next to the regular ones of 0p-0h type) forms the starting point of the present study. An exploratory calculation of this kind within an algebraic framework has already been reported [85, 86] but was confined to the 0^+ band heads. In this chapter an IBM-mixing calculation that describes the three different intrinsic 'shape' configurations is performed, and applied to the very neutron-deficient Pb nuclei.

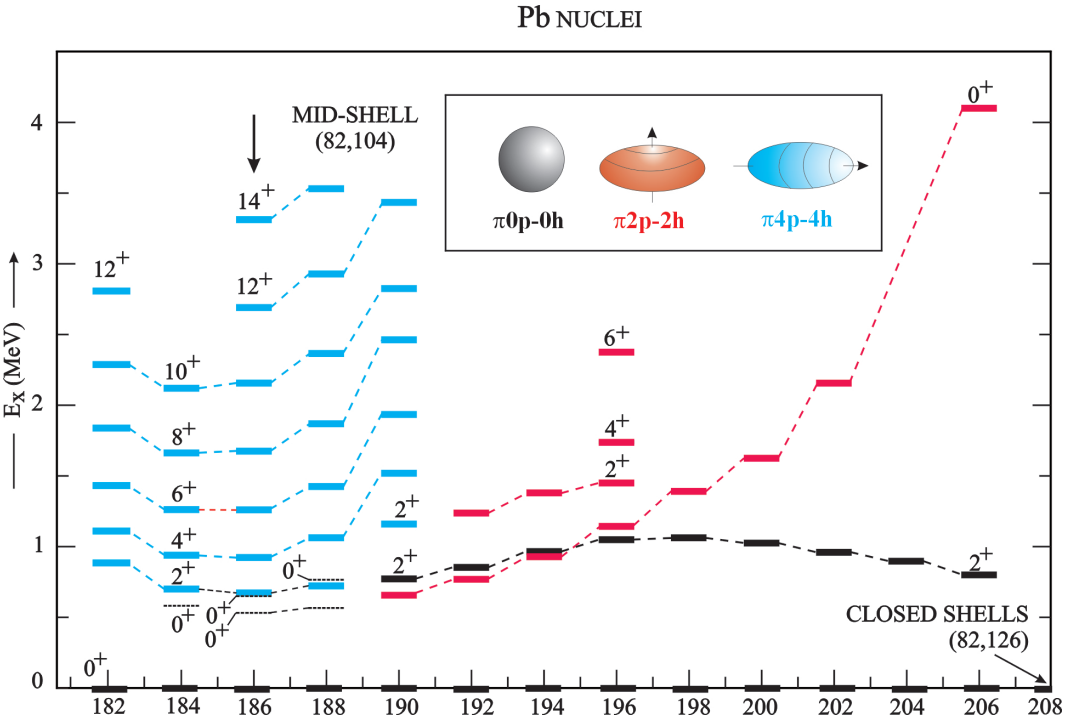

Figure 2.1 Observed systematics of low-lying 0^+ states in even-even Pb nuclei. The first-excited 2^+ state is also given for reference and in the mass region $184 \leq A \leq 190$ known band members of the yrast structure are also shown. This implies that not all observed levels are shown on this figure. References are given in the introduction.

2.2 The configuration mixing model

2.2.1 Hamiltionian

The regular (reg) 0p-0h states are described in terms of N bosons while the intruder 2p-2h and 4p-4h states require $N+2$ and $N+4$ bosons, respectively. The model space thus consists of the sum of three symmetric U(6) representations $[N] \oplus [N+2] \oplus [N+4]$. The model Hamiltonian has the form

$$\hat{H} = \hat{H}_{reg} + \hat{H}_{2p2h} + \hat{H}_{4p4h} + \hat{V}_{mix}. \tag{2.1}$$

The different parts are

$$\hat{H}_{reg} = \epsilon_{reg}\hat{n}_d + \kappa_{reg}\hat{Q}_{reg}\cdot\hat{Q}_{reg}, \tag{2.2}$$

$$\hat{H}_{2p2h} = \epsilon_{2p2h}\hat{n}_d + \kappa_{2p2h}\hat{Q}_{2p2h}\cdot\hat{Q}_{2p2h} + \Delta_{2p2h}, \tag{2.3}$$

$$\hat{H}_{4p4h} = \epsilon_{4p4h}\hat{n}_d + \kappa_{4p4h}\hat{Q}_{4p4h}\cdot\hat{Q}_{4p4h} + \Delta_{4p4h}, \tag{2.4}$$

with the d-boson number operator $\hat{n}_d$ and the quadrupole operator

$$\hat{Q}_i = \left(s^\dagger\tilde{d} + d^\dagger\tilde{s}\right)^{(2)} + \chi_i\left(d^\dagger\tilde{d}\right)^{(2)}, \tag{2.5}$$

where i stands for a regular, 2p-2h or 4p-4h configuration. The parameter Δ_{2p2h} corresponds to the single-particle energy needed to create a 2p-2h excitation, corrected for the gain in binding energy due to pairing. Likewise, Δ_{4p4h} corresponds to the single-particle energy needed to create a 4p-4h excitation (corrected for pairing), with $\Delta_{4p4h} \approx 2\Delta_{2p2h}$. Eigensolutions depend primarily on the ratio ϵ/κ. For $\epsilon \gg \kappa$ the solution is vibrational while for $\epsilon \ll \kappa$ it is rotational. In addition, the parameter χ in the quadrupole operator (3.18) determines whether the solution is SU(3) (axially deformed, $\chi = \pm\sqrt{\frac{7}{4}}$) or SO(6) (triaxially unstable, $\chi = 0$). The Hamiltonians used in (2.1) represent the simplest parametrisation of the IBM which encompasses its different limits, U(5) vibrational, SU(3) rotational and SO(6) γ soft. Often a rotational term $\hat{L}^2$ is added but this is not needed here.

The mixing of the different configurations is induced by $\hat{V}_{mix}$, which is assumed to be of lowest possible order in the s and d bosons,

$$\hat{V}_{mix} = \hat{V}_{mix,1} + \hat{V}_{mix,2}, \tag{2.6}$$

with

$$\hat{V}_{mix,i} = \alpha_i\left(s^\dagger s^\dagger\right) + \beta_i\left(d^\dagger d^\dagger\right)^{(0)} + \text{hermitian conjugate}, \tag{2.7}$$

where $i = 1, 2$ and $\hat{V}_{mix,1}$ mixes the regular (0p-0h) and 2p-2h configurations while $\hat{V}_{mix,2}$ mixes the 2p-2h and 4p-4h configurations. Note that care is taken to introduce different (0p-0h)-(2p-2h) and (2p-2h)-(4p-4h) mixing parameters, (α_1, β_1) and

(α_2, β_2), respectively, and that there is no direct mixing between the 0p-0h and 4p-4h configurations. The latter statement is suggested by the observation that the matrix element of a two-body interaction between 0p-0h and 4p-4h states is zero.

To obtain an estimate of the relation between (α_1, β_1) and (α_2, β_2), assume in first approximation that the dominant component of the 2p-2h and 4p-4h configurations involves pairs of particles (holes) in a single j_p (j_h) shell coupled to zero angular momentum. For a pairing force the following ratio of mixing matrix elements is obtained:

$$\frac{\left\langle 0 \left| \hat{V}_{\text{pairing}} \right| j_p^2(0) j_h^2(0) \right\rangle}{\left\langle j_p^2(0) j_h^2(0) \left| \hat{V}_{\text{pairing}} \right| j_p^4(0) j_h^4(0) \right\rangle} = \frac{1}{2} \sqrt{\frac{(2j_p+1)(2j_h+1)}{(2j_p-1)(2j_h-1)}} \approx 0.5. \tag{2.8}$$

In the limit of large shells, the mixing between the 2p-2h and 4p-4h 0^+ states is thus twice as strong as that between the ground state and the 2p-2h states. In contrast, the corresponding ratio, obtained with the mixing Hamiltonian (2.6) and a U(5) vibrational classification of states, equals

$$\frac{\left\langle s^N \left| \hat{V}_{\text{mix}} \right| s^{N+2} \right\rangle}{\left\langle s^{N+2} \left| \hat{V}_{\text{mix}} \right| s^{N+4} \right\rangle} = \frac{\alpha_1}{\alpha_2} \sqrt{\frac{(N+1)(N+2)}{(N+3)(N+4)}}. \tag{2.9}$$

In the limit of large boson number, α_2 should thus be twice as big as α_1 to recover the ratio in eq. (2.8). In the present application to the Pb isotopes, the boson number N is such that the square root in eq. (2.9) equals about 0.8, by which factor α_2 should be reduced to account for the finite boson number. Another and perhaps more important fact is that both eqs. (2.8) and (2.9) are derived for a spherical configuration. It is clear that deformation may drastically change the ratio of mixing matrix elements and, specifically, it may reduce both matrix elements because of the smaller overlap between states with different deformation. Thus the microscopic estimate $\alpha_2 \approx 2\alpha_1$ cannot be adhered to rigidly and several calculations corresponding to different combinations of mixing matrix elements must be explored.

2.2.2 Parametrisation from known experimental data

The regular configuration

In the even-even Pb nuclei, $126 - N$ valence neutrons form a ground state which is predominantly of seniority zero, $v = 0$. This can be viewed as a condensate of neutron pairs coupled to 0^+. Excited states are first built from one broken pair ($v = 2$) with $2^+, 4^+, 6^+, \ldots$, next two broken pairs ($v = 4$) $0^+, 2^+, 3^+, 4^+, \ldots$ and so on. To describe these spherical states in an IBM context, we consider the Hamiltonian (2.2) with a spherical structure [symmetry limit U(5)] and which has ϵ_{reg} as the only parameter. We fix this parameter to the 2_1^+ state of the heavier Pb isotopes $A = 198$

to 204, where the mp-nh intruder states are high in energy and have little effect on the low-excited spherical states (see fig. 2.1). We do not consider the one broken pair 4^+ (g boson) or 6^+ (i boson),... states, which can only be described within extended boson models. A constant Hamiltonian for this regular configuration, $\hat{H}_{reg} = \epsilon_{reg}\hat{n}_d$, yields a constant excitation energy for the 2_1^+ state, independent of the number of bosons. The excitation energy of the observed states, however, changes slightly with mass number A (because of shell effects). We choose $\epsilon_{reg} = 0.9$ MeV; this value is a compromise between a 2_1^+ state which is somewhat too low and other states that increase too rapidly in energy with angular momentum. A better fixing of ϵ_{reg} could have been obtained by a variation of ϵ_{reg} linear with the number of bosons. For the sake of simplicity this is not done here.

The intruder excitations: 2p-2h and 4p-4h configurations

The spectroscopic information on the neutron-deficient Pb isotopes is limited. We use I-spin symmetry arguments in order to find the IBM parameters of the two intruder configurations in Pb from corresponding bands in neighbouring nuclei where more experimental information is available.

Before deriving the parameters for the 2p-2h configuration in Pb, we first show in fig. 2.2 the correspondence between the experimental 2p-2h intruder band in ^{196}Pb—the only Pb isotope where it is known—(left panel) and the intruder analogue regular 0p-4h ground-state band in ^{192}Pt (middle panel). This 0p-4h band is also shown for other Pt isotopes from mass numbers A = 190 to 200, where the coexisting 2p-6h intruder configuration lies high in energy and has little influence on the 0p-4h band. The right-hand panel of fig. 2.2 shows an IBM calculation of the 0p-4h band in the Pt isotopes which, using a constant Hamiltonian

$$\hat{H} = \epsilon\hat{n}_d + \kappa\hat{Q}\cdot\hat{Q}, \tag{2.10}$$

with $\hat{Q}$ given in eq. (3.18). The band head of the γ band, the 2_2^+ level, is also taken into account in order to restrict the possible parameter values. The parameter χ is fixed in order to reproduce the observed ratio R

$$R = \frac{B(E2: 2_2^+ \rightarrow 0_1^+)}{B(E2: 2_1^+ \rightarrow 0_1^+)}, \tag{2.11}$$

which is 0.00732 in ^{192}Pt [87] and 0.00485 in ^{194}Pt [88]. Theoretical values are 0.00711 and 0.00500, respectively. It is seen that the experimental spectra for Pb and Pt are very similar up to 6^+. Intruder spin symmetry appears to be a good approximation, and so it seems reasonable to use the 0p-4h parameters of Pt to describe the Pb intruder 2p-2h configuration.

In the same way we derive the parameters for the 4p-4h configuration in Pb. In fig. 2.3 we show the observed analogue bands of the 4p-4h intruder configuration

in the Pb isotopes (left panel), the 2p-6h intruder configuration in the Pt isotopes (second panel) and the regular 0p-8h ground-state configuration in the W isotopes (third panel). In the right-hand panel of fig. 2.3, an IBM calculation for this 0p-8h band in the W isotopes is shown, with the Hamiltonian (2.10) again with constant parameters for all isotopes. This calculation also includes the 2_2^+ level, the band-head of the γ band. The parameter χ is fixed from the experimental ratio (2.11) in ^{182}W, which lies in the range 0.0252–0.0295 according to the different references in [89]; the calculated ratio is 0.0276. Again, I-spin symmetry seems to be valid in this case and we use the 0p-8h parameters of W to describe the 4p-4h configuration in Pb.

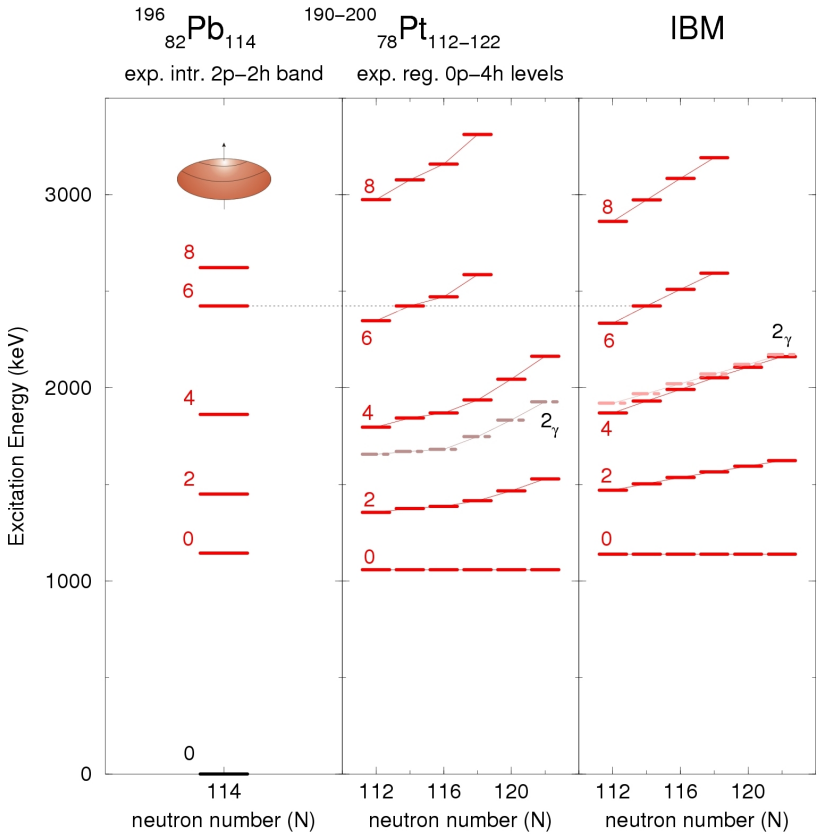

Figure 2.2 Left panel: Experimental [90] excitation energies of the 2p-2h intruder band in ^{196}Pb relative to the regular 0_1^+ ground state. Middle panel: Experimental [37, 53, 54, 55, 56, 57, 58, 59, 76, 91, 92, 93, 94] regular (0p-4h) ground-state bands in the Pt isotopes with $A = 190$ to 200. Right panel: IBM calculation for the Pt isotopes in the same mass range with parameters $\epsilon = 0.51$ MeV, $\kappa = -0.0140$ MeV and $\chi = 0.515$ (kept constant for all isotopes). The Pb and Pt bands are suggested as members of an $I = 1$ intruder-analog multiplet. Energies in Pt and IBM are normalized to the 6^+ excitation energy in the $N = 114$ isotope and by requiring a constant 0^+ energy in other isotopes.

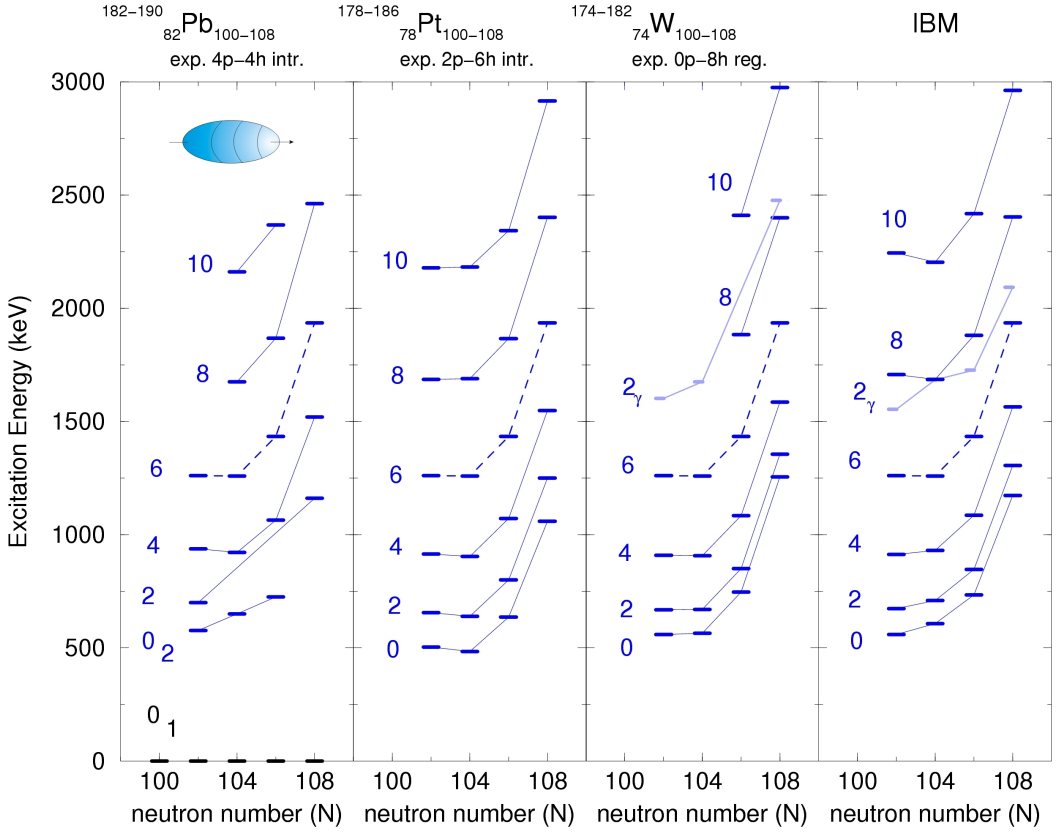

Figure 2.3 Left panel: Experimental [31, 32, 33, 34, 35, 36, 37, 38, 39, 40, 41, 42, 50, 44, 45, 46, 47, 48, 49, 43, 51, 52, 90, 95, 96] 4p-4h intruder bands in the Pb isotopes with A = 182 to 190. Second panel: Experimental 2p-6h intruder bands in the Pt isotopes with A = 178 to 186. Third panel: Experimental [97, 98] regular (0p-8h) ground-state bands in the W isotopes with A = 174 to 182. Right panel: IBM calculation for the W isotopes in the same mass range with parameters $\epsilon = 0.55$ MeV, $\kappa = -0.020$ MeV and $\chi = -0.68$ (kept constant for all isotopes). The Pb, Pt and W bands are suggested as members of an I = 2 intruder-analog multiplet. Energies in Pt, W and IBM are normalized to the 6^+ excitation energy in the corresponding Pb isotope.

2.2.3 Three-configuration mixing in the Pb isotopes

With the three parameter sets $(\varepsilon_i, \kappa_i, \chi_i)$ determined previously for the regular, 2p-2h and 4p-4h configurations, a mixing must now be supplied that reproduces the experimental features of the three-configuration coexistence in the Pb isotopes (the extra parameters $\alpha_i, \beta_i, \Delta_i$). The final set of parameters is given in table 2.1. In table 2.2, we present results on the mixing of the three configurations (reg, 2p-2h and 4p-4h, respectively) in the first three 0^+ excited states. One clearly notices a rapid stabilization, close to 100%, for the 0_1^+ state at the spherical configuration. The 0_2^+ and 0_3^+ states indicate a strong mixing between the 2p-2h and 4p-4h configurations. Rather quickly, a dominance of the 2p-2h configuration is observed from $A = 186$ up to heavier masses in the 0_2^+ state. In table 2.3, we identify, for $^{186}_{82}Pb_{104}$, the bands which contain mainly the 2p-2h (called "2p-2h" band) and the 4p-4h (called "4p-4h" band) configuration for a particular J_i^π value. One notices the "4p-4h" band is related to the 0_2^+ band head and follows up the $2_1^+, 4_1^+, 6_1^+, 8_1^+$ states, whereas the "2p-2h" band is connected to the 0_3^+ band head and follows up the $2_2^+, 4_2^+, 6_2^+, 8_2^+$ states, respectively. The results in tables 2.2 and 2.3 are particularly illuminating in showing the mixing effects within the IBM configuration mixing.

configuration	ϵ	κ	χ	Δ	mixing
regular	0.9	0	—	—	
					$\alpha_1 = \beta_1 = 0.015$
2p-2h	0.51	−0.014	0.515	1.88	
					$\alpha_2 = \beta_2 = 0.030$
4p-4h	0.55	−0.020	−0.680	4.00	

Table 2.1 Parameters of the IBM-calculation of the three coexisting configurations in the Pb isotopes, as shown in fig. 2.4. All parameters are in MeV, except for χ, which is dimensionless.

Note that with constant parameters for all Pb isotopes identical results are obtained for corresponding isotopes that are symmetric around the middle of the shell.

The result of such a mixing calculation is shown in fig. 2.4 (left panel). From the comparison with the experimental situation, see fig. 2.4 (right panel), the slope with which the intruder states gain binding energy towards midshell is too steep, an effect that is independent of the mixing. Apparently, I-spin symmetry is not satisfied completely. A possible cause for these differences between the experimental and theoretical band structures is the fact that the IBM parameters are obtained from separate calculations for the 2p-2h intruder excitations (fig. 2.2) and 4p-4h intruder excitations (fig. 2.3). In the final calculation for the even-even Pb nuclei, which includes the 2p-2h and 4p-4h intruder families together with the regular spherical

configuration, the extra mixing effects will cause specific perturbations that may show up as a breaking of I-spin symmetry and may also affect the A-dependence of the intruder band energies. Possible improvements can be expected from a more elaborate mixing study, treating *all* known data for the neutron-deficient Pb isotopes and relevant nuclei in the $Z = 82, N = 126$ region. A further constraint would also be imposed by the condition that the lowest-lying proton 2p-2h 0^+ excitations approach the observed energy at $E_x \approx 4$ MeV in ^{208}Pb. Such extensive calculations, aiming to describe besides energy spectra and band structures also known electromagnetic (mostly E2 and E0) properties, isotopic and isomeric shifts and nuclear ground-state binding energies, will be pursued in the near future.

Very recently, calculations using boson coherent-states have been carried out by C. Vargas *et al.* [99] for the neutron-deficient Pb isotopes, in order to determine Potential Energy Surfaces (see fig. 5.1), starting from the present IBM parameters (table 2.1). The similarities between the boson coherent-state approach, and the recent mean-field results (see fig 1.9), seem to conform our choice of IBM parameters.

2.3 Conclusion

We have explored in the present chapter the possibility to describe the coexistence and mixing of three different families of excitations, corresponding to different intrinsic structures as observed in the Pb isotopes. In a mean-field approach the three configurations correspond to spherical, oblate and prolate shapes while in a shell-model description they arise as regular 0p-0h states and 2p-2h and 4p-4h excitations across the $Z = 82$ proton shell. Previous studies of such three-configuration systems were limited to the 0^+ band heads (without the associated bands) either in a mean-field [20, 30, 68, 69, 70, 71] or an IBM [85, 86] approach, or, to a phenomenological band-mixing calculation [18, 52], in ^{188,186}Pb, respectively.

The present description is based on the IBM-configuration mixing approach which was originally proposed for two configurations [73, 74, 75, 76]. In an IBM framework the three configurations are described as N-, $(N+2)$- and $(N+4)$-boson states. To reduce the number of parameters that appear in such a configuration mixing calculation, use is made of the concept of intruder-spin symmetry [79], relating configurations with different numbers of particle (N_p) and hole (N_h) bosons (i.e., fermion pairs), but with a constant sum $N_p + N_h = N$. In this way experimental excitation energies in adjacent Pt and W nuclei are used to fix the essential IBM parameters. The final result is a reasonably good description of the observed bands and their variation with mass number A. As outlined at the end of section 2.2.3, ways to improve the present results will need extensive calculations spanning the region of neutron deficient W, Os, Pt, Hg, Pb, Po and Rn nuclei as well as nuclei near the $Z = 82, N = 126$ doubly-closed shell.

0_i^+	configs.	$^{186}_{82}Pb_{104}$	$^{188}_{82}Pb_{106}$	$^{190}_{82}Pb_{108}$	$^{192}_{82}Pb_{110}$	$^{194}_{82}Pb_{112}$	$^{196}_{82}Pb_{114}$
0_1^+	reg	75	93	96	98	99	99
	2p-2h	18	7	4	2	1	1
	4p-4h	7	1	0	0	0	0
0_2^+	reg	20	6	4	2	2	1
	2p-2h	27	67	82	89	92	95
	4p-4h	52	27	14	9	6	4
0_3^+	reg	4	1	1	-	-	-
	2p-2h	51	28	43	-	-	-
	4p-4h	45	71	57	-	-	-

Table 2.2 Magnitudes (in percentages, %) of the three different configurations (reg, 2p-2h, 4p-4h) in the first three 0_i^+ states of the Pb isotopes $186 \leq A \leq 196$, in the IBM calculation of fig. 2.4 (left panel).

"2p-2h band"				**"4p-4h band"**			
	reg	2p-2h	4p-4h		reg	2p-2h	4p-4h
0_3^+	4	51	45	0_2^+	20	27	52
2_2^+	5	65	30	2_1^+	1	32	67
4_2^+	1	77	22	4_1^+	0	22	78
6_2^+	1	81	18	6_1^+	0	17	83
8_2^+	0	83	16	8_1^+	0	16	84

Table 2.3 The magnitudes (given in percentages, %) of the three different configurations (reg, 2p-2h, 4p-4h) in the "2p-2h" and "4p-4h" assigned bands of $^{186}_{82}Pb_{104}$, as shown in the IBM calculation of fig. 2.4 (left panel)

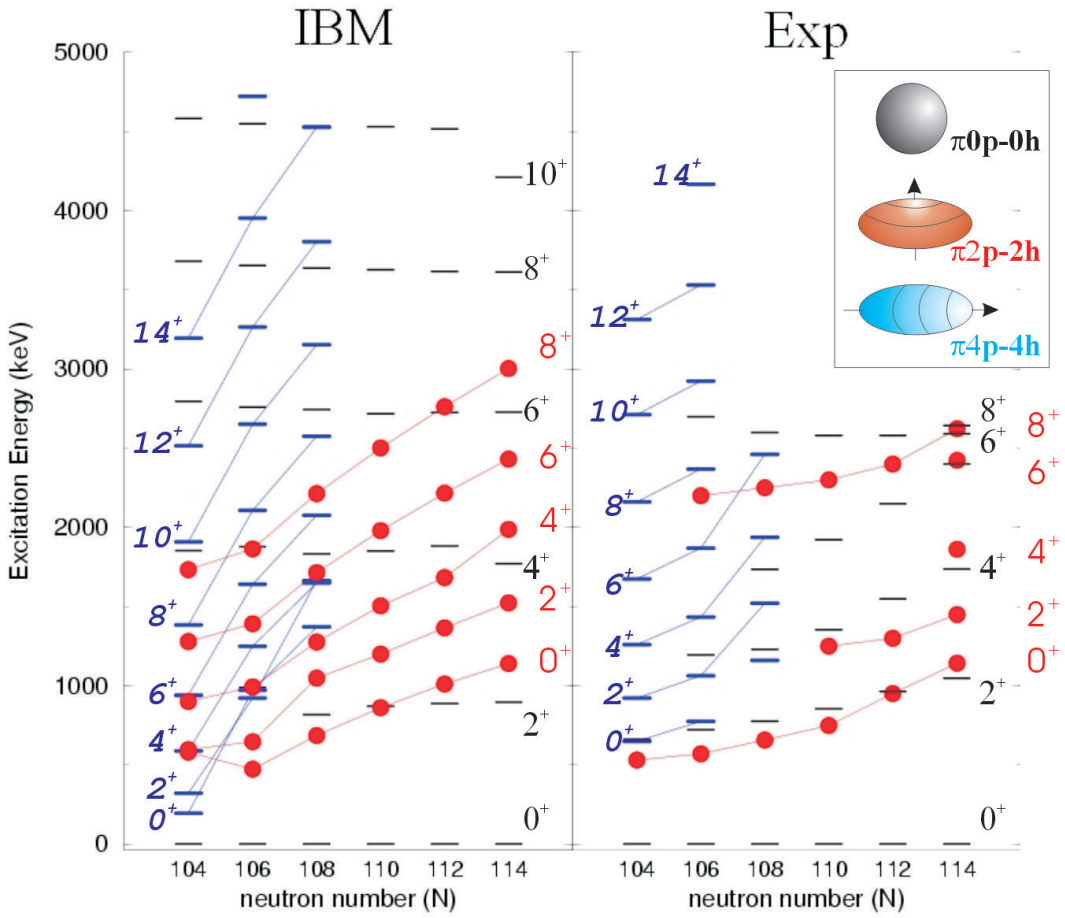

Figure 2.4 Right panel: Experimental [31, 32, 33, 34, 35, 36, 37, 38, 39, 40, 41, 42, 43, 44, 45, 46, 47, 48, 49, 50, 51, 52, 90, 95, 96] spectra of the Pb isotopes with $A = 186$ to 196 containing a regular ground-state spherical band (thin horizontal lines), a 2p-2h intruder band (filled circles) and a 4p-4h intruder band (thick horizontal lines). Left panel: IBM calculation for the Pb isotopes in the same mass region, with parameters determined from results obtained in figs. 2.1-2.3, as given in table 2.1.

Chapter 3

Nuclear binding energies: Global collective structure and local shell-model correlations

3.1 Introduction

In the study of nuclear structure properties, nuclear masses or binding energies (BE) and, more in particular, two-neutron separation energies (S_{2n}), are interesting probes to find out about specific nuclear structure correlations that are present in the nuclear ground state. These correlations, to a large extent, express the global behavior that is most easily seen in a global way and as such, the liquid drop model (LDM) serves as a first guide to match to the observed trends concerning nuclear ground-state masses [100, 101]. There have been extensive global mass studies carried out which aim, in particular, at reproducing the overall trends: from pure liquid-drop model studies (LDM) [102, 103, 104, 105], over macroscopic-microscopic methods [106, 107, 108, 109, 110, 111], over the semi-classical ETFSI (Extended Thomas-Fermi plus Strutinsky integral) [112], towards, more recently, relativistic mean-field [113], and Skyrme Hartree-Fock studies [114].

It is our aim to concentrate on local correlations that are rather small on the absolute energy scale used to describe binding energies (or two-neutron separation energies) but nevertheless point out to a number of interesting extra nuclear structure effects. These can come from various origins such as (i) the presence of closed-shell discontinuities, (ii) the appearance of local zones of deformation, and (iii) configuration mixing or shape mixing that shows up in the nuclear ground state itself. Except for the closed-shell discontinuities, the other effects give rise to small energy changes, about $200 - 300$ keV or less, that were not observed in experiments until recently. However, in the last few years a dramatic increase in the experimental sensitivity, using trap devices or specific mass-measurement set-ups

(ISOLTRAP, MISTRAL, ...) [23, 115], has shifted the level of accuracy down to a few tens of keV (typically $30-40$ keV for nuclei in the Pb region) such that mass measurements are now of the level to indicate local correlation energies that allow to test nuclear models (shell-model studies) [24, 25, 26]. Therefore, interest has been growing considerably and we aim at discussing and analysing, from this point of view, recent mass measurements.

In the first part of the present chapter, we discuss the collective (or global) features of the nuclear binding energy (or the S_{2n} observable) using a simple liquid-drop model (section 3.2) and some general properties of the shell model (section 3.3). In section 3.4 we concentrate on a description of binding energies within the framework of the Interacting Boson Model (IBM), where, besides a study of the global aspects of S_{2n}, the specific nuclear structure correlations (local part) are studied in, and close to, the symmetry limits $U(5)$, $SU(3)$, and $O(6)$. Special attention is given to obtain a consistent description of BE (S_{2n}) values when crossing the mid-shell point. Applications for the $50-82$ shell are presented in some detail. In the second part of this chapter (section 3.5) we concentrate on local modifications of the otherwise smooth BE (S_{2n}) behavior that come from the presence of low-lying intruder states at and near closed shells. We discuss the effect in both, an approximate IBM configuration mixing approach, as well as by studying, in some detail, the macroscopic-microscopic model giving rise to the potential energy surfaces (PES). We apply and discuss both calculations for nuclei in the neutron-deficient Pb region. Finally, in section 3.6 we present a number of conclusions.

3.2 Liquid drop model behavior

Nuclear masses and the derived quantity, the two-neutron separation energy, S_{2n}, form important indicators that may show the presence of extra correlations on top of a smooth liquid-drop behavior. S_{2n} is defined as

$$S_{2n}(A,Z) = BE(A,Z) - BE(A-2,Z), \tag{3.1}$$

where $BE(A,Z)$ is the binding energy defined as positive, (*i.e.* it is the positive of the energy of the ground state of the atomic nucleus) for a nucleus with A nucleons and Z protons.

The simplest LDM [102, 103] will be used as a reference point throughout this chapter because it allows the overall description of the *BE* along the whole table of masses, or for long series of isotopes. More sophisticated macroscopic-microscopic finite-range droplet models, using a folded-Yukawa single-particle potential have been developed [106, 107] and extensive mass tables published [108, 109, 110, 111]. Here, the global trends, even passing through regions of deformed nuclei, have been well described. Deviations that result, usually point towards new local nuclear structure effects. The present computing possibilities have resulted in modern

state-of-the-art mass tables spanning semi-classical EFTSI methods [112], over self-consistent relativistic mean-field models [113], towards a recent Skyrme Hartree-Fock study [114]. Those mass calculations serve as benchmarks for the whole nuclear mass region but local nuclear structure correlations, as well as the exact location of the onset of deformation stay outside the "philosophy" and scope of these important studies.

3.2.1 The global trend of S_{2n} along the valley of stability

To see how the values of S_{2n} evolve globally, through the complete mass chart, we start from can the semi-empirical mass formula [116, 117],

$$BE(A,Z) = a_V A - a_S A^{\frac{2}{3}} - a_C Z(Z-1)A^{-\frac{1}{3}} - a_A(A-2Z)^2 A^{-1}. \tag{3.2}$$

Even though there exist much refined macroscopic models (see references given before), the present simple liquid-drop model (3.2) is a suitable starting point for our purpose in analysing the physics behind the S_{2n} systematics. The S_{2n} value can be written as,

$$S_{2n} \approx 2(a_V - a_A) - \frac{4}{3}a_S A^{-\frac{1}{3}} + \frac{2}{3}a_C Z(Z-1)A^{-\frac{4}{3}} + 8a_A \frac{Z^2}{A(A-2)}, \tag{3.3}$$

where the surface and Coulomb terms are only approximated expressions. If one inserts the particular value of Z, Z_0, that maximises the binding energy for each given A (this is the definition for the valley of stability),

$$Z_0 = \frac{A/2}{1 + 0.0077A^{2/3}}, \tag{3.4}$$

we obtain, for large values of A, the result (see [25]),

$$S_{2n} = 2(a_V - a_A) - \frac{4}{3}a_S A^{-\frac{1}{3}} + (8a_A + \frac{2}{3}a_C A^{\frac{2}{3}})\frac{1}{4 + 0.06A^{\frac{2}{3}}}. \tag{3.5}$$

In the present form, we use the following values for the LDM parameters: a_V = 15.85 MeV, a_C = 0.71 MeV, a_S = 18.34 MeV and a_A = 23.22 MeV [102, 103]. In fig. 3.1, we illustrate the behavior of S_{2n} along the valley of stability (eq. 3.5) for even-even nuclei, together with the experimental data. The experimental data correspond to a range of Z between Z_0+1 and Z_0-2. It appears that the overall decrease and the specific mass dependence is well contained within the liquid-drop model.

3.2.2 The global trend of S_{2n} through a chain of isotopes

We can also see how well the experimental two-neutron separation energy, through a chain of isotopes, is reproduced using the LDM. From Fig. 3.1, it is clear that,

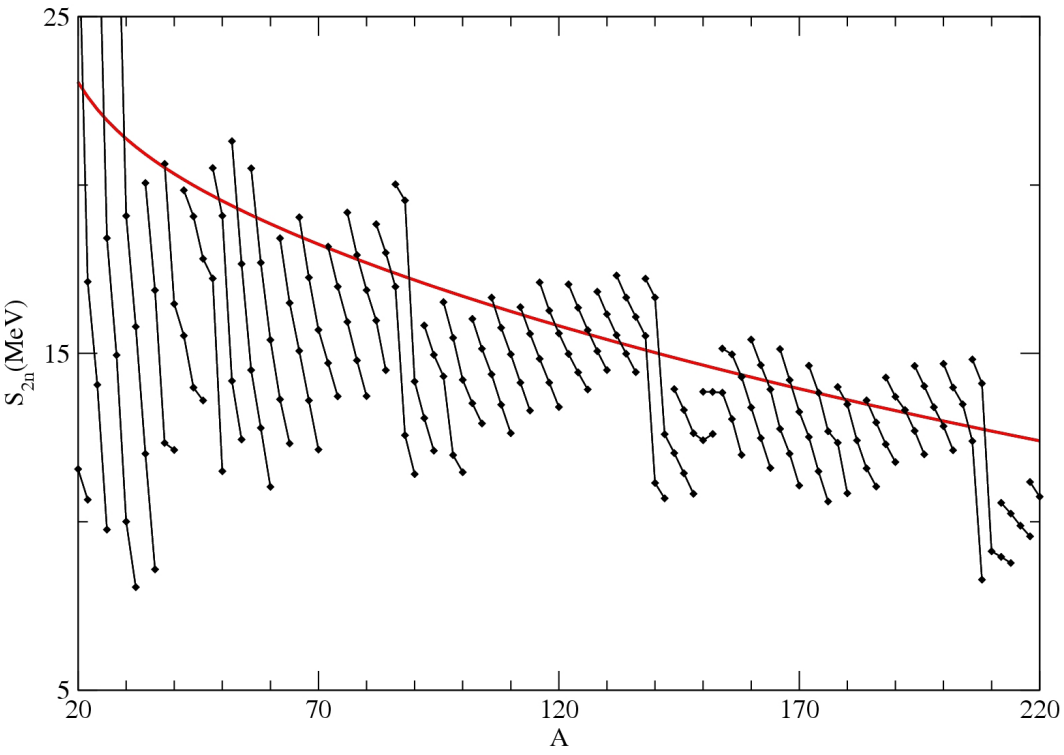

Figure 3.1 Comparison between the experimental S_{2n} (diamonds) values and the LDM prediction (thick full line) along the valley of stability. The experimental data correspond to even-even nuclei around the line of maximum stability. Points connected with lines correspond to nuclei with equal Z.

besides the sudden variations near mass number $A = 90$ (presence of shell closure at $N = 50$) and near mass number $A = 140$ (presence of the shell closure at $N = 82$), the specific mass dependence for series of isotopes comes closer to specific sets of straight lines.

Next, we observe that the mass formula (3.2) is able to describe the observed almost linear behavior of S_{2n} for series of isotopes. The more appropriate way of carrying out this analysis is to make an expansion of the different terms in (3.2) around a particular value of A (or N, because Z is fixed), $A_0 = Z + N_0$, and to keep the main orders. Therefore, we define $X = A - A_0$ and $\varepsilon = X/A_0$. Let us start with the volume term,

$$BE_V(A) - BE_V(A_0) = a_V X. \tag{3.6}$$

The surface term gives rise to,

$$BE_S(A) - BE_S(A_0) \approx -a_S A_0^{\frac{2}{3}} \left(\frac{2}{3}\varepsilon - \frac{1}{9}\varepsilon^2\right) = -a_S \frac{2}{3} \frac{X}{A_0^{\frac{1}{3}}} + a_S \frac{1}{9} \frac{X^2}{A_0^{\frac{4}{3}}}, \tag{3.7}$$

and the contribution of the Coulomb term is,

$$\begin{aligned} BE_C(A) - BE_C(A_0) &\approx -a_C Z(Z-1) A_0^{\frac{1}{3}} \left(-\frac{1}{3}\varepsilon + \frac{2}{9}\varepsilon^2 \right) \\ &= \frac{a_C}{3} Z(Z-1) \frac{X}{A_0^{\frac{4}{3}}} - \frac{2a_C}{9} Z(Z-1) \frac{X^2}{A_0^{\frac{7}{3}}}. \end{aligned} \tag{3.8}$$

Finally, the asymmetry contribution is,

$$\begin{aligned} BE_A(A) - BE_A(A_0) &\approx -a_A \left(A_0 - \frac{4Z^2}{A_0} \right) \varepsilon - a_A \frac{4Z^2}{A_0} \varepsilon \\ &= -a_A \left(1 - \frac{4Z^2}{A_0^2} \right) X - a_A \frac{4Z^2}{A_0^3} X^2. \end{aligned} \tag{3.9}$$

First, it is clear that the coefficients of the linear part are (for $A_0 \approx 100$ and $Z \approx 50$ and taking for a_V, a_C a_S, and a_A the values given in previous section) about two orders of magnitude larger than the coefficients of the quadratic contribution. With respect to the second order terms it is interesting to see the value of each of them: the surface term gives 0.0044 MeV, the Coulomb term -0.0083 MeV, and the asymmetry term -0.23 MeV. As a consequence, in this case, the leading term is the asymmetry one and it is essentially the main source of non-linearities in the BE and therefore, the source of the slope of the S_{2n}. In order to illustrate these results, we present in Fig. 3.2 the different contributions of the LDM (volume, volume plus surface, volume plus surface plus Coulomb and volume plus surface plus Coulomb plus asymmetry term) to the BE and S_{2n} for different families of isotopes. It thus appears that only the asymmetry term induces the quadratic behavior in BE and the linear one in S_{2n}.

In eq. (3.5) we make use of the classical values as discussed in the early papers of Wapstra [102, 103]. This fit, of course, was constrained to a relatively small set of experimental data points. More recent fits, including (i) higher-order terms in the LDM, *e.g.* the surface symmetry correction, a finite-range surface term, droplet correction, etc. and (ii) the much extended range of experimental data points, seem to give rise to an increased asymmetry energy coefficient a_A with values of the order of ≈ 30 MeV [118]. We show, in Fig. 3.2, the results obtained using an increased a_A coefficient, which gives rise to an increased in the absolute value of the S_{2n} slope.

In the present analysis, we have left out the effect of the pairing energy, with a dependence $BE_{pairing} = -11.46A^{-1/2}$ [102, 103], because the net result is an overall shift in the binding energy, but the relative variation in the S_{2n} values, over a mass span of $\Delta A = 20$ units, is of the order of ≈ 100 keV and, as such, is not essential for the plot of Fig. 3.2. Finally it should be stressed that, far from stability and for very neutron-rich nuclei, the asymmetry term can be at the origin of a decreasing trend in the BE when A further increases. This actually corresponds to the well known drip-line phenomenon, but here within a pure LDM approach.

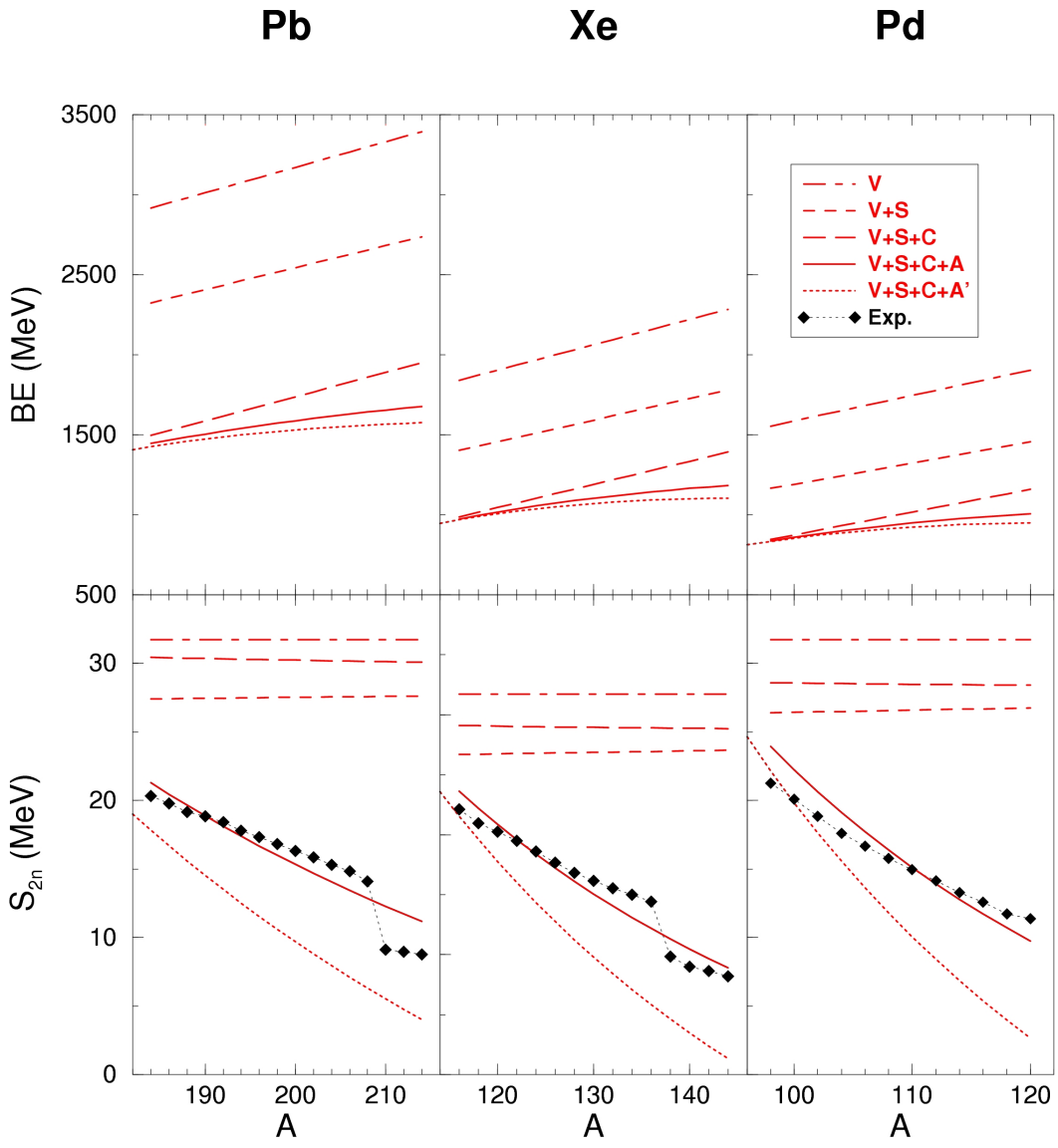

Figure 3.2 Contributions of the different terms of the mass formula to the BE (top row) and S_{2n} (bottom row) for Pb, Xe, and Pd. In the S_{2n} panels are also shown the experimental data. Two different asymmetry terms are considered $a_A = 23.22$ MeV (A), full line, and $a_A = 30$ MeV (A'), dotted line.

3.3 Shell-model description of binding energies

Within the liquid drop model (LDM) description of the binding energy of atomic nuclei, the volume term, the surface and Coulomb energy contributions give rise to an essentially flat behavior in the S_{2n} values. It is the asymmetry term that accounts for an almost linear drop in the quantity S_{2n} within a given isotopic series as a function of the nucleon (or neutron) number A (or N). This expresses the progressively decreasing binding energy needed to remove a pair of nucleons out of a given nucleus.

The asymmetry term shows up already when treating the nucleus as a Fermi gas of independent particles, as a consequence of the Pauli principle. The linear drop in S_{2n} also shows up in a more realistic shell-model description of nucleons moving in an average field, characterised by the single-particle spectrum ϵ_j, that are subsequently coupled to $J^\pi = 0^+$ pairs because of the major attractive binding-energy correlation on top of the monopole binding-energy term. To fix the idea, one should start from a doubly-closed shell nucleus as a reference nucleus in order to describe binding energies (or separation energies) and then treat the interactions amongst nucleons filling a given single-j shell. Talmi has shown [119, 120] that, for a zero-range force (δ-function interaction) using a pair-coupled wave function that has seniority ν as a good quantum number, the contribution to the ground-state configuration can be expressed as

$$BE(j,n) = \langle j^n, \nu = 0, J = 0| \sum V(i,k)|j^n, \nu = 0, J = 0\rangle, \tag{3.10}$$

or

$$BE(j,n) = n\epsilon_j + \frac{n}{2}V_0, \tag{3.11}$$

where $V_0 = \langle j^2, \nu = 0, J = 0|V|j^2, \nu = 0, J = 0\rangle$ is the attractive 0^+ two-body matrix element. This binding energy contribution is essentially equal to the volume part of the liquid-drop model formulation (which scales like A), and scales with the number of interacting valence nucleons moving in the single-j shell-model orbital and contributes with a constant value to the S_{2n} two-neutron separation energy.

More general interactions (finite range forces, the standard pairing force, ...) contribute with extra terms in the expression of the binding energy [119]. Coupling of the ground-state seniority $\nu = 0$ with higher-lying seniority $\nu = 2, 4, \ldots$ configurations also modifies this most simple expression given in (3.11). This then leads to a general diagonal energy that also contains a term quadratic in the number of nucleons n (the specific coefficients depend on the specific forces and coupling) and is given as [121]

$$BE(j,n) = C + \alpha n + \beta\frac{n(n-1)}{2} + [\frac{n}{2}]P, \tag{3.12}$$

provided the seniority ν is a good quantum number. Here, $[n/2]$ stands for the largest integer not bigger than $n/2$. Further, α is in general large and attractive ($\alpha = \epsilon_j + \frac{V_0}{2}$ with $\epsilon \approx -8$ MeV and $\frac{V_0}{2} \approx -(j+\frac{1}{2})$ G, with G the pairing force strength), β is much smaller and repulsive (in agreement with the sign of the asymmetry term in the liquid-drop energy expression) and P describes the odd-even pairing staggering to the binding-energy expression (see Fig. 3.3). Thus, it is the β contribution that causes a linear drop in the S_{2n} value as a function of the nucleon number. This expression has been used to fit S_{2n} values in various mass regions [120, 121, 122]. This shell-model behavior actually describes the long stretches of linear behavior in the S_{2n} curve over a large region of the nuclear mass table, indicating that the above simple structure contains the correct physics and saturation properties of the nucleon-nucleon two-body interactions. From the above discussion, it becomes clear that, in order to correctly reproduce the experimental S_{2n} behavior over a large series of isotopes, one needs a good description of the single-particle energies ϵ_j and their variation over a given mass region. The monopole term [123, 124] is essential in order to correctly reproduce saturation in the nuclear binding starting from a pure shell-model approach, *i.e.* if one starts out, *e.g.* with the single-particle energies in the sd shell-model space around ^{16}O and considers the variation in these single-particle energies through the monopole proton-neutron contribution

$$\tilde{\epsilon}_{j_\rho} = \epsilon_{j_\rho} + \sum \nu^2_{j_{\rho'}} \langle j_\rho j_{\rho'} | V | j_\rho j_{\rho'} \rangle, \tag{3.13}$$

one should reproduce the observed relative energy spacing in the sd shell when reaching the end of the shell near ^{40}Ca.

We shall not start to discuss detailed shell-model calculations here but we like to refer to the very good reproduction of the overall behavior in the S_{2n} value when crossing the full *sd* shell-model region [125], except near $N = 20$ and for the Ne, Na, and Mg nuclei [17, 126].

In the next section, we shall carry out a more detailed study of S_{2n} properties with a shell-model space that is truncated to that part which mainly determines the low-lying collective properties, *i.e.* we will perform the IBM symmetry truncation. We expect essentially to recover the shell-model features as described here. The IBM will allow, however, a more detailed study covering large sets of isotopes in the nuclear mass table.

3.4 IBM description of binding energies

The Interacting Boson Model [10] takes advantage of the group theory for describing low-lying states of even-even nuclei. Such states present a clear *quadrupole* collectivity. The building blocks of the model are bosons with angular momentum $L = 0$ (s bosons) and angular momentum $L = 2$ (d bosons). The number of

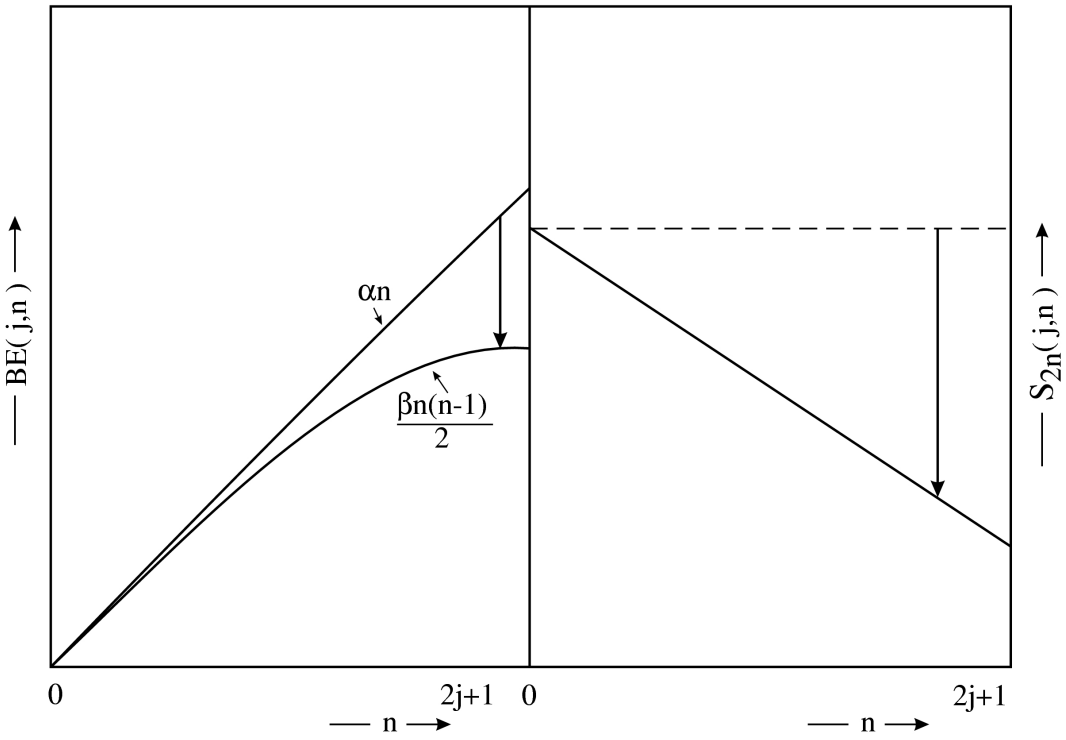

Figure 3.3 Schematic representation of BE (left) and S_{2n} (right) for a shell model Hamiltonian that preserves the seniority v as a good quantum number. The two different contributions to BE (S_{2n}) are plotted separately.

interacting bosons that are present in the system corresponds to half the number of valence nucleons, $N = n/2$, and they interact through a Hamiltonian containing, in the simplest case, up to two-body interactions, being number conserving and rotationally invariant. The original version of the model is called IBM-1 and in this approach no difference is considered between protons and neutrons [10, 127]. In this section we use the IBM-1 version of the model. In the last few decades the IBM has provided a satisfactory description of spectra and transitions rates of medium-mass and heavy nuclei [128]. However in most of the cases the binding energy has not been considered in the analysis. In a recent paper [22] it was pointed out that it is extremely important to include the BE, or equivalently the S_{2n} values, in an IBM study because its value is very sensitive to the Hamiltonian that it is used. Therefore, it is very useful for choosing the most appropriate Hamiltonian in the description of a given nucleus (see fig. 1.10 and 1.11). As was shown by García-Ramos *et al.* in Ref. [22] and will be recapitulated here, in order to study the binding-energy properties, it is necessary to analyse a complete chain of isotopes and not a single nucleus, which makes the study more complicated.

At this point it is convenient to write the definition of S_{2n}. In case we use nucleon particles outside of a closed shell, we define (remind, N denotes the number of nucleon pairs outside of closed shells, not to be confused with the neutron number):

$$S_{2n} = BE(N) - BE(N-1). \tag{3.14}$$

When using a description in terms of holes inside a closed shell, the definition of S_{2n} becomes,

$$S_{2n} = BE(N) - BE(N+1). \tag{3.15}$$

Later (section 3.4.4), we shall present a prescription that contains only a single definition.

For later use (section 3.4.6) we present here a very compact IBM Hamiltonian that will be used throughout this section. This Hamiltonian is not the most general one but is ideal for the purpose of studying binding energies and allows to describe many realistic situations [129]. It can be written as follows,

$$\hat{H} = \epsilon_d \hat{n}_d - \kappa \hat{Q} \cdot \hat{Q} + \kappa' \hat{L} \cdot \hat{L}, \tag{3.16}$$

where $\hat{n}_d$ is the d boson number operator and

$$\hat{L} = \sqrt{10}(d^\dagger \times \tilde{d})^{(1)}, \tag{3.17}$$

$$\hat{Q} = s^\dagger \tilde{d} + d^\dagger \tilde{s} + \chi(d^\dagger \times \tilde{d})^{(2)}. \tag{3.18}$$

The symbol $\cdot$ represents the scalar product. Here the scalar product of two operators with angular momentum L is defined as

$$\hat{T}_L \cdot \hat{T}_L = \sum_M (-1)^M \hat{T}_{LM} \hat{T}_{L-M}$$

where $\hat{T}_{LM}$ corresponds to the M component of the operator $\hat{T}_L$. The operator $\tilde{\gamma}_{\ell m} = (-1)^m \gamma_{\ell -m}$ (where γ refers to s and d bosons) is introduced to ensure the tensorial character under spatial rotations. Note that in realistic calculations $\epsilon_d > 0$ and $\kappa > 0$ [128]. It is common in this approach to use for the E2 transition operator the form

$$\hat{T}(E2) = q_{eff} \hat{Q}, \tag{3.19}$$

in which q_{eff} denotes the effective charge and $\hat{Q}$ has the same structure as in the Hamiltonian (3.18). This approximation is the basis of the so-called consistent-Q formalism (CQF) [130].

The Hamiltonian (3.16) generates the spectrum of the nucleus and in the following will be called "local Hamiltonian". An extra part can be added to this Hamiltonian (3.16) without affecting the spectrum, that will be called "global Hamiltonian".

In the description of BE using the IBM one has to distinguish between two contributions: a global (rather big) part that corresponds to the bulk energy of the atomic nucleus, should change slowly (BE^{gl}) and comes from the "global Hamiltonian", and a local (rather small) part coming from the specific structure of the given nuclei (BE^{lo}), *i.e.* coming from the "local Hamiltonian". However, the global part has to be added *ad hoc* using a given prescription that will be presented in this section. The simplest interpretation of the IBM global part comes from the LDM, and somehow, both contributions must be related. For the different series of isotopes they result into a quadratic behavior in BE and a linear one in S_{2n}. This IBM description resembles the Strutinsky method [131, 132] in the sense that a part (global part) takes care of the main part of the BE, while a second part (local part) modifies this bulk BE and generates the spectrum of the nucleus.

3.4.1 The global part of the *BE* (S_{2n}) in the IBM

The global part of the BE in the IBM (BE^{gl}) comes from that part of the Hamiltonian that does not affect the internal excitation energies. Those terms are related with the Casimir operators of $U(6)$, *i.e.* $\hat{C}_1[U(6)]$ and $\hat{C}_2[U(6)]$ and can be written in terms of the total number of bosons, $\hat{N}$,

$$\hat{H}^{gl} = -E_0 - \mathcal{A} - \frac{\mathcal{B}}{2}\hat{N}(\hat{N}-1). \tag{3.20}$$

Its contribution to the binding energy reads as,

$$BE^{gl}(N) = E_0 + \mathcal{A}N + \frac{\mathcal{B}}{2}N(N-1). \tag{3.21}$$

The corresponding contribution to S_{2n} is linear in the number of bosons:

$$S_{2n}^{gl}(N) = (\mathcal{A} - \mathcal{B}/2) + \mathcal{B}N. \tag{3.22}$$

In order to avoid ambiguities it is assumed in these expressions that N always corresponds to the number of nucleons pairs, considered as particles and is never considered as holes. We come back to this delicate aspect in section 3.4.4.

In the latter expressions, it is implicit that the coefficients $\mathcal{A}$, $\mathcal{B}$ and E_0 are constant for chains of isotopes (fixed Z) when the value of N changes, except when crossing the mid-shell or passing between major shells, *i.e.* it provides a linear contribution. However, this assumption is not clear *a priori*. To find a mathematical proof of the constancy of $\mathcal{A}$ and $\mathcal{B}$ is a difficult task. However, one can find a number of arguments based on LDM, shell-model, and IBM itself, that imply such a constancy.

- A LDM argument: In section 3.2 we noticed that the LDM gives a satisfactory global description of the BE throughout the whole mass table. This description cannot reproduce fine details, but it is able to explain the observed linear

behavior of S_{2n} for series of isotopes. This behavior is the same as the one obtained from (3.22), using $\mathcal{A}$ and $\mathcal{B}$ constants, and therefore supports our hypothesis.

- A shell-model argument: Another justification is based on the shell-model, in particular in the use of the modified surface-delta-interaction (MSDI). It is well known that the surface delta interaction (SDI) gives a good description of energy spectra although it also results in a number of systematic discrepancies with respect to the reproduction of the experimental levels. This discrepancy is especially notable for nuclear binding energies. It was shown that this description could be largely improved when changing the position of the energy centroids for the multiplets with different isospin. The modification of the interaction gave rise to the MSDI [133]. The most important point for our present discussion is that this new element in the two-body interaction, if one keeps the parameters constant, gives rise to a quadratic dependence in the nuclear binding energy, equivalent to the one we obtain in eq. (3.21).

- An IBM argument: A third justification comes from an IBM analysis. It will be shown in sections 3.4.5 and 3.4.6 that our *ansatz* provides an extremely good description of S_{2n} for chains of isotopes in the region from $Z = 50$ to $Z = 82$.

3.4.2 The local part of the BE (S_{2n}) in the IBM: the symmetry limits

The local contribution to the BE (BE^{lo}) comes from the IBM Hamiltonian that gives rise to the nuclear spectrum. This local contribution should be added to the fully linear part presented in previous subsection. A first approximation to this Hamiltonian comes from studying the symmetry limits of the model. Such limiting Hamiltonians do not correspond to realistic Hamiltonians but can be used as a good starting point. In the present discussion, the parameters of the different local Hamiltonians are kept constant, which is not a realistic hypothesis for long chains of isotopes. Note that the global Hamiltonian remains unchanged for the whole chain. Therefore, the following results will be applicable if we cut the chain of isotopes into smaller intervals and if we change the value of the parameters of the local Hamiltonian only between intervals.

The symmetry limits, called dynamical symmetries of the IBM, correspond to particular choices of the Hamiltonian that give rise to analytic expressions for the energy spectra (which is the reason of its usefulness). At the same time the eigenstates exhibit certain symmetries that allow to classify them in a simple way. The symmetry limits appear when the Hamiltonian is written in terms of a particular combination of Casimir operators. Next we succinctly review the three cases that were discussed before [10].

- U(5) limit. The local Hamiltonian that gives rise to the U(5) symmetry limit can be written as,

$$\hat{H}_{U(5)} = \varepsilon\, \hat{C}_1[U(5)] + \alpha\, \hat{C}_2[U(5)] + \beta\, \hat{C}_2[O(5)] + \gamma\, \hat{C}_2[O(3)], \tag{3.23}$$

where $\hat{C}_n[G]$ stands for the Casimir operator of order n of the group G. The ground state of this Hamiltonian can be written as

$$|0^+_{gs}\rangle = |[N], n_d = 0, \nu = 0, L = 0\rangle, \tag{3.24}$$

where [N], n_d, ν, and L are the appropriate labels that completely specify an eigenstate of the Hamiltonian (3.23) (see *e.g.* [10, 127]). The eigenvalue of (3.23) for a general state is obtained as,

$$E_{U(5)} = \varepsilon\, n_d + \alpha\, n_d(n_d + 4) + \beta\, \nu(\nu + 3) + \gamma\, L(L + 1). \tag{3.25}$$

As a consequence $BE_{U(5)}$=0 and $S^{U(5)}_{2n}$=0. It is clear that there is no local contribution to the BE in the case of the U(5) limit.

- SU(3) limit.

In the case of the SU(3) dynamical symmetry, the local Hamiltonian reads as,

$$\hat{H}_{SU(3)} = \delta\, \hat{C}_2[SU(3)] + \gamma\, \hat{C}_2[O(3)]. \tag{3.26}$$

The ground state for this Hamiltonian corresponds to,

$$|0^+_{gs}\rangle = |[N], (\lambda = 2N, \mu = 0), \kappa = 0, L = 0\rangle, \tag{3.27}$$

where [N], (λ, μ), κ, and L are the appropriate labels for completely specifying an eigenstate of the Hamiltonian (3.26) (see *e.g.* [10, 127]). The eigenvalues corresponding to the Hamiltonian (3.26), for a general state, can be written as,

$$E_{SU(3)} = \delta\, (\lambda^2 + \mu^2 + \lambda\mu + 3\lambda + 3\mu) + \gamma\, L(L + 1). \tag{3.28}$$

In this case the binding energy results into the expression,

$$BE_{SU(3)} = -\delta(4N^2 + 6N). \tag{3.29}$$

The value of S_{2n} for particles becomes,

$$S^{SU(3)}_{2n} = -\delta(8N + 2), \tag{3.30}$$

while for holes this becomes

$$S^{SU(3)}_{2n} = \delta(8N + 10), \tag{3.31}$$

where $\delta < 0$ in realistic calculations. It should be noted that the local contribution to S_{2n} is also linear in the number of bosons. This contribution should be added to the global part of the Hamiltonian.

- O(6) limit.

  The O(6) symmetry limit corresponds to the following Hamiltonian,

  $$\hat{H}_{O(6)} = \zeta\,\hat{C}_2[O(6)] + \beta\,\hat{C}_2[O(5)] + \gamma\,\hat{C}_2[O(3)]. \tag{3.32}$$

  The ground state for this Hamiltonian reads as,

  $$|0^+_{gs}\rangle = |[N], \sigma = N, \tau = 0, L = 0\rangle, \tag{3.33}$$

  where $[N]$, σ, τ, and L completely characterise an eigenstate of (3.32) (see *e.g.* [10, 127]). The energy eigenvalues of the Hamiltonian (3.32) can be written as,

  $$E_{O(6)} = \zeta\,\sigma(\sigma+4) + \beta\,\tau(\tau+3) + \gamma\,L(L+1). \tag{3.34}$$

  In this case the binding energy results into the expression,

  $$BE_{O(6)} = -\zeta(N^2+4N). \tag{3.35}$$

  The value of S_{2n} for particles becomes,

  $$S^{O(6)}_{2n} = \zeta(2N+3), \tag{3.36}$$

  while for holes it reads,

  $$S^{O(6)}_{2n} = -\zeta(2N+5). \tag{3.37}$$

  In the more realistic calculations $\zeta < 0$. It should be noted that the local contribution to S_{2n} is again linear in the number of bosons. This contribution should be added to the global part of the Hamiltonian.

At this point, it should become clear that the local IBM Hamiltonian, corresponding to the three dynamical symmetries, does not change the linear behavior of S_{2n} (coming from the global part). In the case of the $U(5)$ limit there is no extra contribution to S_{2n}, while for the $SU(3)$ and $O(6)$ limits only a change in the values of the slope and the intercept of S_{2n} is introduced. The analysis should only be valid within the smaller intervals and thus non-linear behavior in S_{2n} could appear if the character of the nuclei, along a series of isotopes, is changing from one symmetry limit into another one. An extra source for deviations of a linear behavior arises when the parameters of the local Hamiltonian themselves do change from one nucleus to another nucleus, even preserving the dynamical symmetry. Note that the global contribution remains linear.

3.4.3 The local part of the *BE* (S_{2n}) in the IBM: near the symmetry limits

In this subsection we complete the previous analysis, but now we study more complex situations albeit still in an analytical approximation. This will form a good starting point in order to carry out a complete numerical analysis of S_{2n} using the IBM.

Here, we consider the Hamiltonian (3.16), which will prove to be extremely useful for our purpose. This Hamiltonian encompasses the three symmetry limits for particular choices of the parameters and the so called transitional regions. The transitional regions are intermediate situations between the symmetry limits, where one observes rapid structural changes in the nuclei. One can identify three different transitional regions: (a) structural changes between spherical ($U(5)$) and well deformed nuclei ($SU(3)$); (b) structural changes from spherical ($U(5)$) to γ-unstable nuclei ($O(6)$) and (c) structural changes from well-deformed ($SU(3)$) to γ-unstable nuclei ($O(6)$). One observes that the borders of the transitional regions correspond to the dynamical symmetries (indicated between parenthesis).

The idea here is to consider the main part of the local Hamiltonian corresponding to a given symmetry limit plus a small correction term that allows us to explore the transitional region and that can be treated using perturbation theory. Next, we discuss three different situations depending on the main part of the local Hamiltonian.

- Near the $U(5)$ limit.

  The vibrational limit appears when $\kappa = 0$ in Hamiltonian (3.16). If $\kappa \neq 0$ the wave function (3.24) is only an approximate solution to the problem if $|\epsilon_d| >> |\kappa|$. The result is in principle independent of χ, but performing a simple analysis, one notices that the range of applicability of the results depends on χ. So, if one numerically diagonalizes the Hamiltonian (3.16) for $N = 8$ and for different values of κ/ϵ_d, one obtains that, even for a ratio equal to 0.03 and with $\chi = 0$, the overlap $\langle gs|[N], n_d = 0, \nu = 0, L = 0\rangle$ is equal to 0.913. For $\chi = -1$ this overlap equals 0.876, and for $\chi = -\sqrt{7}/2$ it equals 0.833. So it becomes clear that the range of applicability is quite narrow and even diminishes when $|\chi|$ increases.

  In the following discussion we assume $\kappa' = 0$ because its contribution to the BE always vanishes. If one calculates the mean value of (3.16), using the eigenstates (3.24), the result becomes,

$$\begin{aligned} BE &= -\langle 0^+_{gs-U(5)}|\epsilon_d \hat{n}_d - \kappa \hat{Q}\cdot\hat{Q}|0^+_{gs-U(5)}\rangle \\ &= \kappa \langle 0^+_{gs-U(5)}|\hat{Q}\cdot\hat{Q}|0^+_{gs-U(5)}\rangle. \end{aligned} \tag{3.38}$$

  The first term vanishes because $n_d = 0$ in the $U(5)$ ground state (see eqs. (3.24) and (3.25)). In order to calculate the remaining part, we consider the expres-

sion of the quadrupole operator (3.18) and we take into account that every $\tilde{d}$ operator acting directly on the *ket* state, or every $d^\dagger$ operator acting directly on the *bra* state, gives a vanishing contribution. The BE result then becomes,

$$BE = 5\kappa N. \tag{3.39}$$

The two-neutron separation energy for particles can be written as,

$$S_{2n} = 5\kappa, \tag{3.40}$$

while for holes it becomes,

$$S_{2n} = -5\kappa. \tag{3.41}$$

As a consequence, near the vibrational limit, the local Hamiltonian only gives a constant contribution to S_{2n}.

- Near the SU(3) limit.

  A particular case of a rotational nucleus corresponds to the SU(3) limit. In this case $\epsilon_d = 0$ and $\chi = -\sqrt{7}/2$ are the parameters that show up in the Hamiltonian (3.16). If we include $\epsilon_d \neq 0$ such that $|\kappa| >> |\epsilon_d|$, the wave function (3.27) will still be a good approximation to the exact solution. In order to explore up to which values of ϵ_d one can use perturbation theory, we calculate the overlap between the state (3.27) and the exact solution for a system with $N = 8$ bosons. The result we obtain is that, even for a ratio $|\epsilon_d|/|\kappa| = 10$,the overlap is larger than 0.9 (in particular equal to 0.942). So we can use the present approximation in regions quite far from the SU(3) symmetry limit.

  By calculating the expectation value of (3.16), using the state (3.27), the binding energy becomes,

$$\begin{aligned} BE &= -\langle 0^+_{gs-SU(3)}|\epsilon_d \hat{n}_d - \kappa \hat{Q}^{\chi=-\sqrt{7}/2} \cdot \hat{Q}^{\chi=-\sqrt{7}/2}|0^+_{gs-SU(3)}\rangle \\ &= -\epsilon_d \langle 0^+_{gs-SU(3)}|\hat{n}_d|0^+_{gs-SU(3)}\rangle \\ &\quad +\kappa \langle 0^+_{gs-SU(3)}|\hat{Q}^{\chi=-\sqrt{7}/2} \cdot \hat{Q}^{\chi=-\sqrt{7}/2}|0^+_{gs-SU(3)}\rangle. \end{aligned} \tag{3.42}$$

  The expectation value of $\hat{n}_d$ in the SU(3) limit is known [**?**], with as a result,

$$\langle 0^+_{gs-SU(3)}|\hat{n}_d|0^+_{gs-SU(3)}\rangle = \frac{4N(N-1)}{3(2N-1)}. \tag{3.43}$$

  On the other hand $\hat{Q}^{\chi=-\sqrt{7}/2} \cdot \hat{Q}^{\chi=-\sqrt{7}/2}$ is directly related with the SU(3) Casimir operator appearing in eq. (3.26),

$$\hat{Q}^{\chi=-\sqrt{7}/2} \cdot \hat{Q}^{\chi=-\sqrt{7}/2} = \frac{1}{2}\hat{C}_2[SU(3)] - \frac{3}{8}\hat{L} \cdot \hat{L}. \tag{3.44}$$

Finally, one obtains the result,

$$BE = -\epsilon_d \frac{4N(N-1)}{3(2N-1)} + \kappa(2N^2+3N). \tag{3.45}$$

The final expression for S_{2n} in the case of particles becomes,

$$S_{2n} = -\epsilon_d \frac{8(N-1)^2}{3(4N^2-8N+3)} + \kappa(4N+1), \tag{3.46}$$

while in the case of holes it reads,

$$S_{2n} = \epsilon_d \frac{8N^2}{3-12N^2} - \kappa(4N+5). \tag{3.47}$$

The first term in both eqs. (3.46) and (3.47), formally introduces a quadratic N dependence. However, studying the expression for S_2 in more detail, one observes that the final result is almost N independent. In the case of $N \to \infty$, the asymptotic value is 0.667. Already for $N = 8$ one obtains the value 0.670 in the case of particles and 0.669 in the case of holes. As a conclusion, the situation close to the SU(3) limit also gives rise to a linear behavior in S_{2n}.

- Near the O(6) limit.

  The γ-unstable nuclei are well described using the O(6) limit. In this case one should make the choice $\epsilon_d = 0$ and $\chi = 0$ in the Hamiltonian (3.16). If we include $\epsilon_d \neq 0$ such that $|\kappa| >> |\epsilon_d|$, the wave function (3.33) becomes a good approximation to the exact solution. In order to find out how far can one proceed in the choice of the value of ϵ_d, we calculate the overlap between the state (3.33) and the exact solution for a system with $N = 8$ bosons. The result is such that, even for a ratio $|\epsilon_d|/|\kappa| = 10$, the overlap is larger than 0.9 (in particular equal to 0.916).

  The calculation of the expectation value of (3.16), using the eigenstate (3.33), results in the expression,

$$\begin{aligned} BE &= -\langle 0^+_{gs-O(6)}|\epsilon_d \hat{n}_d - \kappa \hat{Q}^{\chi=0}\cdot\hat{Q}^{\chi=0}|0^+_{gs-O(6)}\rangle \\ &= -\epsilon_d \langle 0^+_{gs-O(6)}|\hat{n}_d|0^+_{gs-O(6)}\rangle \\ &\quad +\kappa\langle 0^+_{gs-O(6)}|\hat{Q}^{\chi=0}\cdot\hat{Q}^{\chi=0}|0^+_{gs-O(6)}\rangle. \end{aligned} \tag{3.48}$$

  The expectation value of $\hat{n}_d$ in the O(6) limit is known [**?**], with as a result,

$$\langle 0^+_{gs-O(6)}|\hat{n}_d|0^+_{gs-O(6)}\rangle = \frac{N(N-1)}{2(N+1)}. \tag{3.49}$$

On the other hand $\hat{Q}^{\chi=0} \cdot \hat{Q}^{\chi=0}$ is directly related with the $O(6)$ and $O(5)$ Casimir operators appearing in eq. (3.32),

$$\hat{Q}^{\chi=0} \cdot \hat{Q}^{\chi=0} = \hat{C}_2[O(6)] - \hat{C}_2[O(5)]. \tag{3.50}$$

Finally, the binding energy becomes,

$$BE = -\epsilon_d \frac{N(N-1)}{2(N+1)} + \kappa(N^2+4N). \tag{3.51}$$

The value of S_{2n} for particles results in the expression,

$$S_{2n} = -\epsilon_d \frac{N^2+N-2}{2(N^2+N)} + \kappa(2N+3), \tag{3.52}$$

and for holes it reads

$$S_{2n} = \epsilon_d \frac{N(N+3)}{2(N+1)(N+2)} - \kappa(2N+5). \tag{3.53}$$

Again, the first term introduces a formal quadratic N dependence. However, studying the expressions (3.52) and (3.53) in more detail, one observes that the N dependence almost cancels. In the case of $N \to \infty$ the asymptotic value is 0.5. Already for $N = 8$ one reaches the value 0.486 in the case of particles and 0.489 in the case of holes. As a conclusion, the situations close to the $O(6)$) limit also give rise to a linear behavior in S_{2n}.

Note that the transitional region $SU(3) - O(6)$ cannot be treated using the Hamiltonian (3.16); a treatment based on perturbation theory does not result into a closed expression for the binding energy.

The results obtained in this subsection exhibit the same characteristic as the ones obtained in section 3.4.2, in the sense that all situations that have been analysed always give rise to a linear contribution in S_{2n}. The only way of obtaining deviations from a linear behavior is through the presence of systematic changes of the parameters in the local Hamiltonian. This approach has been explored in detail in [22] and gives rise, indeed, to non-linearities in S_{2n} for the transitional $U(5) - SU(3)$ and $U(5) - O(6)$ regions.

Now that we have carried out the various schematic analyses of S_{2n} in the IBM, we present a more realistic description of binding energies and S_{2n} values in the next subsection.

3.4.4 Crossing the mid-shell

In the previous subsection we have derived closed expressions of S_{2n} for the case of particles and for the case of holes, independently. However, the counting of particles/holes produces some inconsistencies and problems: using the expressions

(3.21) and (3.22), the sign of $\mathcal{B}$ should be changed when crossing the mid-shell. On the other hand, when plotting the binding energies (or S_{2n}) in terms of N (particles or holes) we obtain a "function" that is double valued and can lead to some errors of interpretation. Moreover, we need two definitions of S_{2n}, one for particles and one for holes. A possible outcome of these inconsistencies is to introduce a new variable $\tilde{N}$ that represents the number of valence particle pairs and that is related with the number of bosons N (particles or holes) through the definition,

$$N = \begin{cases} \tilde{N} & \text{for } \tilde{N} \leq \frac{\Omega}{2} \\ \Omega - \tilde{N} & \text{for } \tilde{N} > \frac{\Omega}{2} \end{cases}, \tag{3.54}$$

where $\Omega = \sum(j + 1/2)$ represents the size of the shell, that is the total number of bosons that can be put into that shell. The value of the BE then becomes,

$$BE(\tilde{N}) = E_0 + \mathcal{A}\tilde{N} + \frac{\mathcal{B}}{2}\tilde{N}(\tilde{N} - 1) + BE^{lo}_{IBM}(N(\tilde{N})). \tag{3.55}$$

Using the variable $\tilde{N}$ we have a single definition of S_{2n} for both, particles and holes, that reads,

$$S_{2n}(\tilde{N}) = BE(\tilde{N}) - BE(\tilde{N} - 1), \tag{3.56}$$

or, equivalently,

$$S_{2n}(\tilde{N}) = (\mathcal{A} - \mathcal{B}/2) + \mathcal{B}\tilde{N} + BE^{lo}_{IBM}(\tilde{N}) - BE^{lo}_{IBM}(\tilde{N} - 1). \tag{3.57}$$

Note that the expressions (3.31), (3.37), (3.47), and (3.53) can be used directly taking into account the relation (3.54). The introduction of $\tilde{N}$ is just a formal trick, but it will simplify all further analysis.

Sometimes it might be useful to represent BE or S_{2n} as a function of the atomic number A. In those cases it is trivial to rewrite the equations (3.55-3.56) using A.

Although with the introduction of $\tilde{N}$ we eliminate one ambiguity of the IBM, there still appears a second problem that is intrinsic to the model. In order to illustrate it, we consider a shell-model calculation. It is well known that, making the appropriate changes in the shell-model Hamiltonian, *it does not matter* if one is using particles or holes. Of course, changing from particles to holes when crossing the mid-shell reduces considerably the size of the model space. This freedom is intrinsic to the shell-model because the Pauli principle avoids the over-counting of states within any shell. In the case of the IBM, the situation is completely different. Working in a boson space, one can put an unlimited number of bosons in a shell that has only room for $N_{max} = \Omega$ "bosons". This means that in the boson model space, the Pauli principle, or equivalently the size of the "boson shell", is introduced by hand and, as a consequence, it is *obligatory* to change from particles

to holes when crossing the mid-shell. The relevant point here is that this change induces a discontinuity in the value of S_{2n} when crossing mid-shell. This jump cannot represent a physical effect and is not observed experimentally either. In order to clarify this point, we compare calculations using a pairing Hamiltonian in a single-j shell in the fermion space, with the SU(3) Hamiltonian (3.26)[5, 100]. In the case of pairing, the binding energy and S_{2n} result as

$$BE = G\tilde{N}(\Omega - \tilde{N} + 1), \tag{3.58}$$

and

$$S_{2n} = G(\Omega - 2\tilde{N} + 2), \tag{3.59}$$

respectively, where G denotes the interaction strength and Ω describes the size of the shell. In Fig. 3.4, we plot the expressions (3.58) and (3.59) for $G = 1$ (in arbitrary units) and $\Omega = 10$. One notices a smooth behavior even when crossing the mid-shell. In the case of the SU(3) Hamiltonian one has to use the equations (3.29), (3.30), and (3.31). In Fig. 3.5 we plot these expressions for $\delta = -1$ (in arbitrary units) and $\Omega = 10$. When comparing Fig. 3.5 with Fig. 3.4, one observes clear differences with the pairing Hamiltonian, in particular in the case of S_{2n} (It should be noted that both cases correspond to quite different physical situations. They are only used here in order to see the different behavior when crossing the mid-shell). There is a clear-cut unphysical behavior when crossing the mid-shell. A solution to cope with this inconsistency is obtained when we add the global part of S_{2n} to the local S_{2n} term. Thus, we keep an almost continuous variation in S_{2n} by changing the value of $\mathcal{A}$ and $\mathcal{B}$ when crossing the mid-shell. In the particular case of the SU(3) limit we have just to change the value of $\mathcal{A}$ when crossing the mid-shell in $8\Omega + 12$, for $\delta = -1$ (in arbitrary units). In section 3.4.6 we shall see that, even in realistic calculations, the solution to eliminate the spurious discontinuity in S_{2n} is to change the parameters of the global part (BE^{gl}). It should be noted that in the case of odd Ω, the equations (3.29) and (3.35) become invalid for $N = \Omega/2 + 1/2$. For this value of N, the correct value is zero, while the expressions (3.29) and (3.35) give a value different from zero.

3.4.5 Deriving the global part: calculation of $\mathcal{A}$ and $\mathcal{B}$

Up to now we have carried out a schematic analysis of the S_{2n} observable, coming from the "local Hamiltonian" in the framework of the IBM. We were able though to derive important conclusions. In this subsection we present a new approach for studying S_{2n} values, spectra and transitions rates in a consistent way. In the next section, we apply the method to nuclei belonging to the shell $Z = 50 - 82$. The method that will be used here was first discussed in [22].

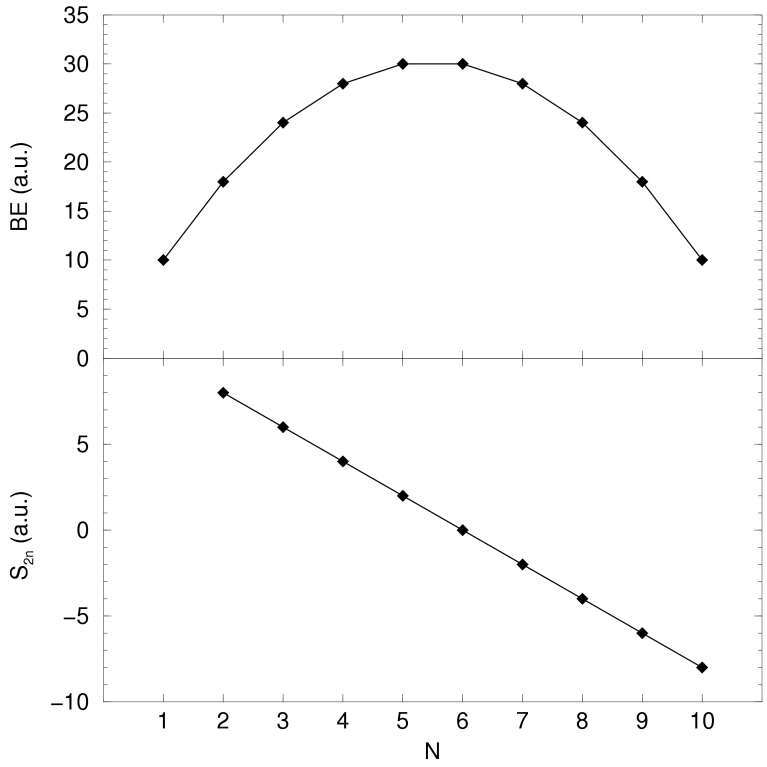

Figure 3.4 BE (top) and S_{2n} (bottom) for a pairing interaction in a single-j shell with $\Omega = 10$ and $G = 1$ (in arbitrary units).

The key point of the method is the assumption that a linear global part (S_{2n}^{gl}), already presented in section 3.4.1 needs to be added to the local contribution. Of course, the coefficients in this global contribution, $\mathcal{A}$ and $\mathcal{B}$, are taken as constant along the chain of isotopes under study, except if crossing mid-shell or moving between major shells (see previous subsection).

In the previous subsections, the local Hamiltonian was taken to correspond to a symmetry limit or to a situation close to this. In the following discussion we consider more realistic Hamiltonians. In principle, one has many possibilities for choosing a realistic Hamiltonian. The parameters of such a Hamiltonian should give rise to a reasonable description of low-lying states of even-even nuclei (energies and transition probabilities). However, in Ref. [22] it was shown that a correct description of spectroscopic properties does not always lead to a corresponding correct description of the nuclear ground state properties, such as S_{2n}. A particular class of Hamiltonian that seems to provide good results for the excited states as well as for the ground state, is described in Ref. [129]. The Hamiltonian used corresponds to (3.16) with $\kappa' = 0$. The main characteristic is that the value of κ is fixed

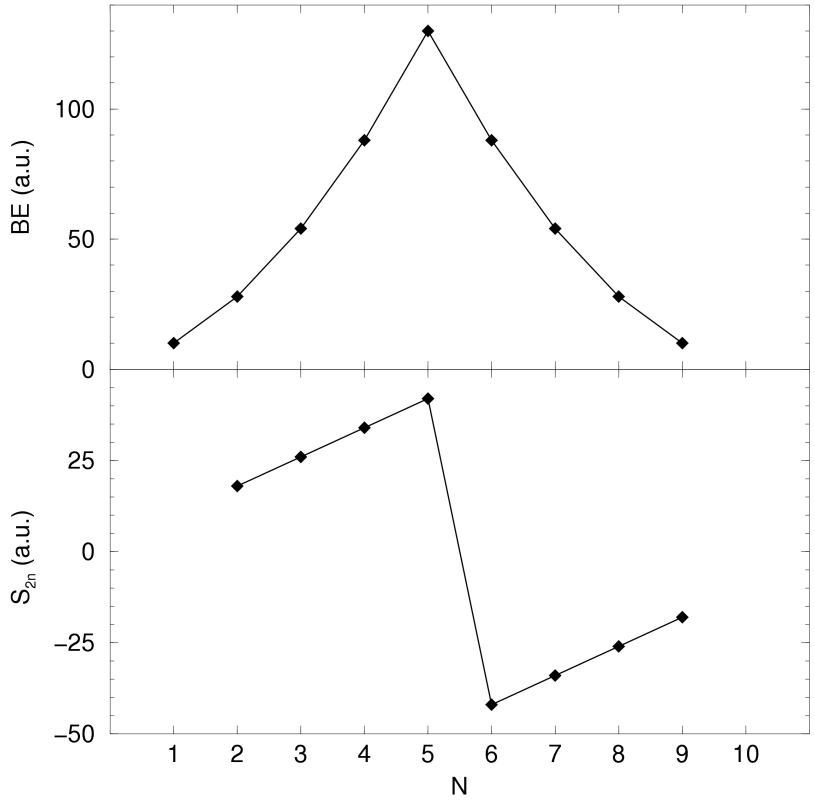

Figure 3.5 BE (top) and S_{2n} (bottom) for a SU(3) IBM Hamiltonian, for $\Omega = 10$ and $\delta = -1$ (in arbitrary units).

for all even-even medium-mass and heavy nuclei to $\kappa = 0.030$ MeV. The values of ϵ_d and χ are adjusted to obtain the best possible description of energy spectra and electromagnetic transition rates (the values of the parameters are given in Ref. [129]). In this framework the main observables that we intend to reproduce are $E(2_1^+)$, $E(4_1^+)/E(2_1^+)$, $E(2_\gamma^+)$, $E(0_2^+)/(E(2_\gamma^+)-E(2_1^+))$, $B(E2;2_\gamma^+ \to 0_1^+)/B(E2;2_\gamma^+ \to 2_1^+)$, and $B(E2;2_\gamma^+ \to 0_1^+)/B(E2;2_1^+ \to 0_1^+)$ (where the label γ refers to the γ band, quasi-γ band or even two-phonon-like band). In the present chapter we take as a guide the values of χ and ϵ_d given in figures 10 and 11 of [129], but the value of ϵ_d will be fine-tuned in order to obtain the best possible description for the energy spectra, but in all cases the differences with respect to the values given in Ref. [129] are smaller than a 10%. It should be noted that the parametrisation of the local Hamiltonian is fixed without considering the S_{2n} values.

Once we have fixed the local IBM Hamiltonian (from Ref. [129]), it is a trivial

task to deduce the linear part of S_{2n} (S_{2n}^{gl}), *i.e.*

$$S_{2n}^{gl} \equiv \mathcal{A} + \mathcal{B}\tilde{N} = S_{2n}^{exp} - S_{2n}^{lo}. \tag{3.60}$$

(Note that for simplification we have made the substitution of $\mathcal{A} - \mathcal{B}/2$ by $\mathcal{A}$). In practice the right hand side of eq. (3.60) is not an exact relation but gives approximately a straight line. As a consequence the linear part is derived from a best fit to the data points, obtained when plotting the right hand side in (3.60).

It should be stressed that the values of $\mathcal{A}$ and $\mathcal{B}$ thus obtained depend on the specific choice of the IBM local Hamiltonian and as a consequence, for the best description of S_{2n}, one cannot mix local and global parts corresponding to different Hamiltonians. That comes from the fact that different local Hamiltonians can give an equally reasonable description of nuclear spectra, but their contribution to the BE value will be probably different, therefore, in order to describe S_{2n} correctly the global contribution ($\mathcal{A}$ and $\mathcal{B}$) will be different. As a consequence the values of $\mathcal{A}$ and $\mathcal{B}$ depend on the local Hamiltonian.

Although we already have a detailed prescription for extracting the values of $\mathcal{A}$ and $\mathcal{B}$, we have to point out how to "operate" when changing between major shells or when crossing the mid-shell point. In principle the values of $\mathcal{A}$ and $\mathcal{B}$ will change when passing between different shells or crossing the mid-shell. That means that we have to consider different separate regions in our analysis.

- Moving between major shells: In this case the values of $\mathcal{A}$ and $\mathcal{B}$ change, especially the value of $\mathcal{A}$ (the intercept). In our calculations the nucleus corresponding to the closed shell is excluded because the prescription that provides the Hamiltonian (3.16) is not applicable and intruder states become important in the description. Therefore, S_{2n} values corresponding to a closed shell and to a closed shell plus two nucleons (of particles) will be excluded from the fit.

- Crossing the mid-shell: As was explained previously, the IBM contains a clear deficiency when crossing mid-shell because the Pauli principle is only included in an approximate way. One of the main manifestation of this fact appears when crossing mid-shell. We already pointed out that a simple way to solve this artefact is to change the global (linear) part of S_{2n} for the second part of the shell. In all practical cases we notice that no data points should be excluded from the calculations as in the previous case. The mid-shell point should be included in the calculation of S_{2n}^{lo} before and after the mid-shell.

3.4.6 Realistic calculations in the shell $50 - 82$

In the present section, we study the value of S_{2n} for the following chains of isotopes: ${}^{114-144}_{54}Xe$, ${}^{120-148}_{56}Ba$, ${}^{124-152}_{58}Ce$, ${}^{128-154}_{60}Nd$, ${}^{132-160}_{62}Sm$, ${}^{138-162}_{64}Gd$, ${}^{148-166}_{66}Dy$, ${}^{150-168}_{68}Er$, ${}^{152-178}_{70}Yb$, ${}^{158-184}_{72}Hf$, ${}^{166-188}_{74}W$, ${}^{170-196}_{76}Os$, and ${}^{176-200}_{78}Pt$, which are precisely the isotopes analysed in Ref. [129]. The superscripts refer to the range of A that we analyse in each series of isotopes.

The main aim of this section is not only to obtain a good description of the experimental S_{2n} [134, 135, 136], but also to show that the hypothesis of constancy for $\mathcal{A}$ and $\mathcal{B}$, *i.e.* the global part of the Hamiltonian gives a linear contribution, is fulfilled along a wide region of nuclei. Somehow both ends are related.

Following the prescription given in subsection 3.4.5, we choose a realistic Hamiltonian for each series of isotopes and we subtract the local contribution of S_{2n}, S^{lo}_{2n}, from the experimental values, S^{exp}_{2n}. With these data we calculate the straight lines that give the best fits. We need to distinguish four regions: (a) $50 < N \leq 66$, (b) $66 < N < 82$, (c) $84 < N \leq 104$, and (d) $104 < N < 126$ (where N represents the total number of neutrons). As can be observed, the points corresponding to the closed shell and to the closed shell plus two neutrons are excluded, while the mid-shell point is taken into account in the calculations. To illustrate the procedure in more detail, we carefully explain the case of the Xe nuclei. In Fig. 3.6 we show the differences $S^{exp}_{2n} - S^{lo}_{2n}$ together with the regression line. One observes three different regions: before mid-shell in the shell $50 - 82$, after mid-shell for the same shell and before mid-shell in the shell $82 - 126$. One notices the correctness of the present description using a straight line for each region, separately. The parameters of the Hamiltonian are given in table 3.1; they correspond to the ones given in [129]. The coefficients of the straight line in each region, from the left to the right are, $\mathcal{A} = 75.5 \pm 9.9$ and $\mathcal{B} = -0.464 \pm 0.084$; $\mathcal{A} = 67.4 \pm 2.1$ and $\mathcal{B} = -0.392 \pm 0.016$; and $\mathcal{A} = 39.90 \pm 0.04$ and $\mathcal{B} = -0.2225 \pm 0.0003$, respectively (all the coefficients are given in MeV). Note that the intercepts and slopes correspond to a representation where we use the atomic number A instead of the number of bosons N or $\tilde{N}$. This criterion will be used along this whole subsection. The error bar derives from the standard deviation in obtaining the best fit and represents a measure of the goodness of the *ansatz*.

We have carried out similar analyses for all the chains of isotopes indicated in the beginning of this subsection, obtaining analogous results. The parameters of the Hamiltonian that has been used are given in reference [129]. In Fig. 3.7 we plot the values of $\mathcal{A}$ and $\mathcal{B}$ for all the isotopes we studied. The panels (a)-(a'), (b)-(b'), (c)-(c'), and (d)-(d') correspond to the four regions defined previously. The error bars correspond to the standard deviation in deriving $\mathcal{A}$ and $\mathcal{B}$. We also present results from calculations using two different values of κ. This is done in order to show the sensitivity of $\mathcal{A}$ and $\mathcal{B}$ with respect to small variations in the value of κ. In both sets of calculations, the values of χ and ϵ_d are identical (strictly speaking,

due to the fine-tuning, ϵ_d is slightly different in both calculations). We can safely conclude that the values of $\mathcal{A}$ and $\mathcal{B}$ are not very sensitive to the choice of κ, and the standard deviations are small enough to justify our *ansatz* that $\mathcal{A}$ and $\mathcal{B}$ are constant within the different mass regions. Note that the values of $\mathcal{A}$ and $\mathcal{B}$ change with Z but remain constant for the whole chain of isotopes (fixed Z), except when crossing the mid-shell or changing of major shell.

In figures 3.8, 3.9, 3.10, and 3.11 we compared the experimental S_{2n} values, S_{2n}^{exp}, with the values predicted by the IBM, combining the linear and the local part. In general, one obtains a rather good description, even in the regions where the nuclear structure character is changing quite rapidly and important deviations from the overall linear behavior appear. We stress that we do reproduce S_{2n} values and, at the same time, the properties of the low-lying states in these nuclei. The IBM results correspond (figures 3.8-3.11) to $\kappa = 0.030$ MeV.

This analysis presented here, together with the results obtained in Ref. [22], points towards an intimate relation between the correct reproduction of the nuclear excited states and nuclear ground-state properties. A simultaneous description guarantees that the Hamiltonian that is used, is appropriate for the nuclei studied over a large mass region.

A	N_ν	ϵ_d	A	N_ν	ϵ_d
114	7	67	130	5	62
116	8	67	132	4	70
118	9	66	134	3	80
120	10	70	138	3	61
122	9	65	140	4	45
124	8	62	142	5	42
126	7	60	144	6	45
128	6	60			

Table 3.1 Parameters for an IBM Hamiltonian for Xe isotopes. With ϵ_d in keV, $\kappa = 30$ keV and $\kappa' = 0$.

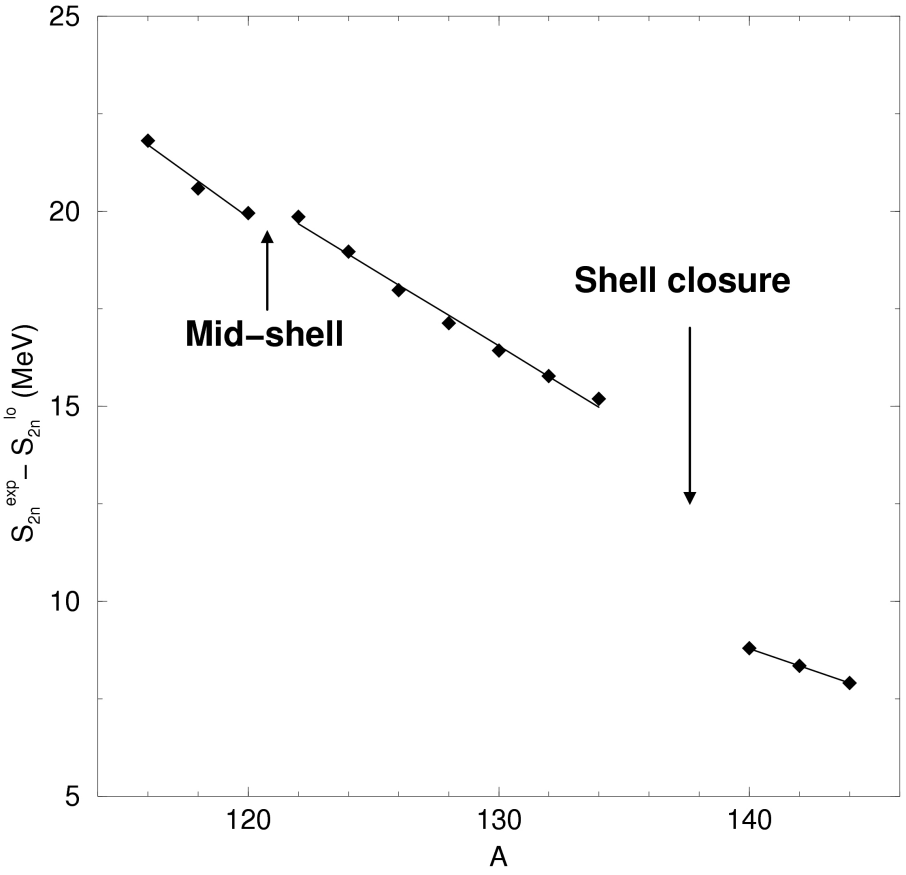

Figure 3.6 Differences $S_{2n}^{exp} - S_{2m}^{lo}$ (full diamonds) together with the regression line for Xe isotopes.

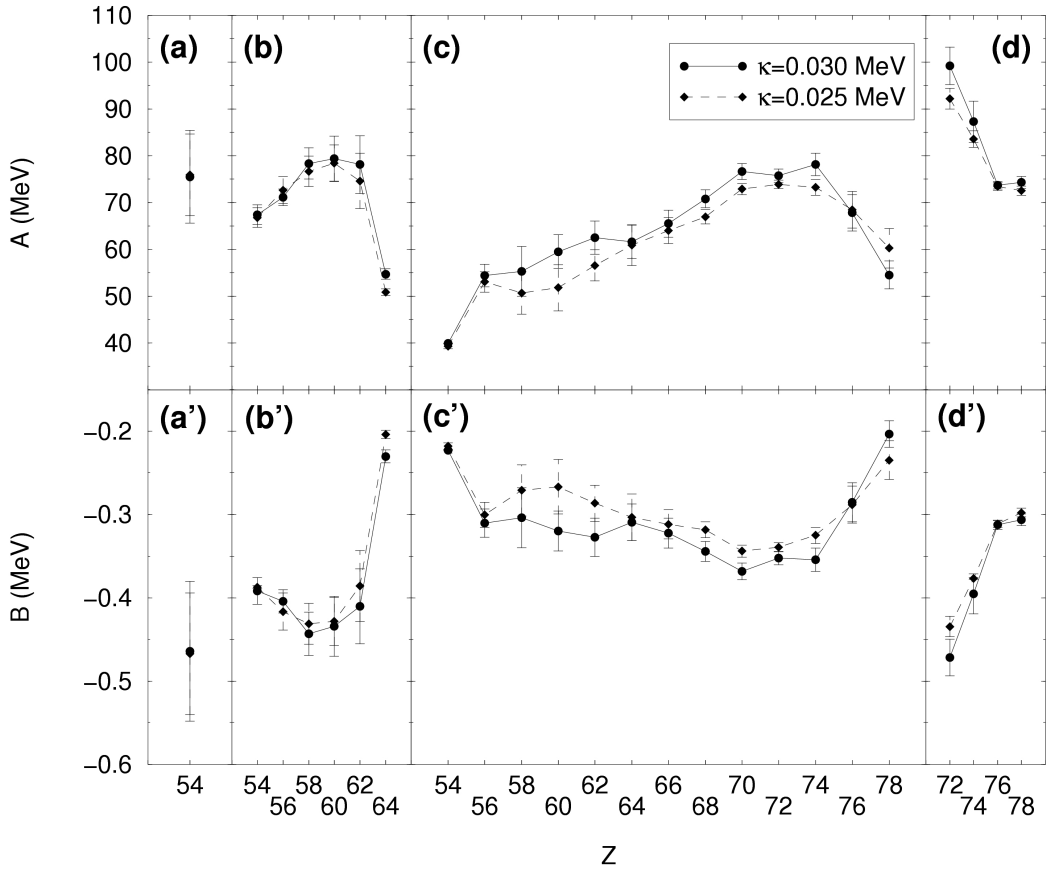

Figure 3.7 Values of $\mathcal{A}$ and $\mathcal{B}$ for different chains of isotopes (see text). Two alternatives calculation with different values of κ are plotted.

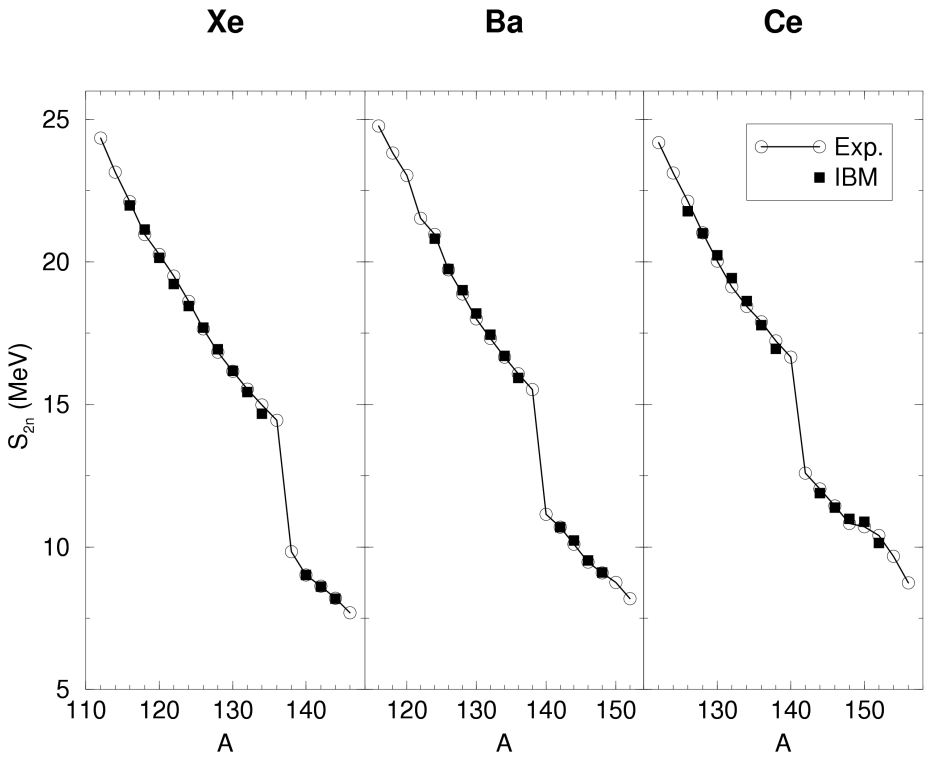

Figure 3.8 Comparison between the experimental S_{2n} and the IBM prediction for Xe, Ba, and Ce isotopes.

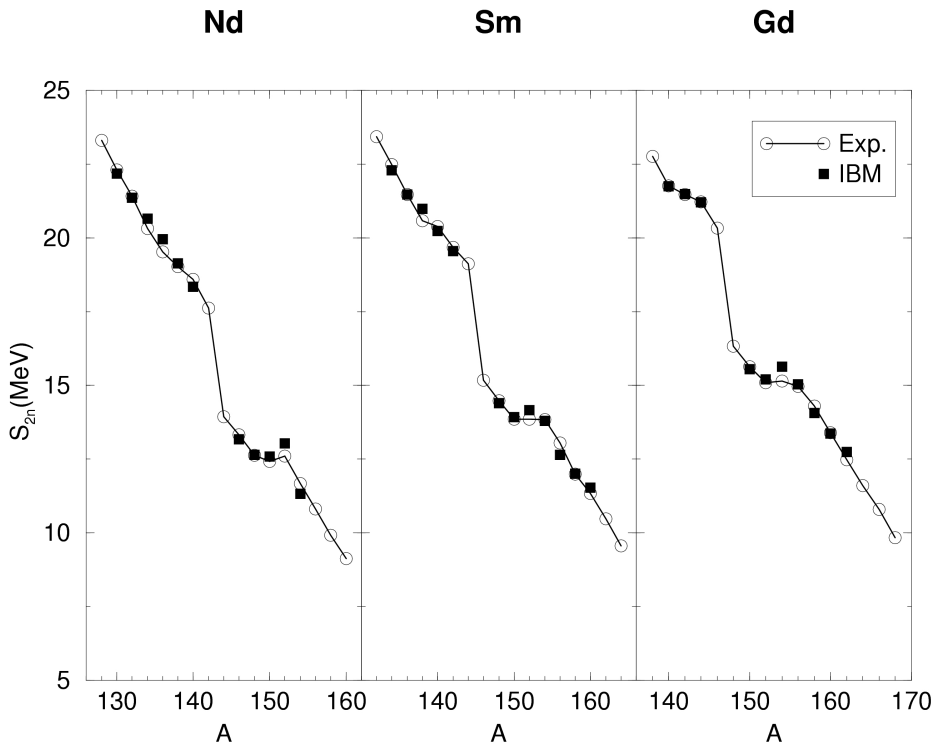

Figure 3.9 Comparison between the experimental S_{2n} and the IBM prediction for Nd, Sm, and Gd isotopes.

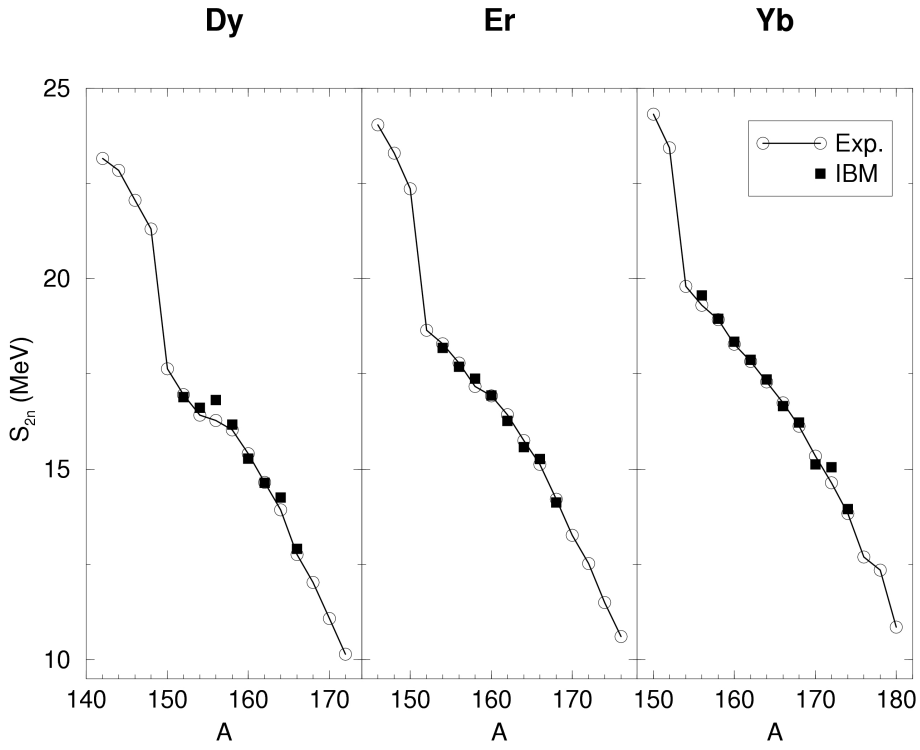

Figure 3.10 Comparison between the experimental S_{2n} and the IBM prediction for Dy, Er, and Yb isotopes.

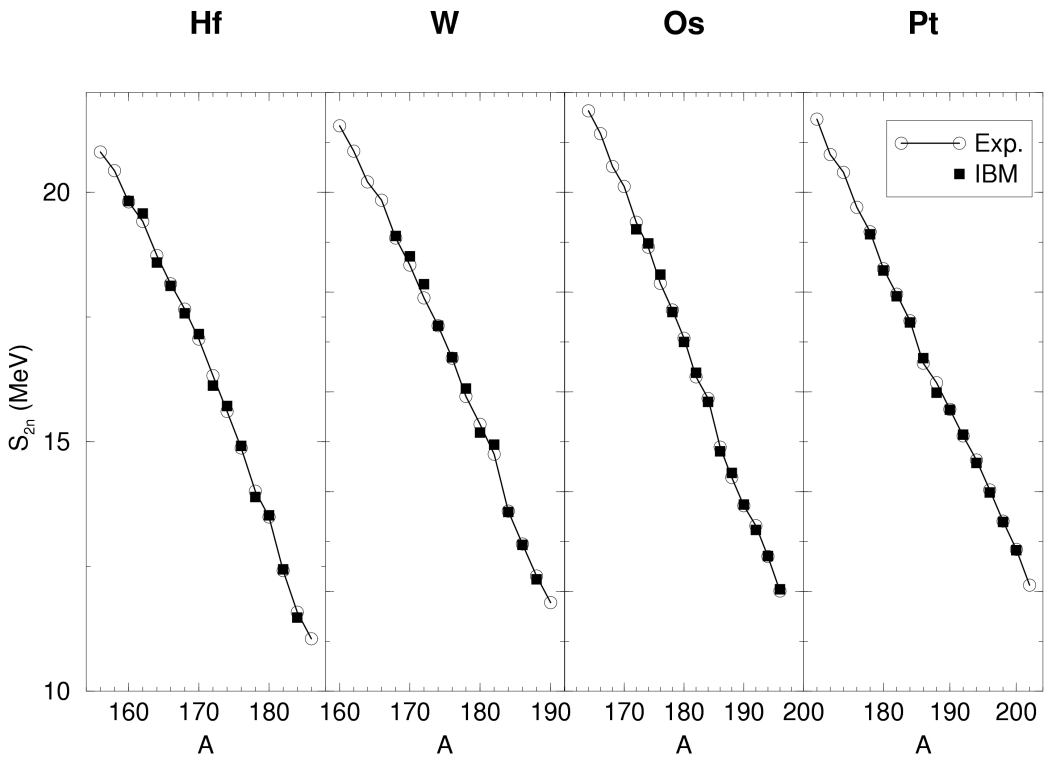

Figure 3.11 Comparison between the experimental S_{2n} and the IBM prediction for Hf, W, Os, and Pt isotopes.

3.5 The effect of intruder states: shape coexistence and shape mixing

In the former sections, we have studied within various approaches to nuclear structure: the liquid-drop approach (section 3.2), the nuclear shell-model (section 3.3) and the symmetry-truncated Interacting Boson Model (section 3.4). We have studied the behavior of an important quantity, *i.e.* S_{2n}, and we have tried to understand its variation over large regions of isotopes, in various mass regions. A consistent set of conclusions follows from the above analyses.

It turns out, however, that if one starts looking to nuclear masses with the highest possible precision [23, 24, 25, 26, 115, 137] one becomes sensitive to localised correlations within the nuclear many-body system. Such high-precision results in the lighter *sd*-shell region, at and very near to neutron number $N = 20$ for the Na, Mg nuclei, have brought evidence for a new zone of deformation, albeit very localised in (Z, N) values [17, 126]. Very recently, Bollen's group has succeeded in performing mass measurements with the Penning trap mass spectrometer ISOLTRAP at ISOLDE/CERN in the neutron deficient region of the Hg, Pt, Pb, Po, Rn, and Ra nuclei [24, 25, 26]. The results are discussed by Schwarz *et al.* [26] and are given in Fig. 3.12 and Figs. 3.13, 3.14, 3.15, and 3.16. Very particular effects in approaching the neutron mid-shell region near $N = 104$ show up.

A possible explanation might originate from the presence of shape coexisting configurations in this particular mass region, which has been discussed in much detail in [17, 138], and a mixing between the intruding configuration and the ground-state, causing local deviations from a smooth linear trend. This is particularly striking in the Hg and Pt nuclei.

Because model spaces within the shell-model quickly become prohibitively large if also particle-hole excitations across the $Z = 82$ closed proton shell are included, standard large-scale shell-model calculations cannot be carried out in a consistent way. Therefore, we discuss two approaches that might allow for such effects to be treated in a consistent approximation: we start from the IBM but now taking into account $2p - 2h$ excitations as the addition of two extra bosons (subsection 3.5.1). We also study the modification of the nuclear ground-state binding energy as derived from a macroscopic-microscopic study, in which potential energy surfaces (PES) are calculated taking into account competing shapes (spherical, prolate and oblate configurations) (subsection 3.5.2).

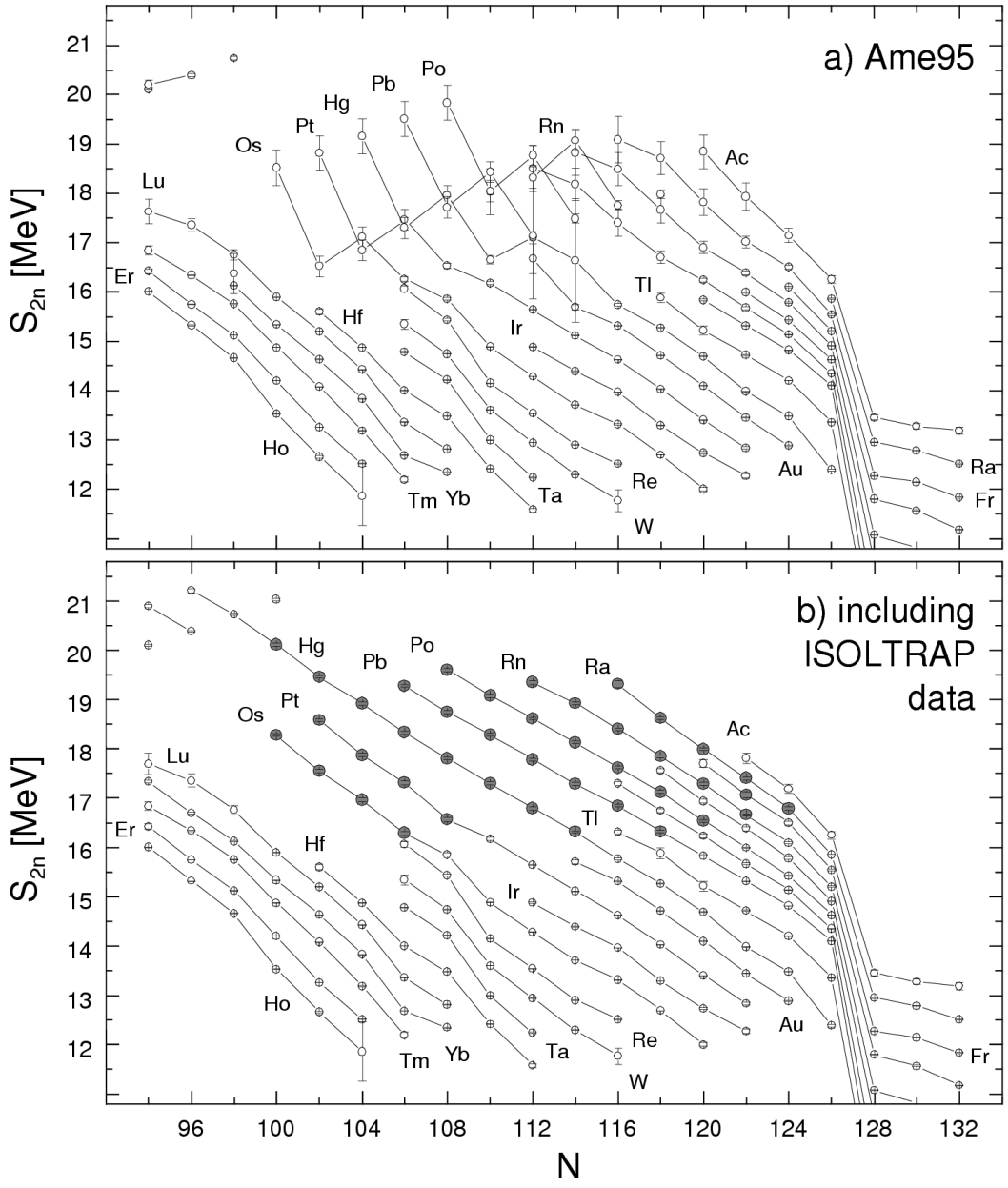

Figure 3.12 Experimental two-neutron separation energies, S_{2n}, in the region of $Z = 80$. a) Experimental values as determined from the analysis of Audi and Wapstra [134], including the update in 1995 [135], b) results obtained redoing the analyses of AME95, including the new ISOLTRAP data [15]. Full circles indicate S_{2n} values that are either obtained for the first time or whose errors were decreased by at least a factor two.

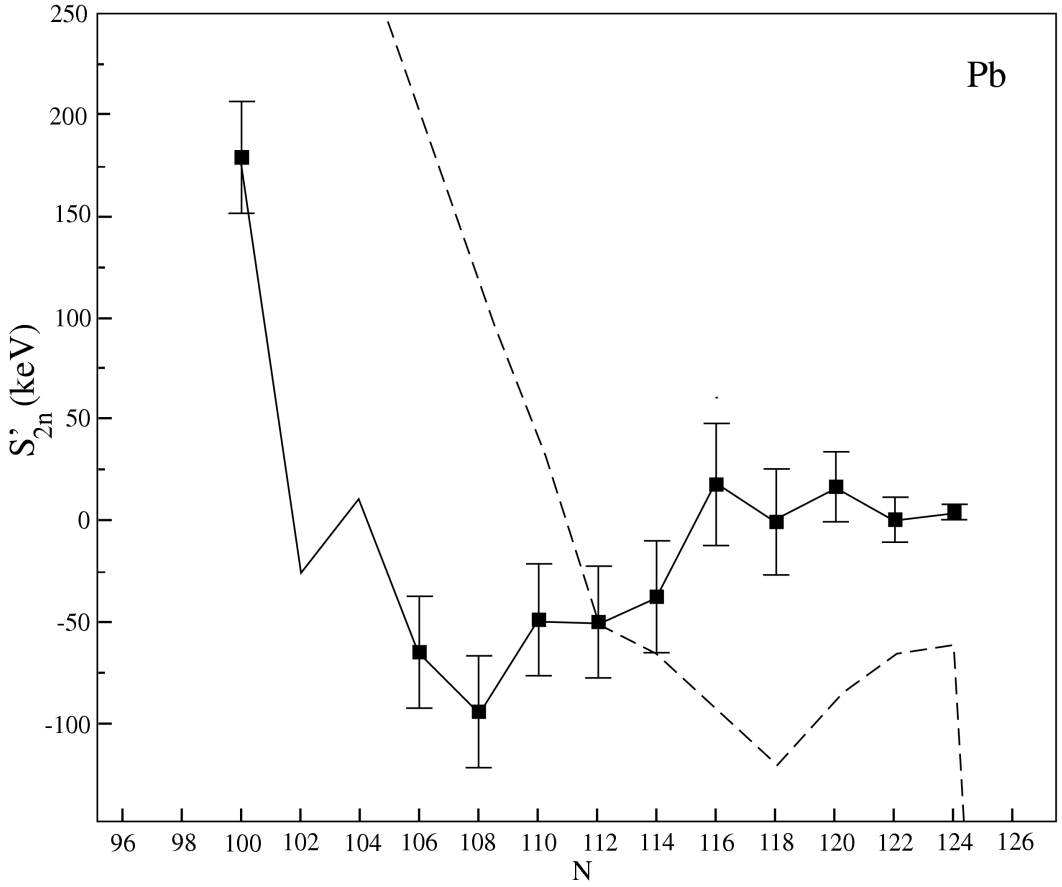

Figure 3.13 S'_{2n} for Pb. Comparison between experimental data (full line connecting dots) and PES results (dashed line).The two points (N=102,104) without data point are derived, containing at least one mass value obtained from mass systematics [45].

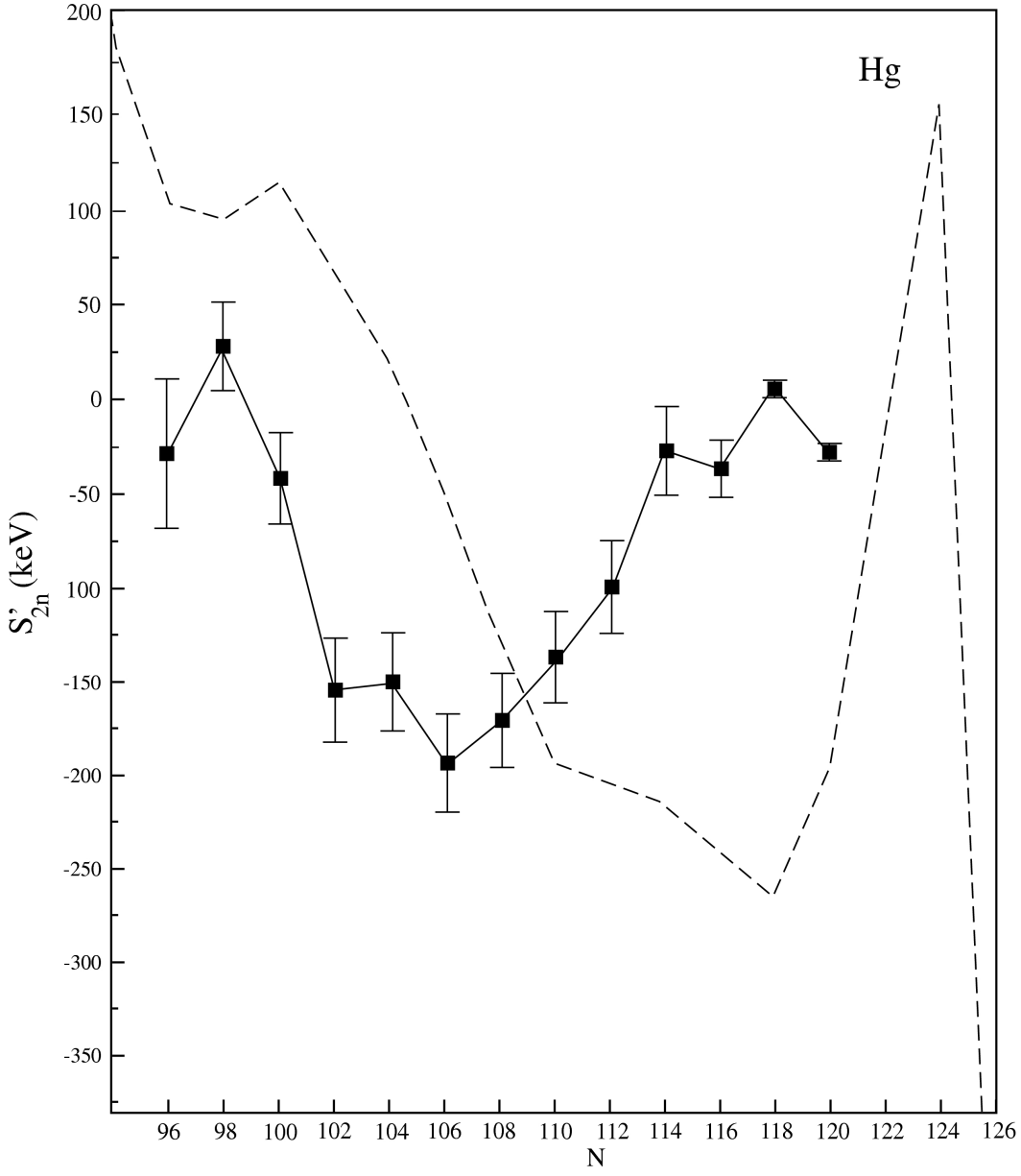

Figure 3.14 S'_{2n} for Hg. Comparison between experimental data (full line connecting dots) and PES results (dashed line).

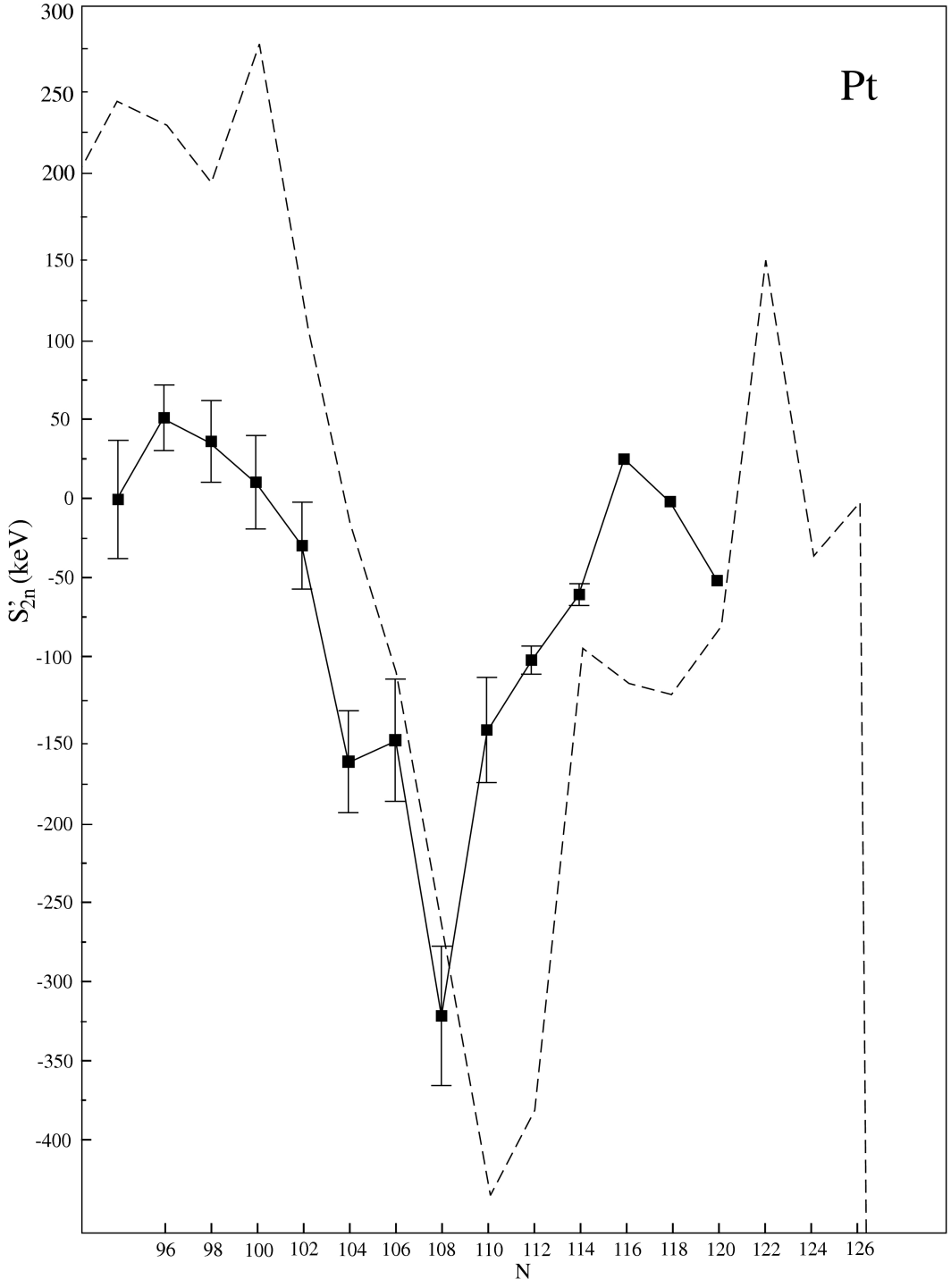

Figure 3.15 S'_{2n} for Pt. Comparison between experimental data (full line connecting dots) and PES results (dashed line).

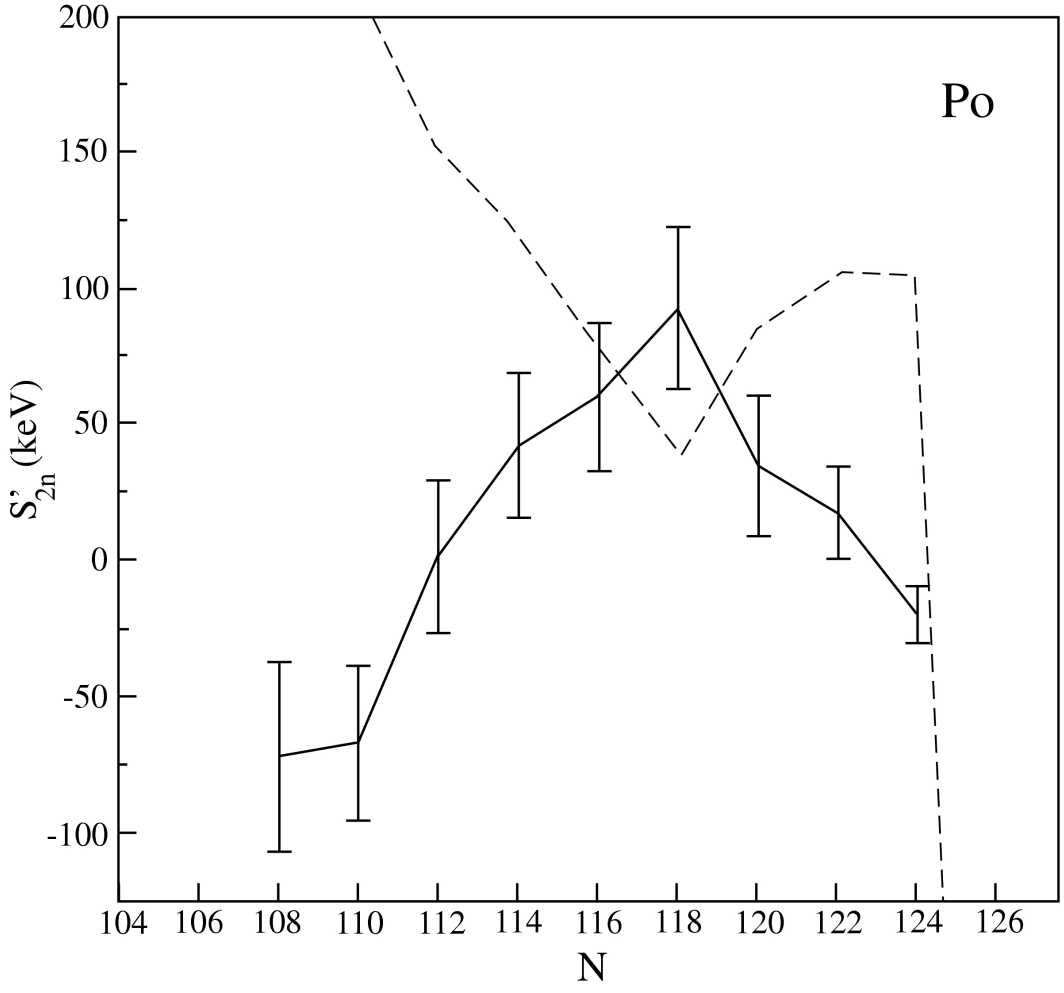

Figure 3.16 S'_{2n} for Po. Comparison between experimental data (full line connecting dots) and PES results (dashed line).

3.5.1 Local nuclear structure effects: intruder excitations near closed shells within the Interacting Boson Model

The effect of low-lying 0^+ intruder excitations, which seems to be related to $mp-nh$ excitations of nucleons across the adjacent closed shells, on energy spectra, electromagnetic properties, nuclear transfer data, etc., has been amply illustrated all through the nuclear mass table in the vicinity of closed shells [17, 138]. This holds in particular for heavy nuclei with the most explicit examples in (and near to) the $Z = 50$ (Sn) region near mid-shell at $N = 66$ and in the $Z = 82$ (Pb) region when approaching the mid-shell at $N = 104$. A full study has been carried out by J.Wood *et al.* [17] which concentrates on the full mass table.

The inclusion of low-lying intruder states in even-even nuclei has been modelled along the IBM by including an extra configuration with two more bosons $(N + 2)$, that may interact with the regular configurations containing N bosons [139, 140, 141, 142, 143, 144]; many calculations along these lines have been performed. Even though detailed calculations may well turn out to have a serious sensitivity to the choice of parameters describing the Hamiltonians corresponding to the two subspaces [145, 146, 147], the general outcome remains very stable and gives the possibility to obtain (i) low-lying 0^+ intruder states that exhibit a very specific mass dependence, approximately described by the expression [148]

$$\Delta E_Q \simeq 2\kappa \Delta N_\pi N_\nu, \tag{3.61}$$

which expresses the extra binding energy that results from the interaction of the extra proton pairs, ΔN_π, with the valence neutron pairs, N_ν, using a quadrupole-quadrupole proton-neutron interaction with κ as the force strength (see Fig. 3.17 left), or, (ii) to come to a "crossing" between the intruder configuration and the regular ground-state configuration (see Fig. 3.17 right). The latter effect causes a more deformed state to become the ground state and will subsequently show up in increased binding energy and, depending on the specific nature of the intruder configuration, possibly gives rise to the appearance of a very localised zone of deformation (island of inversion as called in the $N = 20$ mass region [17, 126, 149, 150, 151, 152]). In both cases, local effects can cause the ground-state to exhibit very specific deviations from the otherwise mainly linear variation of S_{2n}. The former situation (i) will mainly appear when we are sitting in a big shell like in the case in the Sn and Pb mass regions. The second situation (ii), is more likely to show up near sub-shell closure ($Z = 40$, $N = 58$, $Z = 64$, $N = 90$). This effect is depicted schematically in Fig. 3.17 [148].

In the present discussion, we shall mainly concentrate on the Pb region where an extensive data set has become available very recently ([17, 153] and references therein). We have carried out studies within the Interacting Boson Model approach (IBM configuration mixing) in which low-lying intruder configurations are allowed to mix with the regular ground-state configuration. Calculations have been carried

out for the Po isotopes with the aim of understanding the rapid lowering of an excited 0^+ state and the band on top of that [143, 144]. Using a $U(5) - SU(3)$ dynamical symmetry coupling (ds) (using two different sets of coupling matrices) and also a more general IBM-1 Hamiltonian for the intruder excitations (g) [154], we have studied the influence of mixing on the ground-state binding energy and thus on the S_{2n} values. One can see in Fig. 3.18 that the overall trend is rather well reproduced and that in the lightest Po nucleus, where data are obtained, albeit with a large error bar, a local drop of about 400 keV to 150 keV results, depending on how states are mixing (for more details see [144]).

In the Pb nuclei, no specific structure effects outside of a linear variation in S_{2n} show up except at the lowest neutron number observed at present. This is consistent with the excitation energy of the lowest 0^+ intruder state not dropping much below 0.8 MeV [153]. The measured very slow E0 decay rates in the Pb nuclei [155] are consistent with a very weak mixing into the ground state and thus without local binding energy increase.

Calculations in the Pt nuclei [142], using similar methods, in the region where the two different families of states come close and interact with typical mixing matrix elements for the 0^+ states of $100 - 200$ keV, result in a specific variation in the mass dependence of S_{2n} values consistent with the observed data. Independent studies that have attempted to extract the mixing matrix element between the ground-state and intruder-band members, all come close to this value of $100 - 200$ keV as mixing matrix element giving a consistent explanation [143, 144, 156].

Even though it is not possible to derive every single detail of the local S_{2n} variations, all studies and the various results on ground-to-intruder band state mixing point towards the interpretation that it is a localised interaction between the ground state and the specific low-lying intruder 0^+ states which is at the origin of the observed effects. Moreover, there is a clear correlation between the energy where the ground-state and intruder states have a closest approach and the maximal deviation in S_{2n} from a linear variation.

3.5.2 Macroscopic-microscopic calculations

Instead of describing binding energies from a shell-model approach (standard large-scale shell-model calculations or the IBM approximation in which the interactions amongst pairs form the central ingredients), one can use a different method. Here, we start from a model that combines the macroscopic part of the total energy, with a microscopic part. This latter part contains the nuclear shell and pairing correlations near to the Fermi level [100, 101, 131, 132, 157]. In shorthand notation, the total binding energy can be written as

$$BE = E_{LDM} + E_{shell} + E_{pair}. \tag{3.62}$$

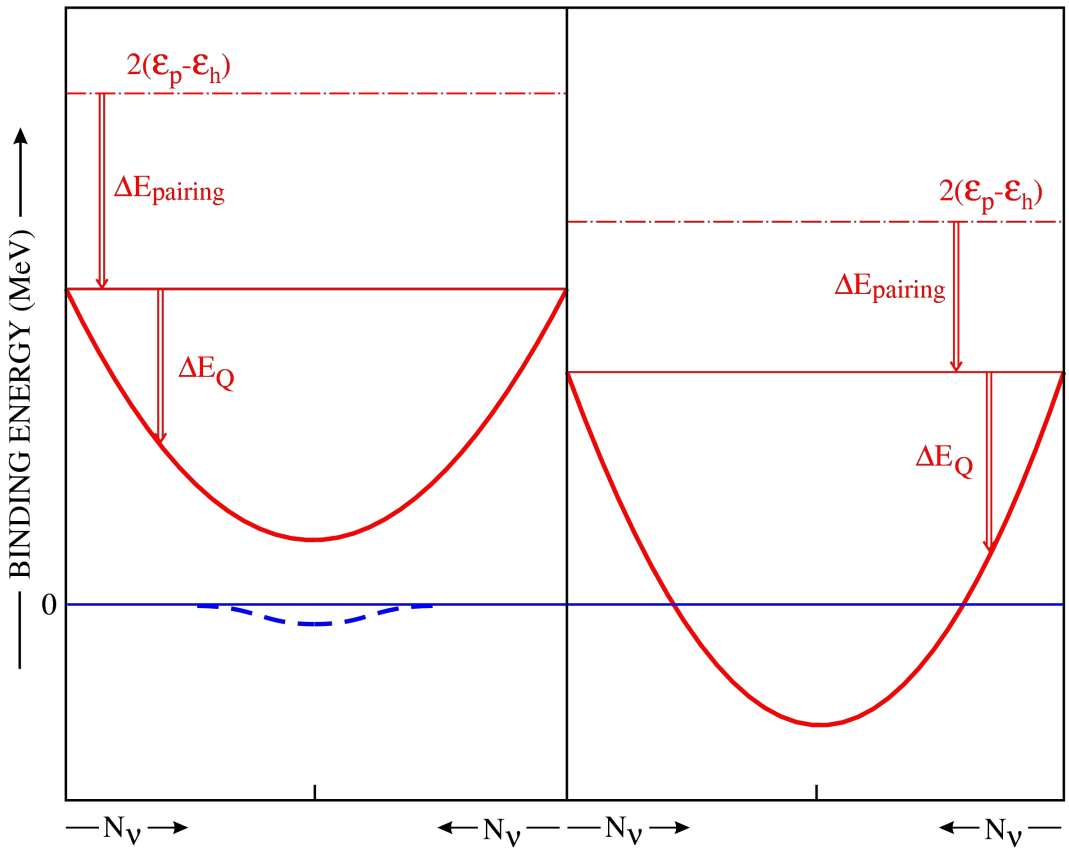

Figure 3.17 Schematic representation of the effect of configuration mixing on the binding energy, plotting the different contributions separately. On the left, it is assume that regular and intruder states seat far in energy. On the right, it is assume that the regular and intruder states cross.

The latter method is called the Strutinsky renormalization method and has been applied in many mass regions (see *e.g.* [106, 107, 108, 109, 110, 111]).

The macroscopic part of the total energy was assumed to be given by a Yukawa-plus-exponential mass formula of Möller and Nix [108, 109]. The shell correction was calculated using the axially-deformed single-particle Woods-Saxon potential [158, 159], with parameters as outlined if Refs. [159, 160, 161]. This average potential has been used previously to determine equilibrium shapes of coexisting configurations [17] in the Pt-Ra region [158, 162, 163, 164, 165]. The shell correction was then calculated according to prescription as given by Brack *et al.* [157],

$$E_{shell} = \sum_{\nu} e_{\nu} - \int_{-\infty}^{\tilde{\lambda}} e\tilde{g}(e)\, de, \tag{3.63}$$

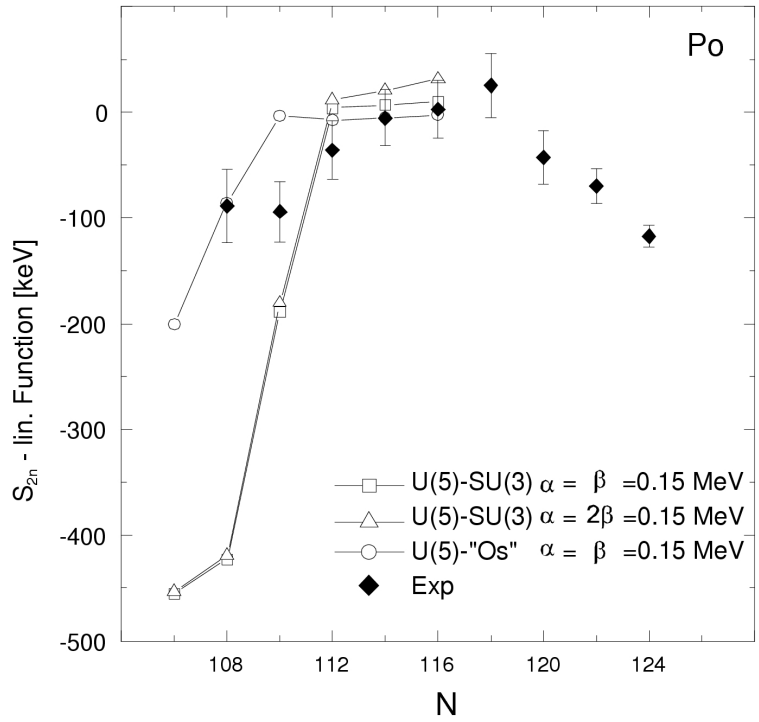

Figure 3.18 Comparison of experimental S'_{2n} values (S_{2n} minus a linear function) with the results of IBM configuration mixing calculations for Po isotopes. Three different kinds of coupling are considered: a $U(5) - SU(3)$ dynamical symmetry coupling (open squares and triangles) and a more general IBM-1 coupling (including g bosons) (open circles).

(with e_ν the single particle energies, $\tilde{g}(e)$ a smoothing function and $\tilde{\lambda}$ the upper integration limit fixed by the number of nucleons present). For the residual particle-particle interaction a standard seniority pairing force has been used. The pairing strengths (for protons and neutrons) used here were those of Ref. [166]. To avoid the well-known problems associated with the BCS treatment of pairing in the region of low level densities, approximate number projection was performed by means of the Lipkin-Nogami (LN) method [167, 168, 169]. The energies of the local minima in the potential energy surface (PES) were obtained by performing a minimisation with respect to the β_4 and β_6 deformations for each value of the quadrupole deformation β_2

Potential energy surface calculations (PES) for a series of isotopes in the Pb region (the Po, Pt, Pb and Hg isotopes) have been carried out before [143, 158, 162, 163, 164, 165] with the aim of studying shape coexistence in the Pb region. Properties of the Pt, Hg, Pb, and Po nuclei are also discussed in the mass tables of Möller *et al.* [107, 108, 109, 110, 111]. A similar study has been carried out recently by R. Wyss [170]. This has been inspired, in particular, by the high-resolution mass

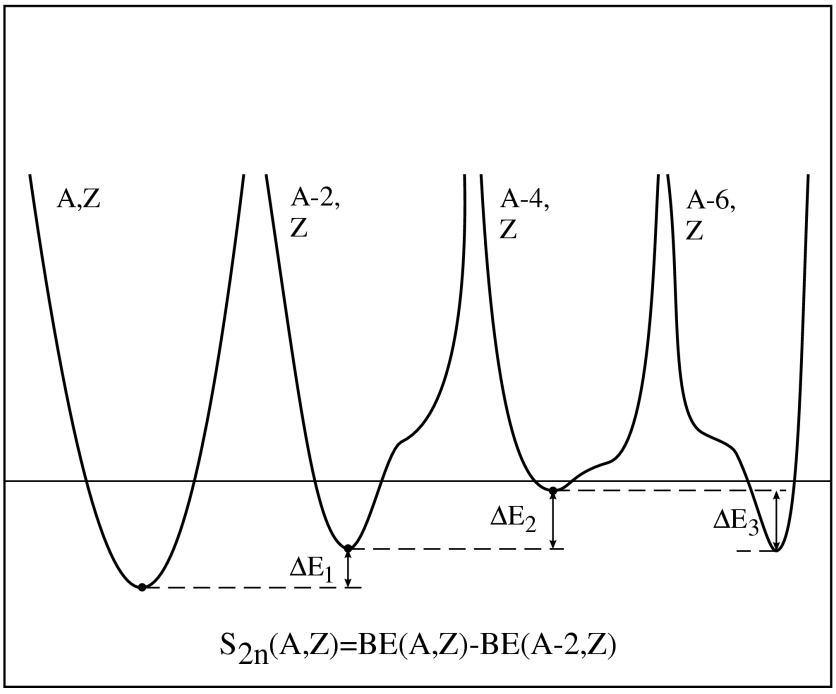

Figure 3.19 Schematic representation of the method for calculating S_{2n} in the study of PES using macroscopic-microscopic models.

measurements carried out by Schwarz *et al.* [26].

In the calculation of the PES, an absolute and several local minima can occur, corresponding to a regular state ($\varepsilon = 0$) and to deformed states ($\varepsilon \neq 0$). Since here, we are interested in two-neutron separation energies, both the binding energies, *i.e.* the absolute minimum, as well as the excitation energies of the local, deformed minima are important. In going from nucleus (A, Z) to the adjacent nucleus, $(A-2, Z)$, in order to derive the S_{2n} value, one has to take differences between the lowest total energy values for the nuclei that are considered (in absolute value). The method is illustrated in Fig 3.19.

We like to discuss in the next two paragraphs the precision with which S_{2n} can be calculated and this is important in the light of later applications to nuclei in the Pb region.

When searching for minima in the potential energy surface (PES), as a function of deformation, a rather dense mesh was used: $\Delta\beta_2 = 0.01$. The behavior obtained was smooth and differences between energy values for neighbouring deformation points were of the order of a few keV, at least close to the minimum. Therefore, the computational error of the minimum energy can be estimated as not exceeding 1 or 2 keV. Of course, the error introduced by approximations of the method itself

(e.g., by only approximate fulfilment of the plateau condition or by use of simple Lipkin-Nogami method for pairing correlations [167, 168]) is much larger, closer to 1 MeV. However, one can expect that taking only differences between energies and not their absolute values cancels these errors substantially.

Inaccuracies could also be introduced through the dependence of energy on Strutinsky's parameters γ ("smoothing range") and p (order of polynomial expansion used in smoothing procedure). As discussed in detail in, e.g., Ref. [171], even for not very exotic nuclei, the plateau condition with respect to these parameters is never fulfilled exactly. A change in γ by $\Delta\gamma \approx 0.2$ can induce a change in shell energy of the order of 1 MeV in a rather irregular way depending on the detailed structure of the single-particle spectrum. As a change in nucleon number by 2 gives rise to a change of shell energy of the order of up to a few MeV, the uncertainties caused by lack of ideal plateau condition can be quite substantial. Again, they are mainly smoothed out by taking differences between adjacent even-even nuclei only. Such irregularities are most likely to show up when deformation changes in passing from one nucleus to the heavier or lighter by 2 nucleons, because the single particle-spectrum is then different for the two nuclei. This latter effect might be partly responsible for the presence of some irregularities (the smaller spikes as seen, e.g., in Fig. 20 for the Pt nuclei).

In the next subsection, we compare these results with the experimental values. One has to stress from the beginning that PES calculations can, at best, give a qualitative description of binding energy differences (S_{2n} values). Dynamical effects obtained by solving a collective Schrödinger equation are not taken care of (no mixing effects between close-lying 0^+ are taken into account when making differences of PES values, purely), in the present discussion.

Going beyond the standard method of calculating PES, one needs to account for mixing of the non-degenerate mean-field solutions. This can be done using the generator coordinate method (GCM), originally developed be Hill, Wheeler and Griffin [172, 173]. Many-body states, obtained from HF+BCS or HFB calculations, are used to construct a more general ground state. At present, this can be done in a consistent way using the same effective interaction. No systematic studies have been performed as yet. Calculations starting from a solution in the collective variables, β and γ and Euler angles, Ω, have been carried out with applications to the $N = 20$ and $N = 28$ shell closure by the group from Bruyères-le-Châtel [174]. Likewise, calculations starting from mean-field wave functions projected on angular momentum and particle number using Skyrme interactions, have been carried out by the Orsay-Saclay-Brussels groups [175] . These calculations confirm specific extra binding energy contributions like the ones discussed in section 3.5.1. So, GCM calculations are becoming within reach for more extended studies in *e.g.* the Pb region because such an approach accounts for the dynamics of the nuclear many-body problem. The shell-model, or, symmetry truncated IBM studies are formulated in the laboratory frame, conserving particle number and angular momentum

from the beginning. In this sense, the two approaches, though starting from a different zero-order picture, essentially cover the same physics.

3.5.3 Applications to the Pb region

The Pb region has shown a number of most interesting features when moving into the neutron-deficient mass region. In the Pb nuclei, low-lying 0^+ excited states have been observed [153]. In the Po nuclei, at the lowest mass numbers reached at present, clear indications exist for a very low-lying 0^+ state that even might become the ground-state [143, 144]. In the Hg and Pt nuclei, clear-cut evidence has accumulated for the presence of shape coexistence [17]. In the Hg nuclei, the oblate shape is observed as being lowest in energy, even for the most neutron-deficient nuclei, whereas for the Pt nuclei, a change from oblate into prolate shapes sets in around mass $A = 188$ and the reverse path back from prolate into oblate around mass $A = 178$. Similar results have been derived before and discussed [162].

It is the aim of the present study to explore how well the mass dependence of the lowest energy minimum in a series of isotopes correlates with the variations in the binding energy (using the two-neutron separation energies S_{2n} as indicator) resulting from the recent high-resolution mass measurements.

On the scale of a S_{2n} plot (MeV energy scale) (see Fig. 3.12), no details can be seen of the "intruder" correlations (expected to be of the order of a few hundreds of keV). Therefore, we split up a S_{2n} curve in two parts: a linear part and a part that contains local correlations (deformation effects, specific mixing of configurations with the ground state, ...). In order to visualise deviations from a linear behavior of the S_{2n} values around neutron number, $100 \leq N \leq 110$ (the mid-shell region), where nuclear shape coexistence and shape mixing is known to occur, the linear curve was fitted to available experimental data outside of this range (see [24, 25, 26]). We shall concentrate on these differences $S'_{2n}(exp) \equiv S_{2n}(exp) - S_{2n}(lin-fit)$ (and similarly in defining $S'_{2n}(th)$ as the difference of the theoretical value with the linear fit). In all following figures (unless stated explicitly), we use these reduced quantities. In Fig. 3.20, we give an overview of the $S'_{2n}(th)$ values, obtained for the Pt, Hg, Pb and Po nuclei. We shall give a more extensive discussion of these results in comparing them with the data in the various subsections. Note the differences with IBM in obtaining $S_{2n}(lin-fit)$ (S^{gl}_{2n}).

The Pb $(Z = 82)$ isotopes

The $S'_{2n}(exp)$ values are given in Fig. 3.13. It is clear that down to the value at $N \simeq 110$, only a moderate lowering is observed (down to $\simeq 50$ keV). Beyond mid-shell neutron number ($N < 104$), a rather important increase in $S'_{2n}(exp)$ results. The relative variation in this quantity, moving out of the closed shell at $N = 126$

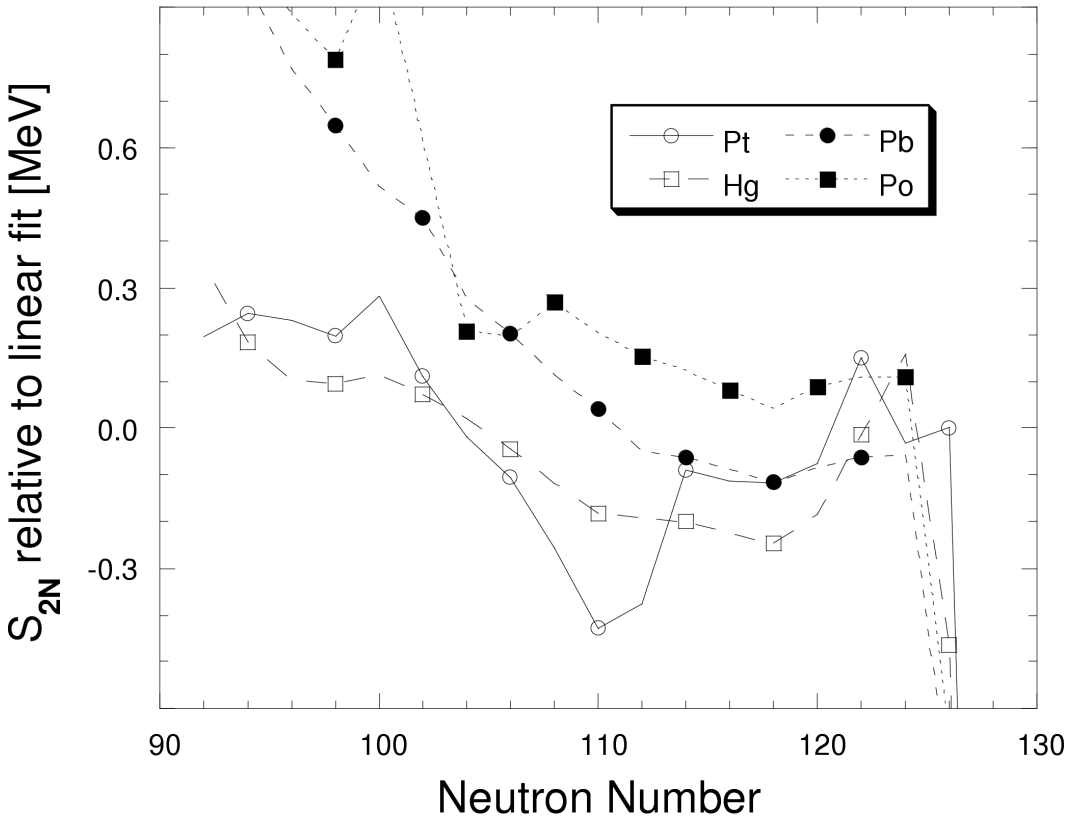

Figure 3.20 Theoretical S'_{2n} values, $S'_{2n}(th)$, for Pt, Hg, Pb and Po using macroscopic-microscopic PES calculations.

towards mid-shell and beyond, relative to the linear fit (which is approximating the local liquid-drop variation very well) is a reflection of the neutron shell-plus-pairing energy correction $\delta E = E_{shell} + E_{pair}$. These latter energy corrections causes the neutron closed shell at $N = 126$ to become more strongly bound (compared to a linear variation) and the mid-shell region to become less strongly bound (compared to the linear variation). The fact that for the Pb nuclei, one has, at the same time, a closed proton shell at $Z = 82$, makes these variations relatively small on an absolute scale and effects of deformation (occurrence of oblate and/or prolate shapes) cannot easily be observed on the present energy scale used. The theoretical values $S'_{2n}(th)$, as plotted on the same figure 3.13, are derived starting from a deformed Woods-Saxon in calculating the PES curves. The theoretical curve takes a large jump down approaching the neutron closed shell at $N = 126$ and then remains moderately flat down to $N = 114$. Then, a smooth but steady increase is observed in passing through the mid-shell region (reflection of the behavior of δE). The theoretical increase, though, advances the experimental increase by a couple

of mass units. It is clearly very interesting that masses for even lighter Pb isotopes could be determined to test this behavior.

The Hg $(Z = 80)$ **and Pt** $(Z = 78)$ **nuclei**

The experimental reduced S_{2n} plots, S'_{2n}, look rather similar (see figures 3.14 for Hg and 3.15 for Pt isotopes). Both show a systematic decrease in the separation energy for N decreasing towards mid-shell at $N = 104$. The plot for Hg shows a smooth valley with a minimum around -200 keV. Pt however, shows a sudden and steep minimum of -300 keV for $^{186}_{78}Pt_{108}$. Starting from mid-shell, the separation energies increase again for decreasing N.

One can check (see [17] for the specific energy spectra) that around mid-shell $N = 104$ two band structures are present. Apart from the first one, known from heavy nuclei, that correspond to an oblate but weakly deformed structure, there appears another band that can be interpreted as a rotational spectrum corresponding with a prolate shape of larger deformation. In the Hg nuclei, this second band only approaches the ground state to $\simeq 400$ keV, whereas in the Pt nuclei, the prolate structure becomes the ground-state band. As a conclusion, the even-even $^{178-186}Pt_{100-108}$ nuclei will have deformed ground states [26].

For the Hg nuclei, we show in Fig. 3.14 a comparison between the reduced PES calculations, resulting in the theoretical $S'_{2n}(th)$ values and the corresponding experimental $S'_{2n}(exp)$ values. We observe a rather good overall agreement, except for the fact that in the theoretical curve a more pronounced flat region is obtained for neutron numbers in the interval $110 \leq N \leq 120$, and the fact that below mid-shell, the theoretical values become slightly positive. The first region ($110 \leq N \leq 120$) can be understood by the fact that the oblate minimum for these Hg nuclei starts to develop, giving rise to a relative increase in the binding energy over a spherical liquid-drop behavior (the linear reference line at zero). The oblate minimum deepens down to $N = 112 - 114$ and then moves out again in the region $N = 98 - 100$, approaching the liquid-drop reference line (see Fig. 3.21).

For the Pt nuclei, the experimental and theoretical S'_{2n} values are plotted in Fig. 3.15. Concentrating on the theoretical curve, one can relate the general structure with the PES curves and their variation with decreasing neutron number. At first, around neutron number $N = 122-124$, the oblate minimum starts to develop, deepening in going from $N = 124$ down to $N = 118$. At the same time, a prolate minimum takes shape and the minima for the oblate and prolate shape are almost degenerate at $N = 110$. The prolate minimum takes over and this minimum starts becoming less deep at neutron number $N = 106$. At $N \simeq 96$, the prolate and oblate minima become degenerate again, but now as much less pronounced and deep minima (see Fig. 3.22). This changing structure reflects the variation of the theoretical S'_{2n} values, a structure that is also observed quite clearly in the experimental data.

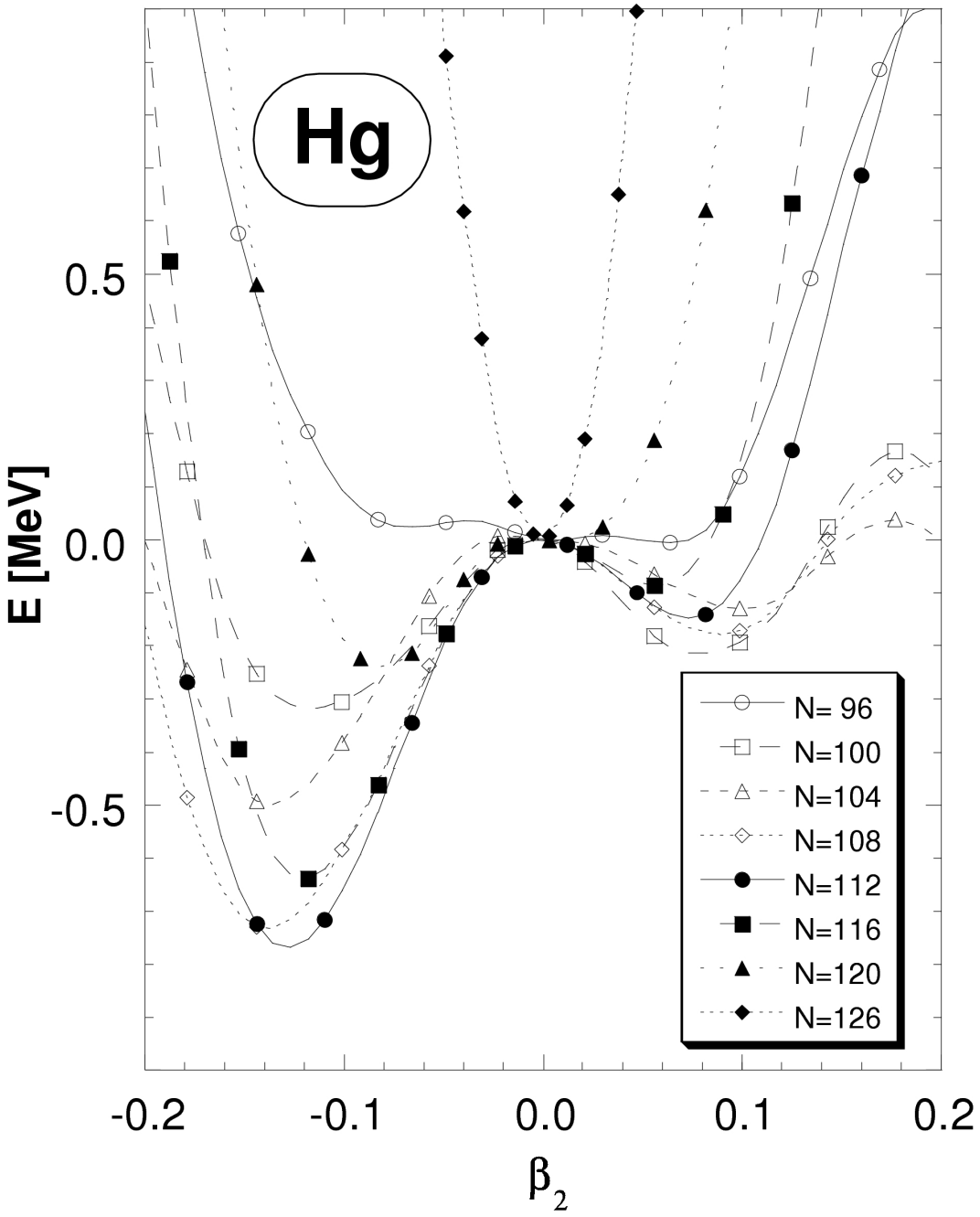

Figure 3.21 Energy surface (PES) as a function of the deformation parameter β_2 for different isotopes of Hg.

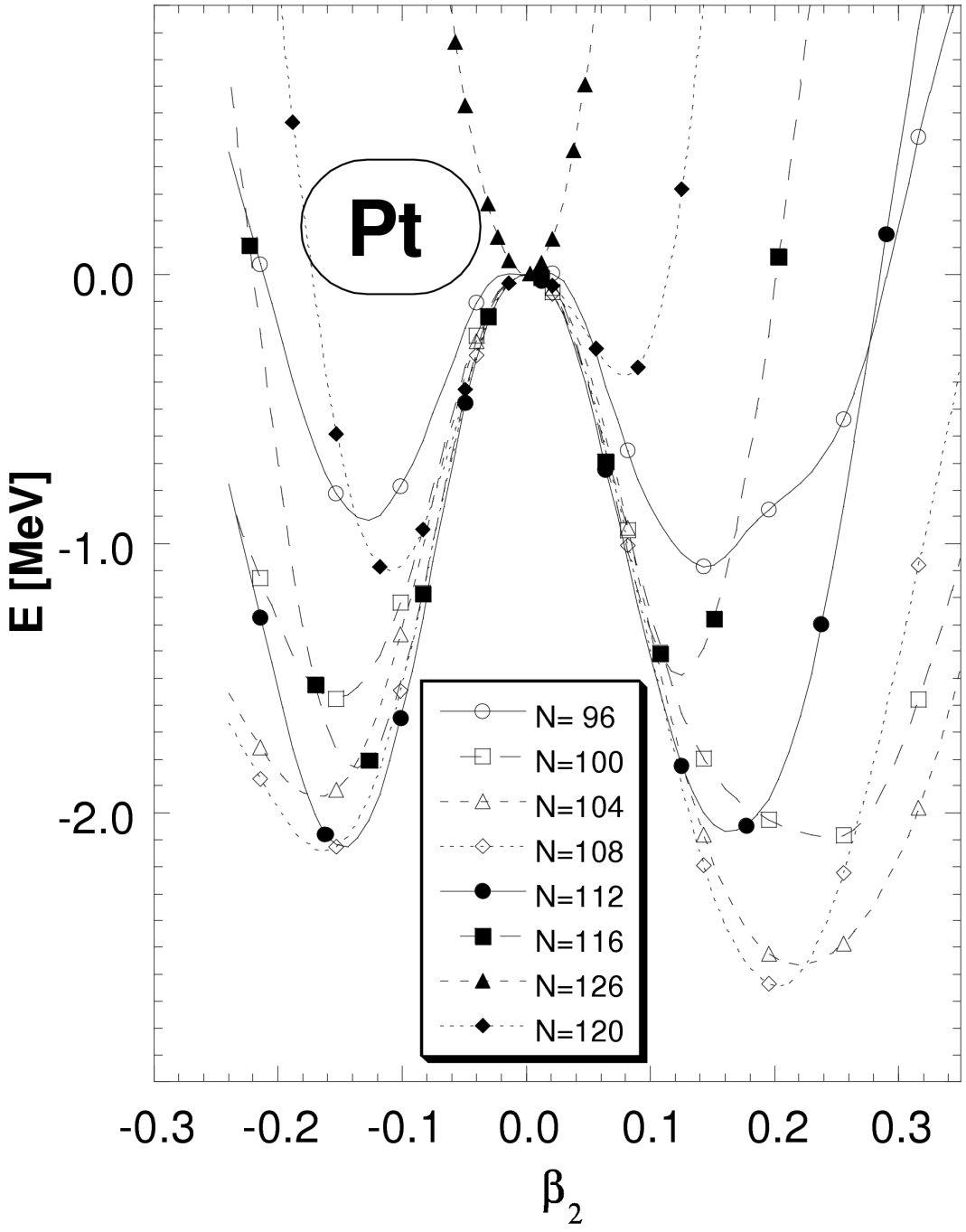

Figure 3.22 Energy surface (PES) as a function of the deformation parameter β_2 for different isotopes of Pt.

The Po $(Z = 84)$ isotopes

The Po nuclei have recently been described using particle-core coupling and IBM studies [143, 144] and there, it has been discussed extensively that an intruder 0^+ excited state is clearly dropping in energy with decreasing neutron number N (from $N = 118$ down to $N = 108$) and might even become the ground-state itself for these very neutron-deficient Po nuclei. Inspecting now the experimental $S'_{2n}(exp)$ values (see Fig. 3.16), it looks like the on-setting drop (below the reference linear fit line) from $N = 118$ down to $N = 108$ is strongly correlated with the above drop in energy of the intruder 0^+ state.

In the results of the PES calculations (see also [143, 170] and Fig. 3.23), the spherical minimum stays particularly stable down to $N = 118$ but then an oblate minimum starts coming on and deepens systematically, relative to the spherical minimum. In this respect, the comparison between the experimental and theoretical S'_{2n} values goes rather well, down to $N = 118$, in view of the energy scale used on the Fig. 3.16. At neutron number $N = 118$, the theoretical and experimental curves are going opposite ways. For the theoretical results, below $N = 118$ down to $N = 108$, the oblate minimum is developing relative to the spherical minimum with a prolate minimum quickly entering the picture that already is the lowest one (compared to the oblate minimum and the spherical point), see Fig. 3.23. The difference with the Hg and Pt nuclei is, that in those cases (below $Z = 82$), very quickly, the oblate and prolate minima appear much below the energy corresponding with the spherical point. In Po, on the contrary, this is not the case. Potential minima develop at oblate and prolate shapes, but the spherical point dominates down to $N = 106$ (see Fig. 3.23). It is this difference that causes the theoretical $S'_{2n}(theo)$ curve to move up (relative to the linear fit). The clear differences then point out either, that the PES situation in the Po nuclei is not so well reproduced, or, that dynamical effects, originating from mixing between the wave functions, localised at the various collective minima and the spherical point, play an important role. The latter effect, which is absent in any of the comparisons made in this section (the Pb, Hg, Pt and Po nuclei) implies that in the present comparison we cannot expect detailed agreement: only a qualitative correlation between trends in the theoretical and experimental S'_{2n} can be expected. Of course, the measurement of masses in the even more neutron-deficient nuclei is extremely important. One might get access to the study of effects of (i) collective (deformation versus spherical shape) correlations and (ii) specific local configuration mixing inducing extra binding energy in the nuclear ground-state configurations.

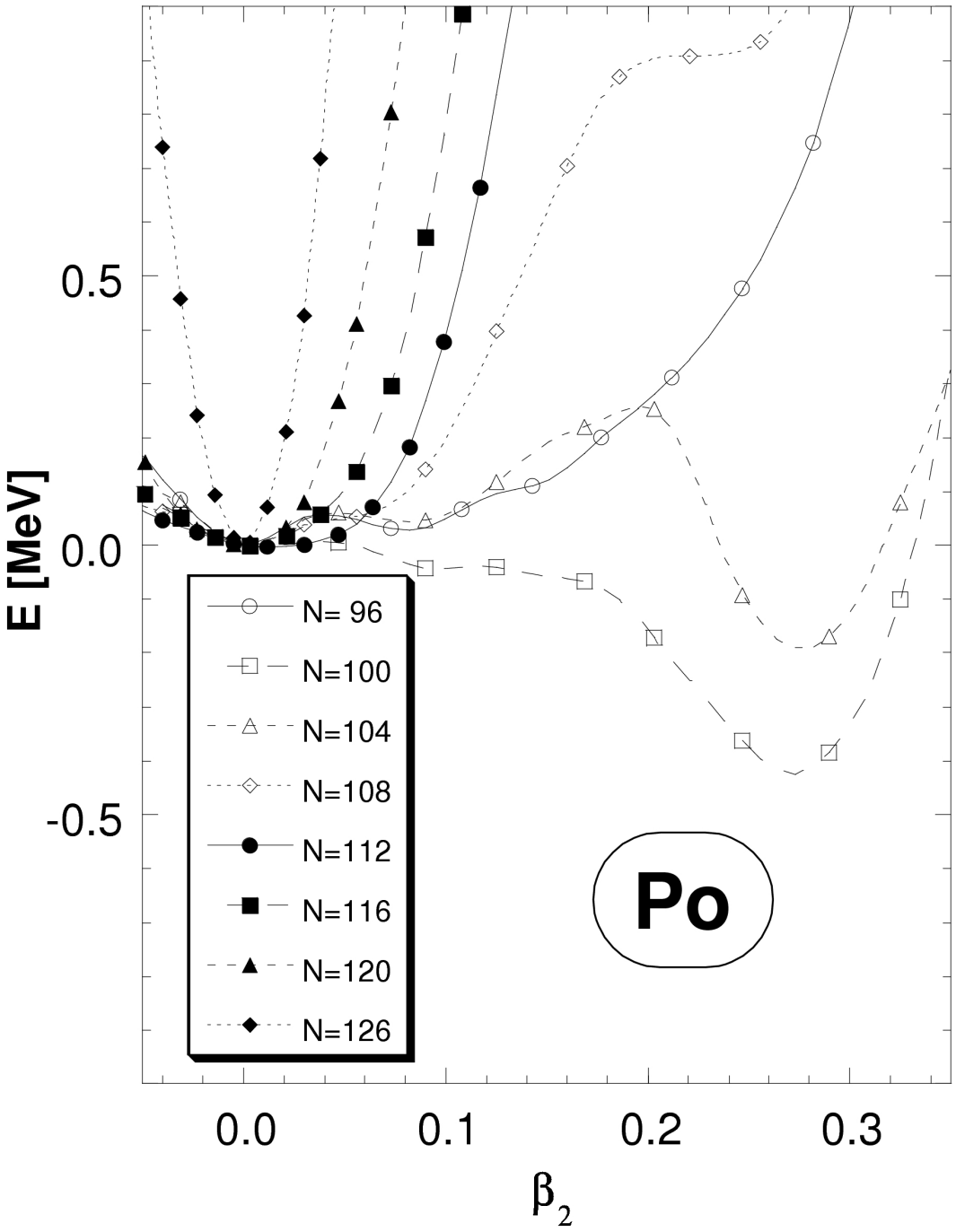

Figure 3.23 Energy surface (PES) as a function of the deformation parameter β_2 for different isotopes of Po.

3.5.4 A short conclusion

As a conclusion to section 3.5, we can say that mixing between intruder and regular states has an influence on both nuclear energy spectra and nuclear binding energies. However, we are still far from a detailed description of the consequences of mixing on the separation energies, as has become clear from the previous plots (see figures 3.13,3.14, 3.15, and 3.16).

Even though the many parameters appearing in the macroscopic-microscopic model to evaluate nuclear masses and PES, those parameters are fitted to an enormous mount of data in a complex fitting procedure; they remain untouched after that. Only a few of them (see also section 3.2.1) are really fitted to all masses; the other ones are fitted to selected data sets. Therefore, the masses derived this way (and derived S_{2n} values) cannot be used to account for all localised nuclear structure correlations (at and near closed shells, the precise onset of regions of deformation), which is also not the aim of the many mass studies [107, 108, 109, 110, 111, 112, 113, 114]. Only after including dynamical effects (like *e.g.* the GCM approach) can one expect to cover both, the full global and local mass behavior.

It should be stressed that in the case of the IBM calculations, the parameters of the local Hamiltonian have been chosen independently from the "S_{2n} problem". They were obtained from an independent fit of the energy spectra in this mass region for both, the regular and intruder states. As far as the two-neutron separation energies are concerned, the IBM results can count as a prediction for the actual S'_{2n} values.

3.6 Conclusions

In the present chapter, in which we have studied nuclear binding energies and their global properties over a large region of the nuclear mass table, we also concentrated on local deviations from a smooth behavior and made use of the two-neutron separation energy, S_{2n}, as an important property to explore the nuclear mass surface. The latter local variations could stem from the presence of shell or sub-shell closure, the appearance of a localised region of deformation or might originate in specific configuration mixing with the ground state that causes local increased binding energies to show up.

The very recent high-resolution measurements that have been carried out, in particular at the ISOLTRAP and MISTRAL set-ups at ISOLDE/CERN have allowed to study nuclear masses with an unprecedented precision of 10^{-5} and as such brings the interest of mass measurements from tests of global mass formulae or HF(B) studies into a realm that allows tests of shell-model calculations.

Here, we have discussed up to what level calculations - making use of global macroscopic models, macroscopic-microscopic calculations, the shell-model and the Interacting Boson Model - can give a correct overall description of the nuclear

mass surface (along the region of the valley of stability as well as for series of isotopes). It has become clear that, if one starts from a simple liquid-drop approach, the observed almost linear drop in the S_{2n} value is accounted essentially through the asymmetry term. This term causes nuclei to become less bound when moving out of the region where $Z \approx \frac{A}{2}$ in a systematic way and even turns to a linear variation in (3.9) when the neutron excess is becoming really large. The liquid drop approach is able to give the correct overall mass dependence in S_{2n} along the stability line as well as for long series of isotopes. It is observed though that the experimental slope is somewhat less pronounced compared to the liquid drop behavior (see Fig. 3.2), but here, more sophisticated macroscopic-microscopic calculations have resulted into impressive results.

The above features also result from a shell-model approach in which we treat a given mass region approximately starting from a reference (doubly)-closed shell nucleus and have the valence nucleons filling a single-j shell model orbital. Using a zero-range δ interaction, a linear variation with the number of nucleons, n, in describing the binding energy $BE(j, n)$ results. For more general interactions, still keeping seniority, v, as a good quantum number, a linear plus quadratic n dependence is obtained with the coefficient of the quadratic part contributing with a repulsive component to the total binding energy of the shell. This term is similar in nature and relative magnitude to the asymmetry term of the liquid-drop model description. Finally, a linear drop in the value of S_{2n} results.

There is a clear need to do better and try more detailed shell-model calculations. At present, the limitations of standard large-scale diagonalization constrain the calculations to the fp shell. Recent, new developments, starting from diagonalizations in a basis generated from Monte-Carlo sampling of the essential nuclear degrees of freedom (Monte-Carlo shell model diagonalization: MCSMD) have resulted in highly encouraging results that may open new possibilities to cover both, global and local nuclear properties in a consistent and unified way [176, 177]).

There are remaining problems connected with deriving absolute binding energies since one needs a good description for the variation with A or N of the single-particle energies ϵ_j. Some prescriptions are in use [123, 124], but there remains a difficulty for pure shell-model studies.

In plotting the value of S_{2n} versus the number of nucleon pairs, the shape is close to linear. Deviations, however, show up that must be due to the subsequent filling of a number of single-particle orbitals and to the correlation energy that results from the interactions in which pairing and proton-neutron forces play a major role. A pair approximation, as used within the Interacting Boson Model, can then be used to take into account both the global and local components of nuclear binding energy. We have discussed a procedure which starts from simultaneous treating binding energies and excitation energies in extracting parameters for the linear and quadratic $U(6)$ Casimir invariant operators. This approach bases on the assumption that the added global part to the IBM result is the same for a chain of isotopes.

It should be stressed that the linear part will change when changing between major shells and even when crossing the mid-shell region. This latter fact turns out to be an intrinsic deficiency of the IBM due to the fact that the Pauli principle is included only in an approximate way (there is no reference any more to the subsequent filling of a set of single-particle orbitals with a maximal number of nucleons). In section 3.4.5, we have reported a detailed prescription in order to obtain a consistent description of binding energies, energy spectra and transition rates in the framework of the IBM.

In a second part of this chapter, we have concentrated particularly on local deviations from the above global description. The possibility to study nuclear masses with the highest possible precision has become available over the last years, in particular at the ISOLTRAP and MISTRAL set-ups at ISOLDE/CERN. Here, precisions of the order of 30 keV on a total mass of a heavy Pb nuclei (≈ 1600 MeV) is reached. This has given rise to a number of unexpected features in the masses of neutron-deficient nuclei in the region of Pt, Hg, Pb, Po, Rn, Ra [24, 25, 26]. Before, similar local deviations had been observed in the region of light $N = 20$ nuclei for Na, Mg [126, 17, 149, 150, 151, 152].

In the present chapter, we have pointed out the necessity to incorporate configuration mixing of the regular ground state with low-lying 0^+ intruder states that approach the 0^+ ground-state in the neutron mid-shell region ($N \approx 104$) for nuclei near closed-shell configurations. We have carried out detailed calculations for the Po nuclei. Similar calculations for the whole Pb region will be carried out elsewhere in a consistent way. At the same time, calculations for the potential energy surfaces(PES) of the given nuclei in the Pb region have been performed, using the macroscopic-microscopic model with the universal deformed Woods-Saxon parametrisation. Here, the various shapes: spherical configuration, oblate and prolate deformed shapes and their relative ordering, as a function of neutron number, is instrumental in understanding local ground-state energy deviations from the background liquid-drop behavior. We observe a good correlation between the experimental values of S'_{2n} and the calculated ones on the 100 keV-scale. These results are encouraging in the light of lack of dynamical effects: we just compare energy minima for different shapes without taking into account mixing that will inevitably occur between such close-lying states.

Resuming, we have shown, in a first part, that both, a liquid-drop approach (macroscopic-microscopic models in general) as well as the shell model and the IBM describe the global part of the S_{2n} value essentially identical. The linear drop is mainly connected to the asymmetry term (in the LDM), the quadratic terms (in the shell model) and the quadratic $U(6)$ Casimir invariant (in the IBM), but all three contain the same physics. Both, the overall drop in S_{2n} for the whole mass region, as well as in specific long isotopic series are well accounted for. The experimental drop is overall less steep. In particular, in the case of the IBM we have shown that it is possible to give a consistent description of ground-state and excited-state

properties. This description is able to reproduce the experimental S_{2n} values rather well. Finally, in a third part, deviations in nuclear binding from the global trend are showing up in various localised regions. In the Pb region, it is most probably the effect of mixing of low-lying intruder configurations (oblate and/or prolate shape configurations) into the ground-state that turns out to be responsible for increased binding energies in the neutron-deficient region. Using configuration mixing in the IBM, detailed studies can be carried out and a consistent study is planned for the Pb region and for other (sub)shell-closures. The PES study of static properties on the other hand is able to give a good guidance to the interpretation of the specific deviations that have been observed in the Pb region.

Thus nuclear mass measurements are becoming increasingly important since they have progressed now to the level of testing microscopic studies (shell-model effects, localised zones of nuclear deformation, ...). This will become clearly an important line of research in future projects.

Chapter 4

Nuclear Shell Model Approach to Nuclear Binding Energies

4.1 Differences between pairing and zero-range effective interactions for nuclear binding energies

4.1.1 introduction

With the advent of a wide variety of beams of exotic nuclei, it is important to understand the physics that can be extracted from the measurement of various observables. Even with the weakest exotic beam intensities (ranging below 1p/s), it is possible to measure masses with advanced trapping instruments. This will allow the possibility of exploring the binding energies of long isotopic chains, especially on the neutron rich side of stability. These binding energies are determined by the shell model single-particle energies and by the residual interactions amongst the valence nucleons. One can therefore use such data to extract information on either of these two important ingredients in nuclear structure.

However, to do so requires an understanding of the predictions for binding energies with different residual interactions. Two of the most important and studied of these are the monopole pairing and the delta interactions, both designed to reflect the key short-range nature of the residual interactions and to reproduce typical spectra of nuclei near closed shells.

Although the basic properties of these interactions have long been known, some key differences in their predictions are not well appreciated. Specifically, the explicit juxtaposition of the predictions of these interactions for binding energies across a shell have not, to our knowledge, been presented before. It is therefore the purpose of the present section to first recall some characteristic features of these forces, originally elucidated decades ago, and then to apply these results to understand the evolution of binding energies across a shell.

We will show that, although the pairing and delta forces are often considered to be similar, and do produce similar *excitation* spectra, they are fundamentally different in the way they affect particles filling a j-shell (in particular in their "saturation" properties), and they produce entirely different predictions for binding energies across a shell. Data on long iso-chains of nuclei, which will be forthcoming with new radioactive beam facilities, will therefore allow a distinction between these interactions.

We start by focussing on characteristic aspects of these interactions. For simplicity, we consider a large single j-shell although we comment at the end on the more realistic multi-j nature of major shells. The reader is referred to [5, 100, 119, 120, 133, 178] for discussion of these interactions: these discussions form the basis for the present discussion and the key elements that we will be exploit below.

4.1.2 Pairing force, delta interaction and nuclear binding energies

In the study of nuclear structure properties, in particular when concentrating on the interactions amongst identical nucleons, the pairing force takes on a special role [100]. It has been devised in order to describe the special features of the effective nucleon-nucleon force in the nuclear medium, e.g., favoring $J^\pi = 0^+$ coupled configurations over any other angular momentum state. This particular property is indeed observed when studying energy spectra where identical nucleons essentially determine the outcome [5, 100, 119, 120, 133, 178]. Similarly, effective forces in the nuclear medium have been devised acting in coordinate space, all containing essentially the effective short-range characteristics which give rise to the above generally observed energy spectra for identical nucleons interacting inside the atomic nucleus [5, 133, 179]. At the extreme side, the zero-range or delta-interaction requires the nucleons to be at the same place in coordinate space in order to contribute to nuclear binding, e.g., $\delta(\vec{r}_1 - \vec{r}_2)$. Even though the resulting energy spectra with either pairing or short-range forces compare rather well concerning the preference of binding nucleons into $J^\pi = 0^+$ states over the other angular momentum components, there appear a number of subtle differences between the pairing force and the zero-range force that we wish to discuss in order to point out their consequences.

The pairing force, defined in occupation number representation as

$$H_{pairing} = -G\Omega_j S^+(j)S(j), \tag{4.1}$$

with the definition of the pair creation operator

$$S^+(j) = \frac{1}{\sqrt{\Omega_j}} \sum_{m>0} (-1)^{j+m} a^+_{jm} a^+_{j-m}, \tag{4.2}$$

describes well the short-range properties of effective nucleon-nucleon interactions. Because of the very definition of the pairing force, there is no reference to coordi-

nate space and so the statement cannot be rigorously correct. What the pairing force does, is scatter nucleons isotropically in the space of magnetic substates $(m, -m)$ and scatter every substate pair $(m, -m)$ into any other substate pair $(m', -m')$ with equal amplitudes (when making the appropriate choice for the phases) [5, 100]. One can calculate this magnetic subspace scattering matrix of dimension Ω_j (considering time-reversal as a conserved quantity) for any other force [119, 120] and it turns out that for the zero-range delta-interaction, scattering is no longer fully isotropic although there is a very strong preference for it. The matrix elements fall off slowly when moving away from the diagonal. At the other extreme, low-multipole forces like the quadrupole-quadrupole interaction, described by the Legendre polynomial $P_2(\cos\theta_{1,2})$, essentially result in pure forward scattering, i.e., the scattering goes preferentially from an initial state $(m, -m)$ into the same state as the final state $(m, -m)$ [5]. For large values of j, $j \to \infty$, the m-state scattering matrix becomes diagonal.

Next, we point out that the specific gap between the $J^\pi = 0^+$ angular momentum coupled state and the higher angular momentum states in short-range coordinate space forces does not derive from a single multipole but results from a coherent effect of all multipoles, contributing to a given $(j)^2(0^+)$ configuration, i.e., from $k = 0$ up to $k = 2j - 1$. This can be derived exactly using the zero-range delta-interaction force [5, 100, 119, 120, 133, 178] and there one observes that for large-j values, the different multipole energy contributions that lower specifically the $J^\pi = 0^+$ state with respect to the unperturbed energy all become equal in amplitude having the same phase (see figure 4.1). So one cannot single out a given set of multipoles as the essential ones in producing the specific property for nucleons to couple preferentially in the $J^\pi = 0^+$ state. They are all equally important.

The difference in the pairing and δ-function forces leads to important effects. When using the pairing force (see eq. (4.1)), and building a basis of $J^\pi = 0^+$ coupled configurations, which for seniority $\nu = 0$ becomes $(S_j^+)^{\frac{n}{2}}$, one can evaluate the binding energy exactly. Breaking up pairs into higher angular momentum states, e.g. , $J^\pi = 2^+, 4^+, \ldots$ corresponding to seniority $\nu = 2$, and even into more broken-pair components with seniority $\nu = 4, \ldots$, the following general expression for binding energy results [5, 100, 120]

$$BE^{\text{pairing}} = \frac{G}{4}(2\Omega_j - n - \nu + 2)(n - \nu), \tag{4.3}$$

which reduces, for seniority $\nu = 0$ states, to

$$BE^{\text{pairing}} = G(\Omega_j - N + 1)N. \tag{4.4}$$

Here, n describes the number of (valence) particles and $N = \frac{n}{2}$ the number of (valence) *pairs*. So we can easily deduce the pairing force contribution to the two-

neutron separation energy. Starting from eqs. (4.3) and (4.4), one obtains

$$S_{2n}^{\text{pairing}} = G\,(\Omega_j + 2 - n) = G(\Omega_j + 2 - 2N), \tag{4.5}$$

(here now, n and N refer to neutrons only, of course). These results, obtained many years ago [119] for a single-j shell, imply that with the shell fully filled with nucleons, the total binding energy is given by the diagonal expression $-G\Omega_j$. For a typical value of $G = 0.25$ MeV (using the prescription that $G \simeq 25/A$ MeV, and for $A = 100$) and for $j = 11/2$ ($\Omega_j = 6$), this gives a rather small value of only 1.5 MeV for the total binding energy of the closed shell. This results because the pairing force counts the number of pairs moving in the j-shell in which the Pauli effect plays an essential quenching role. This result is illustrated in figure 4.1, where binding energies for the seniority ($\nu = 0$) 0^+ state in the $1h_{11/2}$ configuration is shown.

If we now use the zero-range $\delta(\vec{r}_1 - \vec{r}_2)$ force, and the same basis as we used when discussing the binding energy effects for the pairing force, a totally different result emerges. This may seem strange at first because one has an intuitive "feeling" that pairing and zero-range forces should give rise to very much identical results. This is approximately so for the energy spectrum (see figure 4.2). However, the zero-range interaction does not scale with the number of *pairs* as does the pairing force but scales with all the fermions that are interacting.

This is shown in figure 4.3, where we denote a pair by the combination of two crosses connected with a dashed line. Then the actual interactions between nucleons can "cross" between pairs and the arguments of the zero-range force, $\vec{r}_1$ and $\vec{r}_2$, will become identical to the whole set $\vec{r}_1, \vec{r}_2, ..., \vec{r}_{2j+1}$. That is, each nucleon has an equal short range interaction with *each* of the other ones. In contrast, for a pairing force, the interaction is only *within* a single pair. The zero-range force will then result in a much larger diagonal binding energy that is obtained by evaluating the expression [119, 120]

$$\langle j^n, \nu, JM| \sum V_{i,k} |j^n, \nu, JM\rangle = \langle j^\nu, \nu, JM| \sum V_{i,k} |j^\nu, \nu, JM\rangle + \frac{n-\nu}{2} V_0, \tag{4.6}$$

(this holds exactly for any odd-tensor interaction where seniority is a good quantum number, and the zero-range interaction, operating in the above configuration, acts like an odd-tensor interaction). If we concentrate on the ground state and thus construct the $\nu = 0$ state, the above expression gives the much simpler result [119, 120]

$$\langle j^n, \nu = 0, JM| \sum V_{i,k} |j^n, \nu = 0, JM\rangle = \frac{n}{2} V_0, \tag{4.7}$$

which holds for $n = 0, 2, 4, \ldots \rightarrow 2j + 1$. Thus, the binding energy changes completely (see figure 4.2), giving rise to a linear behavior in n (in contrast to the "roll-over" in the binding energies for a pairing force past mid-shell). As a result, the binding energy of the filled shell for a δ -interaction amounts to $\Omega_j V_0$ where V_0 denotes the relative binding energy of the $J^\pi = 0^+$ configuration with respect to its unperturbed energy. A good estimate for this value is $V_0 = G\Omega_j$. Thus, we notice that the total binding energy contribution for the filled shell now becomes $G{\Omega_j}^2$.

The difference between the pairing force and zero-range delta-function force thus becomes very important when one studies binding energies. Even though the detailed spectroscopic properties are not so different (the pairing force as well as the zero-range force both give rise to a n-independence in the energy spectra when filling up the shell-model orbital j with n identical nucleons), the use of the pairing force turns out to be a poor choice when studying binding energy effects. The pairing force over-saturates, whereas the zero-range force perfectly saturates. That is, the binding energy contribution for each successively added pair of nucleons decreases with n for a pairing force but is a constant for the zero-range delta interaction.

If one looks at a more realistic case, e.g., filling up nucleons within the major shell between 50 and 82 nucleons (see chapter 3 and [180, 181]), one should consider the specific shell-model sequence of orbitals, and one cannot just put all particles in a large degenerate shell. with $j = 31/2$ (or $\Omega_j = 16$). In this case one fills in sequence, e.g., the $2d_{5/2}, 1g_{7/2}, 1h_{11/2}, 2d_{3/2}$ and $3s_{1/2}$ orbitals. The arguments discussed above for a δ-interaction can then be used and, as a result, one obtains a sequence of straight lines, each characterized by a slightly different slope which is fixed by the value of V_0 or by the Slater integral for that particular orbital. So we need an extra index $V_0(j)$ [5, 119, 120, 133]. As a result, one is able to reproduce correctly the trend of increasing binding energies all through a large shell.

One should remark that for other short-range forces that do not belong to the class of odd-tensor forces, extra corrections can show up and the expression for the binding energy in even-even nuclei in a given j-shell is modified to the result [119]

$$BE^{\text{general}} = \alpha n + \beta \frac{n(n-1)}{2} + P\left[\frac{n}{2}\right], \tag{4.8}$$

provided seniority v remains a good quantum number (cfr. eq. (3.12)). The value of α represents [120, 121] the binding from the single-particle energies, the value of β is much smaller and repulsive and P expresses the accumulating binding energy (see eq. (4.7)) for a short-range force when going through a chain of isotopes. This more general expression is important in order to obtain a more detailed description of binding energies within a simple shell-model approach. This will not be discussed here [180, 181]. Of course, attempts to treat binding energies consistently, within a shell-model context, also have to cope with the problem of modifications

in the mean-field itself (varying single-particle energies ϵ_j) as a function of the filling of shells. This "monopole" issue is discussed in detail by Zuker et al. [123, 124].

4.1.3 Conclusion

To conclude, we have discussed some simple but subtle differences characterizing two forces that are extensively used in the study of nuclear structure properties. Even though their relative excitation energy spectra ressemble each other very closely, important differences show up in evaluating binding energies for a filled shell-model orbital. We point out that the major difference comes from the fact that the pairing force acts in angular momentum space or the space of magnetic substates $(m, -m)$ whereas the zero-range delta-function force only acts when the two interacting nucleons appear at the same spatial coordinates. In that respect, we also point out that, in coordinate space, the special preference of nucleons to be bound in $J^\pi = 0^+$ states comes from a coherence effect of all contributing multipoles. These characteristics lead to important differences in the predictions for the two classes of interactions for binding energies. Specifically, the total binding energy across a shell increases linearly for a δ- interaction but maximizes at mid-shell and decreases past mid-shell for a monopole pairing interaction. These differences could be significant when long isochains of nuclei are studied with beams of exotic nuclei.

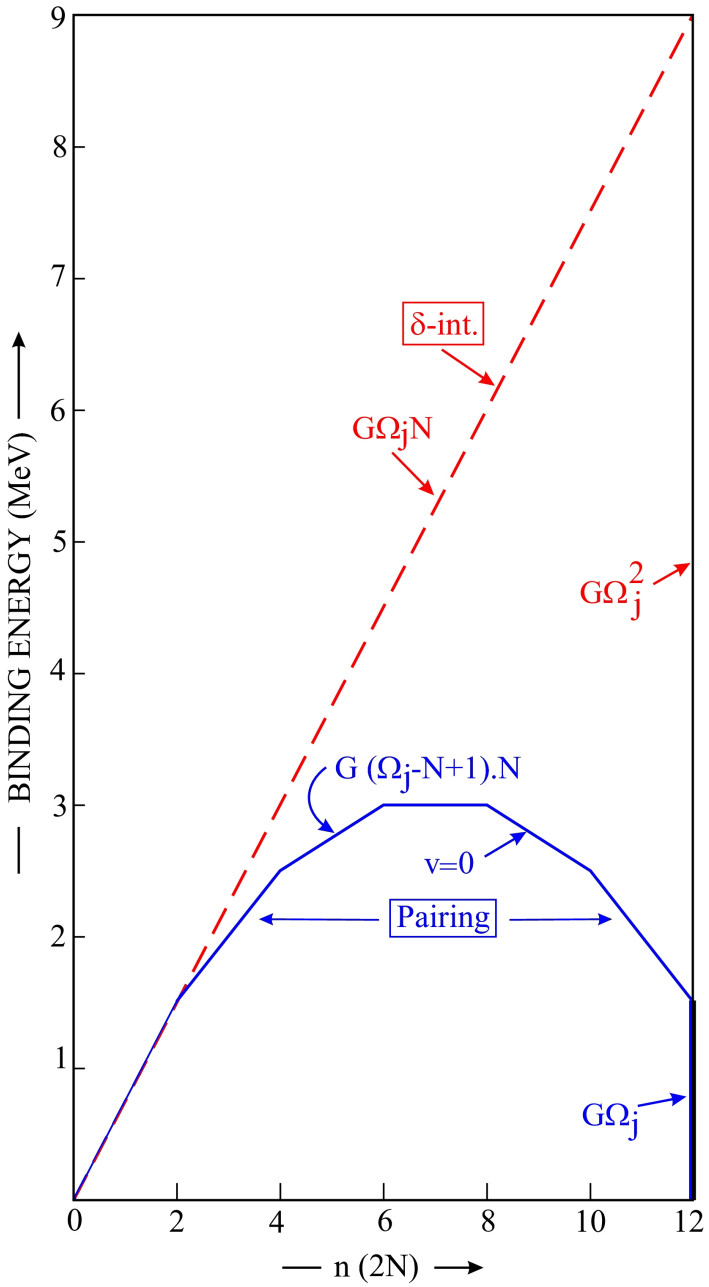

Figure 4.1 Comparison of the binding energy for n particles (number of pairs $N = \frac{n}{2}$) filling the $1h_{11/2}$ orbital with Ω_j =6 using the pairing force (eq. (1)) and the zero-range delta-function force.

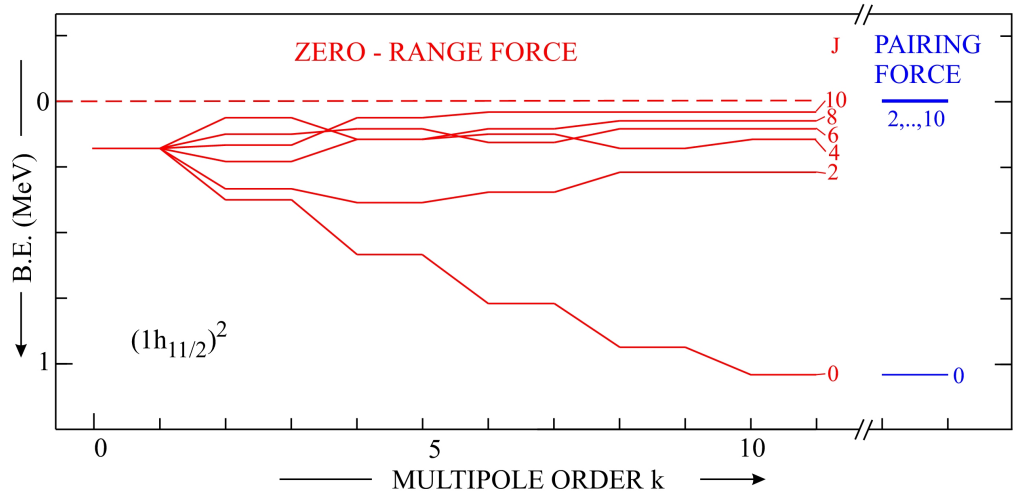

Figure 4.2 Multipole decomposition for the two-body matrix elements, $\langle(1h_{11/2})^2; JM|V|(1h_{11/2})^2; JM\rangle$, using a zero-range force. On the extreme right of the figure, the spectrum for a pure pairing force is added for comparison.

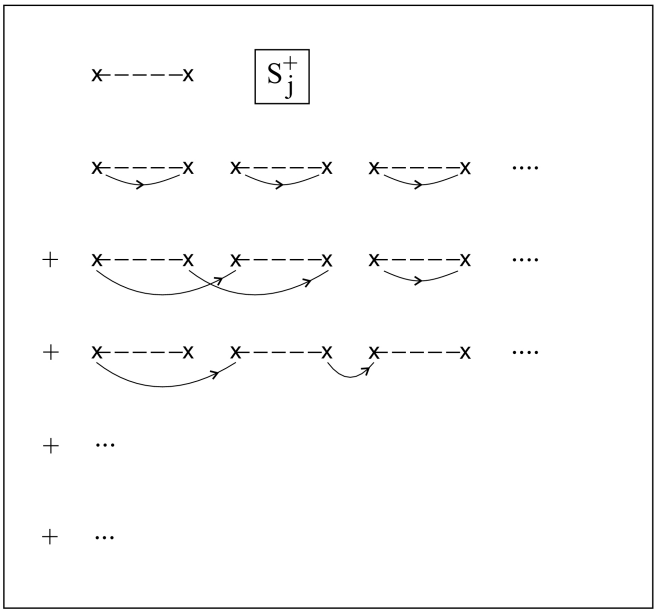

Figure 4.3 Diagrammatic drawing of all the possible two-body interactions, using a $\delta(\vec{r}_1 - \vec{r}_2)$ force with a pair state $(S_j^+)^{\frac{n}{2}}$. Crosses, connected with dashed lines, represent a given nucleon pair. The full lines (with arrows) then represent possible combinations for interacting nucleons (there are $2j+1$ crosses). Each line indicates one of the $\frac{n(n-1)}{2}$ possible terms.

4.2 Proton-neutron quadrupole interactions: an implicit contribution to the pairing field

4.2.1 Introduction

The pairing force, which expresses in the most succint way the preference of nucleon pairs to become bound into $J^\pi = 0^+$ states in the atomic nucleus, has been widely used in many applications in the study of nuclear structure properties [5, 100, 120, 133]. Compared to the use of many other effective forces that have been used, both of finite but short-range character or, constructed explicitly starting from the nuclear G-matrix and free nucleon-nucleon scattering, the pairing force has besides its extreme simple structure, lead to study and solve the classification of nucleons that occupy the available single-particle orbitals. The quasi-spin scheme [100, 120], or, closely related the introduction of the seniority quantum number v [119], leads to single-j and degenerate many-j shell exact solvable models. They can be used as benchmarks to compare other more detailed calculations with.

Another important characteristic of the nucleon-nucleon effective interaction acting inside atomic nuclei is expressed through the long-range components of this interaction [182]. The low multipoles and the quadrupole component, in particular, are essential in generating low-lying nuclear collective phenomena.

Both components have formed a keystone to understand the many facets of nuclear structure: from few nucleons near to closed-shell configurations as well as in those situations where many valence protons and neutrons are actively present outside closed shells. They are essential ingredients of any shell-model (or present large-scale shell-model) calculation, even though in most of them either model interactions are constructed explicitely or deduced from more realistic nucleon-nucleon potentials (see refs. [126, 183, 184, 185, 186] to cite just some recent shell-model studies).

In the present section 4.2, we like to point out that the quadrupole-quadrupole proton-neutron force can, to lowest order in perturbation theory, be seen as leading to an implicit extra contribution to the pairing field, thus renormalizing the original pairing force strength. In subsection 4.2.2, we succintly indicate the results of pure pairing in single-j shell, and explicitely evaluate the proton-neutron quadrupole-quadrupole contribution to the ground-state energy and observe that its effect leads to an extra pairing contribution. In subsection 4.2.3 then, we give some application in various mass regions in order to estimate the effect of this induced 'pairing-like' contribution. In the conclusion, we indicate that this extra effect may well be interesting when studying nuclear structure properties not too far from closed shells in which the interactions amongst identical nucleons dominate the proton-neutron interaction effects.

4.2.2 Shell-model correlations

As discussed in the introductory section, the interplay of the pairing force and the proton-neutron low multipole deformation-driving force components are essential ingredients of any shell model calculation. The aim of the present section is to point out that, to lowest order, the proton-neutron quadrupole part can be incorporated in an implicit way as a renormalization of the pairing force strength. Of course, this means that applications will stick to regions near to closed shells where the proton-neutron energy contribution is not the dominant part since then, one has to treat both components (pairing and low-multipole proton-neutron part) on equal footing.

We first give a short reminder of the pairing correlation energy part, considering the nucleons are filling a single-j shell (or a set of degenerate-j shells). Secondly, we study the proton-neutron energy correction (quadrupole interaction) to be superposed to the pairing part.

Pairing energy corrections

Let us consider the most simple case of a pure pairing force: n identical valence nucleons interacting in a single-j shell, with a given strength G,

$$\hat{H} = -G \sum_{m,m'>0} a^{\dagger}_{jm} a^{\dagger}_{j-m} a_{j-m'} a_{jm'} (-1)^{2j+m+m'}. \tag{4.9}$$

The ground state of such a system corresponds to a state where the nucleons are coupled in pairs to angular momentum $J = 0$. As a consequence the ground state has seniority $v = 0$,

$$|n, v = 0\rangle = (S^{+}_{j})^{n/2}|0\rangle, \tag{4.10}$$

where

$$S^{+}_{j} = \frac{1}{\sqrt{\Omega}} \sum_{m>0} (-1)^{j+m} a^{+}_{jm} a^{+}_{j-m}. \tag{4.11}$$

The binding energy of this system results,

$$BE^{\text{pairing}} = \frac{G}{4}(2\Omega - n + 2)n = G(\Omega - N + 1)N, \tag{4.12}$$

where N is the number of valence nucleon pairs and Ω is the shell degeneracy, $\Omega = j + 1/2$. In a system with valence protons and neutrons, interacting through pairing forces between alike nucleons, one has to consider the equation (4.12) for protons and for neutrons separately. As an illustration of the pairing interaction (see figure 4.4), we shown the spectrum of a pure pairing force. From expression

(4.12), the pairing contribution to the two-neutron separation energy can be easily deduced, with as a result

$$S_{2n}^{\text{pairing}} = G(\Omega_\nu + 2 - n_\nu) = G(\Omega_\nu + 2 - 2N_\nu), \tag{4.13}$$

where n_ν is the number of valence neutrons, N_ν the number of valence neutrons pairs and $\Omega_\nu = j_\nu + 1/2$ is the shell degeneracy for neutrons. Note that there is no contribution from the proton side because the number of protons is the same in both neighboring isotopes.

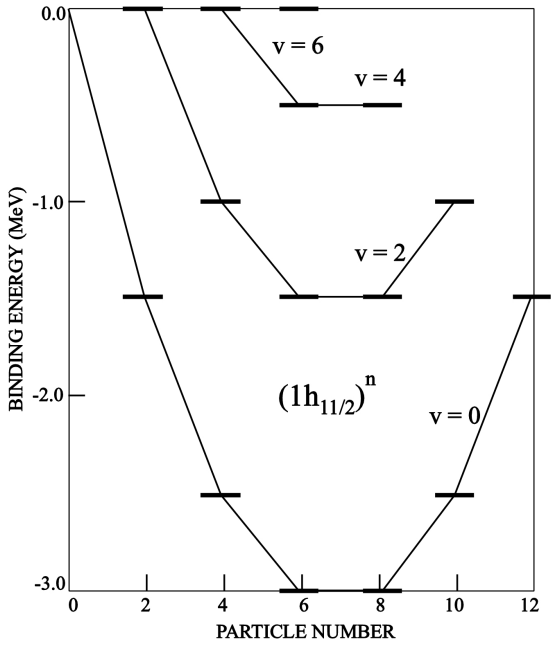

Figure 4.4 Spectrum for a pure pairing force within the $1h_{11/2}$ orbital, *i.e.* for the $(1h_{11/2})^n$ spectrum, with seniority $v = 0$, $v = 2$, $v = 4$, and $v = 6$ as a function of the particle number n. The pairing strength G has been chosen as $G = 0.25$ MeV. Taken from [5].

The quadrupole energy contribution

As discussed before, it is our aim the study the extra energy contribution in the ground state that is due to the proton-neutron quadrupole-quadrupole interaction. The quadrupole proton-neutron Hamiltonian can be written as,

$$\hat{H} = \kappa \hat{Q}_\pi \cdot \hat{Q}_\nu, \tag{4.14}$$

where $\hat{Q}$ is the quadrupole operator for protons and neutrons, respectively, and $\cdot$ stands for the scalar product. The main characteristic of the quadrupole operator

is that it induces the breaking of pairs, promoting pairs coupled to $L^\pi = 0^+$ into pairs coupled to $L^\pi = 2^+$, thereby changing the seniority quantum number υ and causing a core-polarization effect [187]. To a first approximation the ground state of the system will change from a condensate of proton and neutron pairs coupled to $L^\pi = 0^+$ (4.10) to a superposition of this state together with a new one where one-proton and one-neutron pairs coupled to $L^\pi = 2^+$ are induced,

$$|N_\pi \otimes N_\nu\rangle = |S_{j\pi}^{N_\pi} \otimes S_{j\nu}^{N_\nu}; L = 0\rangle + \xi |S_{j\pi}^{N_\pi - 1} D_{j\pi} \otimes S_{j\nu}^{N_\nu - 1} D_{j\nu}; L = 0\rangle, \tag{4.15}$$

where

$$D_j^+ = \sum_{m>0} (-1)^{j-m} \langle jmj - m|20\rangle a_{jm}^\dagger a_{j-m}^\dagger \tag{4.16}$$

will create a pair of nucleons coupled to $L = 2$.

Taking into account that the quadrupole contribution is small with respect to the pairing interaction, in order to fully determine the state (4.15), the most straightforward way is to use perturbation theory. Doing so, the expression of the mixing coefficient results,

$$\xi = \frac{\kappa\alpha}{\Delta E_\alpha}, \tag{4.17}$$

where

$$\alpha = \langle S_{j\pi}^{N_\pi} \otimes S_{j\nu}^{N_\nu}; L = 0|\hat{Q}_\pi \cdot \hat{Q}_\nu|S_{j\pi}^{N_\pi - 1} D_{j\pi} \otimes S_{j\nu}^{N_\nu - 1} D_{j\nu}; L = 0\rangle \tag{4.18}$$

and

$$\Delta E_\alpha = -E_{2_\pi^+} - E_{2_\nu^+}. \tag{4.19}$$

$E_{2_\rho^+}$ ($\rho = \pi, \nu$) are the excitation energies of states with one $L = 2$ proton or neutron pair, respectively. Those energies will be positive for $\kappa < 0$.

The energy correction due to the quadrupole force will be given by the matrix element of the Hamiltonian (4.14) using the state (4.15) resulting a binding energy, for a system where the driving forces are pairing and quadrupole interactions:

$$BE = BE^{\text{pairing}} + 2\frac{\kappa^2\alpha^2}{-\Delta E_\alpha}, \tag{4.20}$$

where BE^{pairing} corresponds to equation (4.12). Note the minus in front of ΔE_α because the latter equation refers to the binding energy.

Due to the schematic structure of the states appearing in (4.18) it is possible to obtain a more explicit expression of this matrix element using the Racah algebra

reduction formulae [119]. First step is the decoupling of the proton and neutron sectors,

$$\begin{aligned}\alpha &= \frac{1}{\sqrt{5}}\langle (S_{j\pi})^{N_\pi}; L=0\|\hat{Q}_\pi\|(S_{j\pi})^{N_\pi-1}D_{j\pi}; L=2\rangle \\ &\times \langle (S_{j\nu})^{N_\nu}; L=0\|\hat{Q}_\nu\|(S_{j\nu})^{N_\nu-1}D_{j\nu}; L=2\rangle. \end{aligned} \tag{4.21}$$

Using the appropriate reduction formulae one arrives to,

$$\alpha = \frac{1}{\sqrt{5}}\sqrt{N_\pi(\Omega_\pi - N_\pi)}\sqrt{N_\nu(\Omega_\nu - N_\nu)}\frac{\langle\hat{Q}_\pi\rangle\langle\hat{Q}_\nu\rangle}{\sqrt{(\Omega_\pi-1)(\Omega_\nu-1)}}, \tag{4.22}$$

where,

$$\langle\hat{Q}_\pi\rangle = \langle S_{j\pi}\|\hat{Q}_\pi\|D_{j\pi}\rangle = \frac{2}{\sqrt{2j_\pi+1}}\langle j_\pi\|\hat{Q}_\pi\|j_\pi\rangle, \tag{4.23}$$

and

$$\langle\hat{Q}_\nu\rangle = \langle S_{j\nu}\|\hat{Q}_\nu\|D_{j\nu}\rangle = \frac{2}{\sqrt{2j_\pi+1}}\langle j_\pi\|\hat{Q}_\nu\|j_\pi\rangle. \tag{4.24}$$

The expressions (4.23) and (4.24) can be even more simplified if one assumes the harmonic oscillator as single particle basis and uses the expression for the quadrupole operator,

$$\hat{Q} = \sum_i r_i^2 Y_2(\theta_i, \varphi_i) \tag{4.25}$$

resulting into

$$\begin{aligned}\langle\hat{Q}_\rho\rangle &= \frac{2}{\sqrt{2j_\rho+1}}(N_{ho}+\frac{3}{2})\langle j_\rho\|Y_2(\theta,\varphi)\|j_\rho\rangle \\ &= \sqrt{\frac{5}{\pi}}(N_{ho}+\frac{3}{2})\frac{\frac{3}{4}-j_\rho(j_\rho+1)}{\sqrt{(2j_\rho-1)j_\rho(j_\rho+1)(2j_\rho+3)}}, \end{aligned} \tag{4.26}$$

where $\rho = (\pi,\nu)$, $Y_2(\theta,\varphi)$ is the spherical harmonic with $L = 2$ and N_{ho} is the number of quanta of the shell.

After these simple calculations one obtains a closed expression for the binding energy,

$$BE = BE^{pairing} + \frac{2}{5}\frac{\kappa^2}{-\Delta E_\alpha}\frac{N_\pi(\Omega_\pi - N_\pi)N_\nu(\Omega_\nu - N_\nu)}{(\Omega_\nu-1)(\Omega_\pi-1)}\langle Q_\pi\rangle^2\langle Q_\nu\rangle^2. \tag{4.27}$$

If we are now interested in the study of binding energies within a set of isotopes (thus Ω_π and N_π are fixed numbers) and by defining the coefficient $\overline{C}$ as follows,

$$\overline{C} = \frac{2}{5}\frac{\kappa^2}{-\Delta E_\alpha}\frac{N_\pi(\Omega_\pi - N_\pi)}{(\Omega_\nu-1)(\Omega_\pi-1)}\langle\hat{Q}_\pi\rangle^2\langle\hat{Q}_\nu\rangle^2. \tag{4.28}$$

we now obtain a "correlated" binding energy expression in the ground state

$$BE^{correlated} = BE^{pairing} + \overline{C}(\Omega_\nu - N_\nu + 1)N_\nu - \overline{C}N_\nu. \tag{4.29}$$

If it would turn out that $\overline{C}$ is much smaller in magnitude compared to G, then the third contribution can be quite small and the total "correlated" binding energy becomes

$$BE^{correlated} = (G + \overline{C})(\Omega_\nu - N_\nu + 1)N_\nu. \tag{4.30}$$

and one obtains a form, identical to the original pairing energy expression, albeit with a new coupling strength. In the next subsection, we shall evaluate in detail the value the coefficient $\overline{C}$ can reach to in order to see how well, the idea that proton-neutron quadrupole-quadrupole forces can, to lowest order, be absorbed into the pairing force between the identical nuclei is a valid one.

One interesting point is that, starting from the above equations (4.29) and (4.30), one deduces that for the two-neutron separation energy the linear part drops out and now one obtains a strictly linear behavior in N_ν with the result

$$S_{2n}^{quadrupole}(N_\nu) = (G + \overline{C})(\Omega_\nu + 2 - 2N_\nu) - \overline{C}. \tag{4.31}$$

This is essentially the same result as was obtained using a pure pairing force (see equation (4.13)) except for the small correction factor $\overline{C}$ (which we still have to prove). It is quite surprising that the lowest-order effect induced by proton-neutron residual quadrupole forces (it can be show that this holds for higher multipoles too) comes about as a 'renormalization' of the original pairing force.

It must be pointed out that, to lowest order, the same results are obtained if 0^+ coupled pairs (for protons and neutrons) are changed into 4^+ states, or even higher angular-momentum states. Again, one effectively incorporates that part of the proton-neutron interaction in the original pairing force by renormalizing the pairing strength further and one produces a linear variation of S_{2n}.

4.2.3 The pairing and quadrupole strength: some specific applications to check how well the above approximation works

The goal of this subsection is to calculate the correction factor $\overline{C}$ and compare this value to the estimate for the pairing strength, in various mass regions.

- The pairing strength G.

  An average value of G for medium-mass and heavy nuclei is $25/A$ MeV [188]. However, this averall value can change significantly in different mass regions, ranging from $G = 19/A$ MeV, for the regions $Z \sim 40 - 50$, to $G = 30/A$ MeV for Pb nuclei [189].

As an example, for $_{52}$Te isotopes ($A \approx 106 - 152$) the pairing strength is $G \approx 0.15$ MeV, and for $_{42}$Mo isotopes ($A \approx 84 - 128$) $G \approx 0.18$ MeV.

- The quadrupole strength $\overline{C}$.

  In order to estimate the value of $\overline{C}$, we assume that the different major shells consist of single-j shells where the diferent levels are taken as degenerate. In table 4.1, we show the values of j and degeneracies for different major shells or subshells in the regions $Z \sim 40$ and $Z \sim 50$. As example of isotopes with $Z \sim 40$ we can consider $_{48}$Cd ($N_\pi = 1$), $_{42}$Mo ($N_\pi = 1$), $_{44}$Ru ($N_\pi = 2$), and $_{46}$Pd ($N_\pi = 2$), and with $Z \sim 50$ 52Te ($N_\pi = 1$), $_{54}$Xe ($N_\pi = 2$), $_{56}$Ba ($N_\pi = 3$), and $_{58}$Ce ($N_\pi = 4$). For both shells we take as number of quanta $N_{ho} = 4$, which covers a shell from 40 to 70 nucleons and is in agreement with table 4.1.

  Another ingredient necessary for calculating $\overline{C}$ (see equation (4.28)) is $\Delta E_\alpha = -E_{2^+_\pi} - E_{2^+_\nu}$ which can be estimated from experimental energy systematics of the first 2^+ excitation energy [5]. That gives for the $Z \sim 50$ region a maximum value of $\Delta E_\alpha =\simeq -2$ MeV [190] and for the $Z \sim 40$ region, a slightly higher value $\Delta E_\alpha =\simeq -2.5$ MeV [187]

  The final element for calculating $\overline{C}$ is the value of κ. There exist realistic values of the quadrupole strength in the context of the IBM [10, 191], κ_0, that can be easily related with the value of κ appearing in equations (4.14) and (4.28) through the following expression [187]:

$$\kappa = \frac{5\kappa_0\sqrt{\Omega_\pi\Omega_\nu}}{\sqrt{\frac{2}{\Omega_\pi - 1}}\sqrt{\frac{2}{\Omega_\nu - 1}}\langle j_\pi \| \hat{Q}_\pi \| j_\pi \rangle \langle j_\nu \| \hat{Q}_\nu \| j_\pi \rangle}. \tag{4.32}$$

  As can be verified from table 4.2.3 and in figure 4.5, the term $|\langle j_\rho \| Q_\rho \| j_\rho \rangle|$ increases linearly with j_ρ, but this tendency compensates with a factor Ω_ρ, which gives as result that the value of κ is almost independent of the value of j_ρ (Ω_ρ). On the other hand the values of $\langle \hat{Q}_\rho \rangle$ and $\langle \hat{Q}_\rho \rangle^2$ (the third factor in (4.28)) do not change dramatically with j_ρ in the range $j_\rho = \frac{3}{2} - \frac{31}{2}$. This is an important outcome because that implies that the value of $\overline{C}$ is not strongly dependent on the particular j (Ω) value of the proton or neutron orbitals (degeneracies) that the nucleons are occupying.

  After this discussion one can evaluate the value of $\overline{C}$. In table 4.3, we present the values for different nuclei in the regions $Z \sim 40$ and $Z \sim 50$. Note that two alternatives shell closures have been used.

  As one can notice from table 4.3, the induced correction, stemming from the proton-neutron interaction to the pure pairing can be, at maximal of the order 10-15% of the regular pairing strength, depending somewhat on the degeneracy of the proton and neutron shell-model spaces that are used for describing the various series of isotopes.

$Z \sim 40$		
Shell	Degeneracy	j
$Z = 40 - 50$	$\Omega_\pi = 5$	$j_\pi = 9/2$
$N = 50 - 64$	$\Omega_\nu = 7$	$j_\nu = 13/2$
$N = 50 - 82$	$\Omega_\nu = 16$	$j_\nu = 31/2$
$Z \sim 50$		
Shell	Degeneracy	j
$Z = 50 - 82$	$\Omega_\pi = 16$	$j_\pi = 31/2$
$Z = 50 - 64$	$\Omega_\pi = 7$	$j_\pi = 13/2$
$N = 50 - 82$	$\Omega_\nu = 16$	$j_\nu = 31/2$

Table 4.1 Degeneracies and associated single-j shell configurations for regions $Z \sim 40$ and $Z \sim 50$.

j_ρ	$\langle Q_\rho \rangle$	$\langle Q_\rho \rangle^2$	$\langle j_\rho \| Q_\rho \| j_\rho \rangle$	j_ρ	$\langle Q_\rho \rangle$	$\langle Q_\rho \rangle^2$	$\langle j_\rho \| Q_\rho \| j_\rho \rangle$
3/2	-3.10	9.62	-3.10	17/2	-3.45	11.92	-7.32
5/2	-3.31	11.00	-4.06	19/2	-3.45	11.94	-7.72
7/2	-3.38	11.46	-4.78	21/2	-3.45	11.96	-8.11
9/2	-3.41	11.67	-5.40	23/2	-3.46	11.97	-8.47
11/2	-3.43	11.78	-5.94	25/2	-3.46	11.98	-8.82
13/2	-3.44	11.85	-6.44	27/2	-3.46	11.99	-9.48
15/2	-3.44	11.89	-6.89	31/2	-3.46	12.00	-9.79

Table 4.2 Values for $\langle Q_\rho \rangle$, $\langle Q_\rho \rangle^2$ and $\langle j_\rho \| Q_\rho \| j_\rho \rangle$ (see expressions 4.23, 4.24 and 4.26) for j_ρ going from 3/2 to 31/2

$Z \sim 40$				
Shells	Mo	Cd	Ru	Pd
$\Omega_\pi = 5, \Omega_\nu = 16$	0.0062	0.0062	0.0093	0.0093
$\Omega_\pi = 5, \Omega_\nu = 7$	0.0059	0.0059	0.0079	0.0079
$Z \sim 50$				
Shells	Te	Xe	Ba	Ce
$\Omega_\pi = 16, \Omega_\nu = 16$	0.0091	0.017	0.0240	0.029
$\Omega_\pi = 7$, $\Omega_\nu = 16$	0.0036	0.006	0.0073	0.073

Table 4.3 Values of $\overline{C}$ (in MeV) for different nuclei and different mass regions.

The quadrupole constant $\overline{C}$ is over a factor from 5 to 25 smaller than the pairing constant G. Therefore, pairing and quadrupole interactions give rise to contributions to the binding energy that exhibit the same structure (except for some smaller corrections). This number dependence occurs through the common factor $(\Omega - N + 1)N$ with Ω the degenarcy of the shell that is filling up with identical nucleons.

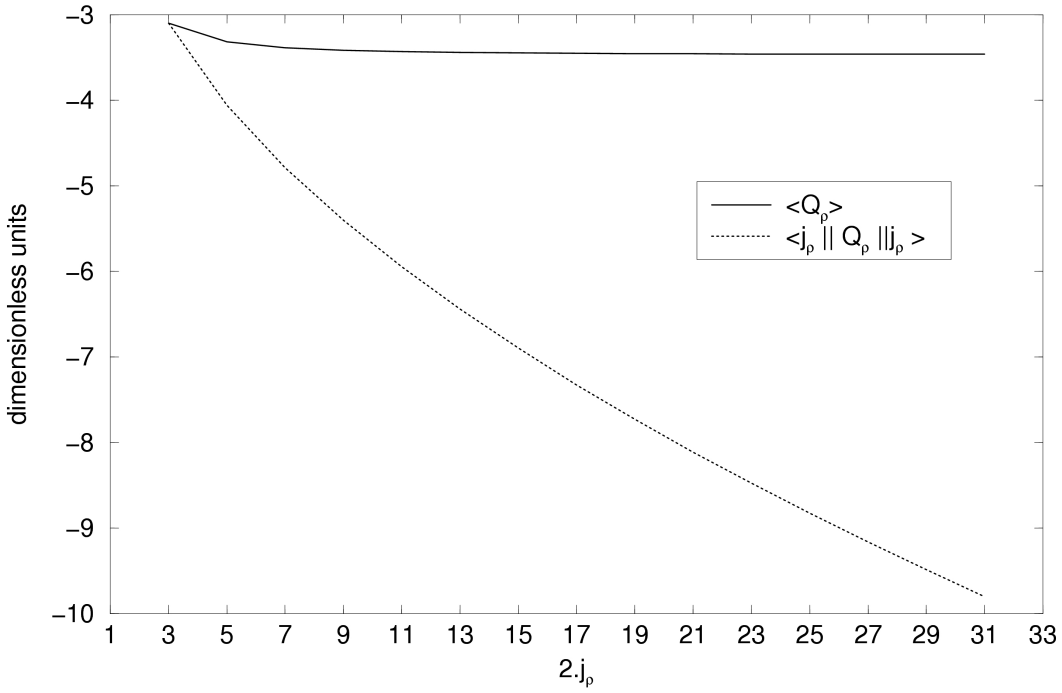

Figure 4.5 Plot of the values for $\langle Q_\rho \rangle$ and $\langle j_\rho \| Q_\rho \| j_\rho \rangle$ for j_ρ going from 3/2 to 31/2. As one can see, $\langle Q_\rho \rangle$ is nearly a constant for changing j_ρ.

4.2.4 Conclusion

In trying to understand the shell-model correlations amongst the nucleons outside of closed shells one can, at present, use large-scale shell-model calculations. From these studies, it becomes clear that the pairing force acting amongst identical nucleons and the proton-neutron low-multipole force components do form the essential elements that need to be incorporated, albeit in different ways of sophistication. In the present section, we have concentrated onto the salient features of the shell-model with nucleons (protons and neutrons, separately) filling single-j shell configurations, simplifying the residual interactions to pairing (identical nucleons) and considering the lowest-order effect of the proton-neutron quadrupole interaction.

It is shown that this latter effect renormalizes the pairing energy (between 5 to 25%). Thus, the proton-neutron quadrupole interaction, if one keeps within series of isotopes (or isotones) in the immediate vicinity of closed shells, creates an "implicit" pairing field to a very good approximation.

Chapter 5

Conclusion and Outlook

In the study of the nuclear many-body problem, several nuclear models have been developed over the years that are able to explain how nuclear structure evolves over large mass regions of the nuclear chart. Often, they are also able to give a detailed description of the properties of the individual nuclei. These models however, are fine-tuned to those regions of the nuclear chart where experimental information is available. Only after the 1990's, state-of-the-art experimental techniques such as Radioactive Nuclear Beams (RNB) have made it possible to also explore more exotic regions of the nuclear chart, such as regions with superheavy nuclei or exhibiting an unusual neutron-to-proton ratio. Extrapolating the predictions from the existing theoretical models towards these new exotic regions of the nuclear chart, often results in large contradictions with the experimental findings, and also between the theoretical predictions themselves. This raises the question whether we have effectively understood how protons and neutrons are organised within the atomic nucleus, and how nuclear structure depends on nuclear mass, nuclear excitation or rotational energy, ...

The study of the atomic nucleus contributes to the general understanding of several areas of interest in physics, as e.g. the understanding of the dynamics of many-body systems. Many-body systems have too many constituents to allow for an exact mathematical solution, but on the other hand, they have too few constituents for the application of statistical methods. The different approaches to the atomic nucleus (macroscopic, microcopic, application of symmetries, ...) can be applied to the many-body problems of other fields in physics as well. The interactions that are in play in the nuclear many-body problem are some of Nature's basic forces (the strong force, the weak force and the electromagnetic force). Studying their behaviour in the nuclear medium, might learn us about how the light elements, like D, ^{3}He,^{4}He,^{7}Li, have formed from a hot soup of subatomic particles, during the early moments of the Universe. All heavier elements have been (and are still being) produced in stars or in supernovae, usually involving very exotic

nuclei as crucial stepstones in the synthesis process. Only recently, large regions of new exotic nuclei on the nuclear chart came into the range of experimental facilities. Unclosing the Terra Incognita of the nuclear chart already showed new nuclear structure phenomena that theoretical models had not predicted. Neutron halo and neutron-skin nuclei are probably some of the best examples. The large number of theoretical publications that followed immediately upon these experimental discoveries, illustrates very well the spontaneous feedback that exists between theoretical and experimental nuclear physics.

Also the present research work was strongly inspired by recent results at the fore-fronts of experimental nuclear physics.

- A. Andreyev *et al.* reported in Nature on three coexisting nuclear shapes in the $^{186}_{82}$Pb isotope [14] and brought the "long-known" phenomenon of nuclear shape coexistence back to the fore-fronts of both experimental and theoretical nuclear physics. It challenged us to find a theoretical description that would be applicable to the whole $Z \sim 82$ region, where several isotope series are known to exhibit shape coexistence phenomena.

- High-resolution mass measurements have been carried out recently for the $Z \sim 82$ region, especially at ISOLTRAP (ISOLDE/CERN), using the Penning-trap technique. The unprecedented precision of typically 10^{-5} makes it possible to check nuclear masses for the presence of small local correlations that are expected to show up as a fingerprint for shape-coexistence effecs [15]. It challenged us to find a theoretical description that is able to incorporate these local structure effects in a coherent way into the global nuclear-mass.

The results obtained in the present study will now be reviewed in the light of the above two points.

Shape Coexistence in the neutron-deficient Pb isotopes

One of the reasons for the continuous theoretical interest in nuclei that exhibit coexisting shapes, is that the phenomenon arises because of inhomogeneities (shell or sub-shell gaps) in the single-particle level densities near the Fermi surface. Prediction of such multiple nuclear shapes therefore can serve as a sensitive test for the nuclear potentials in use, as well as for residual interactions. Nuclear shape coexistence phenomena have been observed all over the nuclear chart, especially near to the magic numbers of protons and neutrons [17]. The neutron-deficient lead isotopes show a particularly interesting and spectroscopically rich situation, with an energy spectrum where three different families of excited states coexist at low energies.

Several approaches have been used to interprete this complex spectroscopy. In a **mean-field approach**, the spectra of the Pb isotopes are understood as reflecting several competing minima in an axial quadrupole energy landscape, corresponding to spherical, oblate (disk shaped) and prolate (cigar shaped) deformations (see fig. 1.9). However, as M. Bender *et al.* remark, in the neutron-deficient Pb region, shape coexistence can not be completely described at the level of mean-field models [20]. The minima obtained as a function of the quadrupole moment are often shallow and it is not clear *a priori* whether they will survive dynamical effects such as quadrupole vibrations. Pure **phenomenological shape mixing** has also been used as an approach to interprete the experimental findings. In this model, the physically observed states are the results of the interaction between the several configuration. They are thus a superposition of spherical, oblate and prolate configurations, where the relative weights in the mixing are determined by a fit to the experimental data. [18]. In the **shell-model picture**, the three different families of excitation states are generated by two-particle two-hole (2p-2h) and four-particle four-hole (4p-4h) proton excitations across the $Z = 82$ shell gap mainly, next to the regular configuration with a closed proton shell. The excitation energies of the proton multi-particle multi-hole (mp-mh) states are lowered by the residual quadrupole-quadrupole interaction. From this point of view, the mean-field oblate minimum can be associated with the proton 2p-2h configuration, and the prolate one with proton 4p-4h states. Many-particle many-hole excitations can not easily be handled in full-scale shell-model calculations, in particular, for the large model spaces required for the description of heavy open-shell nuclei. They are, therefore, treated with the help of algebraic models like the **Interacting Boson Model** (IBM).

We have followed the latter approach in chapter 2, where we have associated the proton 0p-0h, 2p-2h and 4p-4h excitations across the $Z = 82$ closed proton shell, by configurations with N, $N + 2$ and $N + 4$ bosons, respectively. Parameters associated with the proton mp-mh excitations have been fitted to the neighbouring Pt and W isotopes, exploiting the Intruder-spin (I-spin) symmetry, and allow an important restriction on the number of parameters. This approach is promising to describe the nuclear shape coexistence phenomenon for the whole $Z \sim 82$ region within the same framework, and can offer a fruitful line of research for the near future. Also from the pure theoretical point of view, the I-spin symmetry leads to the more complicated but very interesting non-compact algebraic $U(6,6)$ group, that partly has been explored in its nuclear context in a series of papers [81, 82, 83, 84]. This clearly deserves a deeper investigation. The final results offer a reasonably good description of the observed bands and their variation with mass number A (see fig. 2.4).

Our choice of parameters seem to be confirmed by recent calculations for the neutron-deficient Pb isotopes, using the boson coherent-state approach, carried out by C. Vargas *et al.* [99]. Starting from the IBM parameters as deduced in chapter 2 (table 2.1), a Potential Energy Surface (PES) is calculated that resembles very

well those obtained within a mean-field approach (compare fig. 5.1(d) with fig. 1.9). Only the mixing strength as deduced in chapter 2 (parameters α and β in table 2.1) appeared to be too large, as only two (spherical and prolate) of the three minima remain in the final PES surface (fig 5.1). However, the precise strength of the mixing between different coexisting configurations, is a theoretical question that is still unanswered, also in other mass regions. In this boson coherent-state approach, it appears that a reduction of the mixing strength, again leads to three minima in the Potential Energy Surface of fig. 5.1(d), which otherwise is very similar in appearance to the surface shown in fig. 1.9(d).

We have already started investigations into the precise role of the mixing in the neutron-deficient lead isotopes, concentrating on the ^{188}Pb isotope, where recently more experimental information on electromagnetic transition rates has become available [18]. B(E2)-values, not incorporated yet in the study of chapter 2, are expected to give more insight in the nature of the physically observed nuclear energy levels. The low-lying excited states in the neutron-deficient lead isotopes appear as rather strongly mixed states, so that their identification as primarly regular, primarly 2p-2h or primarly 4p-4h becomes extremely difficult. Electromagnetic E2 transition rates can therefore serve as a good guideline to classify excited states into a band, following the simple fact that intra-band E2 transitions (transition rates between excited states within the same band) should always be much stronger than inter-band E2 transitions (transitions between excited states from different bands). A comparison between the experimental energy spectrum and the theoretical one for ^{188}Pb is shown in fig. 5.2. The former IBM-mixing program, which we used to carry out the calculations described in chapter 2, only gave the total B(E2) transition rates between the final nuclear states. The IBM-mixing program has been modified so that it now becomes possible to trace back the contributions from the different configurations in each electromagnetic transition (E0, E2, ...). It is interesting to study how the situation looks like in the adjacent neutron-deficient Pb isotopes. This clearly deserves a more thorough study, which will be addressed in the near future, and falls out of the scope of the present work.

Local correlations in the global nuclear-mass behaviour: a consistent description

Models that study nuclear masses all over the chart of isotopes have evolved from liquid drop studies, over macroscopic-microscopic models, towards - in the last years - Hartree-Fock and Hartree-Fock-Bogoliubov studies. Recently, the precision with which mass measurements are carried out, has improved a lot. Even for nuclei far from stability, as e.g. the neutron-deficient nuclei in the Pb region, mass measurements now are able to show small local correlations, of only some hundreds of keV. These data give important information about specific nuclear structure effects (local areas of deformation, nuclear shape coexistence, ...).

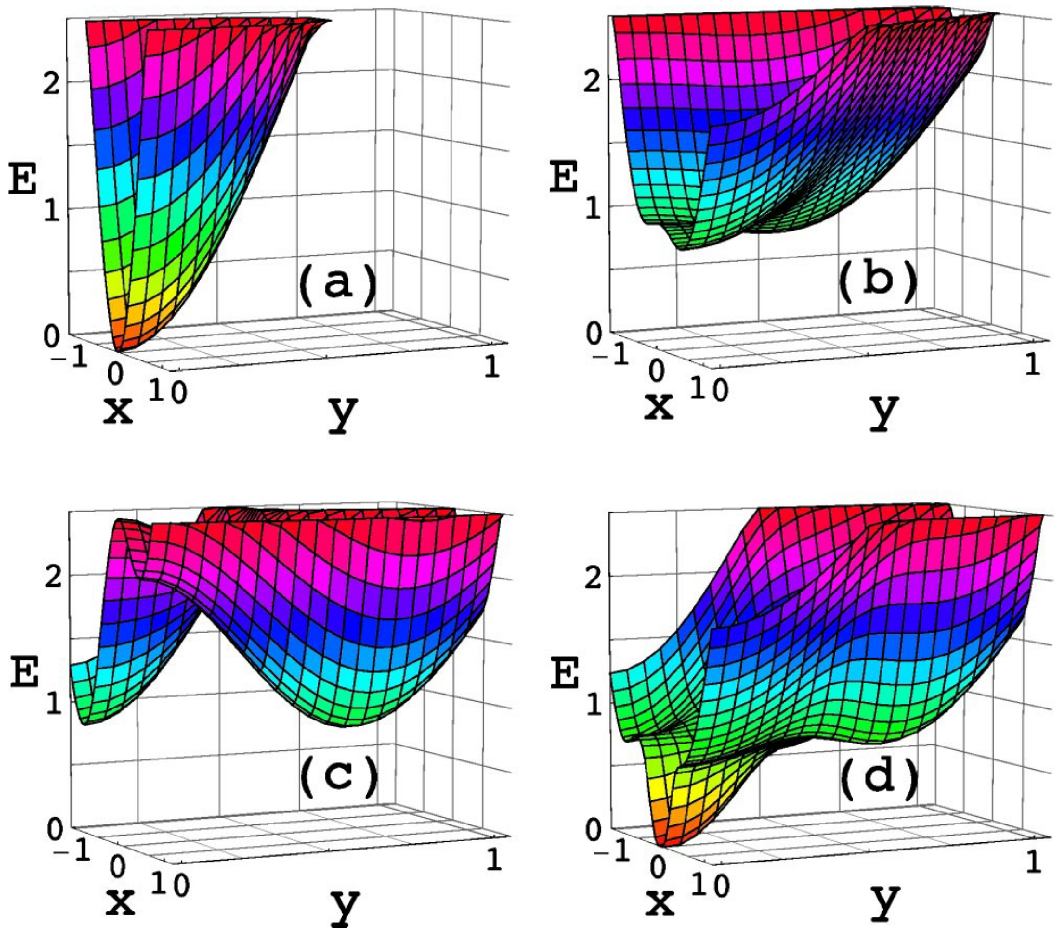

Figure 5.1 Potential energy surfaces (PES) for ^{186}Pb within the approach of the boson coherent-states, where the deformation parameters $x \equiv \beta\sin(\gamma{+}30^\circ)$ and $y \equiv \beta\cos(\gamma{+}30^\circ)$ run from -1 to 1, and 0 to 1, respectively. The vertical axis gives the nuclear excitation energy in MeV. The four plots show (a) the 0p-0h configuration before mixing, (b) the 2p-2h configuration before mixing, (c) the 4p-4h configuration before mixing, and (d) the lowest eigenpotential of after mixing. Compare with the PES results in fig. 1.9 from a recent mean-field approach. Taken from [99].

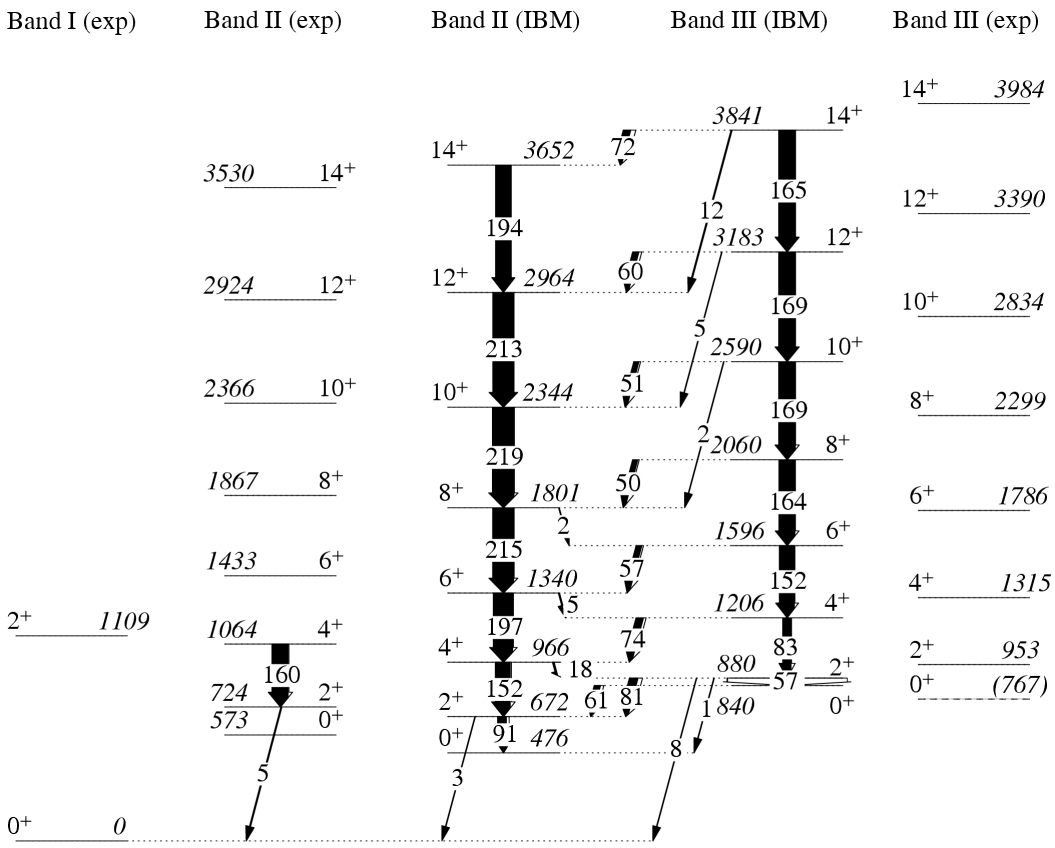

Figure 5.2 Experimental and theoretical (IBM) level scheme for the 2p-2h and 4p-4h bands in ^{188}Pb. From left to right, the experimental 4p-4h, the IBM 4p-4h, the IBM 2p-2h and the experimental 2p-2h bands are reproduced. The arrows denote the B(E2)-values for a given transition, expressed in e^2b^2. Taken from [192].

A realistic study of these local correlations requires detailed shell-model calculations, which cannot be carried out easily for open-shell nuclei with a large number of valence nucleons, especially for the large model spaces required. However, schematic interactions have been constructed within the context of the nuclear shell model that give adequate descriptions of the energy spectra in the vicinity of closed shells. In chapter 4, the local contributions to the nuclear binding energy coming from some of the most widely used schematic interactions are studied. In section 4.1 we studied the pairing force and the delta-interaction. Although these two forces describe nuclear excited states in a similar way, we came to the conclusion that the way in which they contribute to the nuclear binding energy is very different. As the pairing force scales with the number of free pairs in an orbital, the contribution to the nuclear binding energy will maximize at mid-shell and decrease past mid-shell. The use of the pairing force thus turns out to be a poor choice when studying binding energy variations over a number of single-particle orbitals. On the other hand, for a delta-interaction, which scales with the total number of particles in a orbital, the contribution to the binding energy increases linearly when filling the orbital. The differences between the two interactions could show to be significant when studying long isochains of isotopes. In section 4.2 the contributions to the nuclear binding energy from the pairing force and the proton-neutron quadrupole interaction are studied. It appears that the contribution from the proton-neutron quadrupole interaction has the same dependence on the number of valence pairs in an orbital as the contribution from the pairing force. To a first approximation, the proton-neutron quadrupole interaction will result in a "renormalization" of the strength of the pairing force. In a further study, it will be interesting to check how well this "normalized" pairing force describes pair excitations in heavy nuclei, and how well it can describe local correlations in the behaviour of experimental nuclear binding energies.

A way to circumvent the numerical problems of large-scale shell-model calculations in heavy nuclei is offered by the symmetry-based truncation of the shell-model basis space within the Interacting Boson Model (IBM). The IBM is able to give a good description of the low-energy part of nuclear energy spectra, even in those regions of the nuclear chart where it is know that nuclear structure changes rapidly, as e.g. in regions with nuclear shape transitions or shape coexistence (see chapter 2). It has been pointed out recently that nuclear ground-state properties (masses, binding energies, separation energies, ...), that are often omitted in an IBM analysis, are important to determine the most appropriate Hamiltonian in the description of a given isotope series. This is especially the case where otherwise there might be a certain parameter freedom (see fig. 1.10 and 1.11). In chapter 3 a procedure is described within the IBM, that starts from simultaneously treating binding energies and excitation energies, to give a consistent description of both the global nuclear mass behaviour and the local deviations that contain detailed nuclear structure information. Some technical problems are addressed that

arise at neutron mid-shell, where one changes from a parametrization using boson-particles to a parametrization using boson-holes. In the second part of chapter 3, applications of the model have been presented for the 50-82 shell, where we have concentrated on local modifications of the otherwise smooth behaviour of the nuclear binding energies, that come from the presence of low-lying intruder states at and near closed shells. These effects are discussed both within an IBM configuration mixing approach, as well as implicitely within the macroscopic-microscopic model, using potential energy surface calculations (PES). Nuclear mass measurments are becoming increasingly important, since they now have progressed to the level of testing microscopic studies (shell-model effects, local zones of deformation, configuration mixing or shape mixing that shows up in the nuclear ground state, ...). This will clearly become an important line of research in the near future.

Chapter 6

Nederlandstalige Samenvatting

In de studie van het veeldeeltjessysteem van de atoomkern, zijn door de jaren heen verschillende theoretische modellen ontwikkeld, die in staat zijn te verklaren hoe de structuur van de kern evolueert doorheen grote massagebieden van de nuclidenkaart. Vaak zijn ze ook in staat om een gedetailleerde beschrijving te geven van eigenschappen van individuele atoomkernen. Deze modellen zijn echter opgesteld voor die gebieden van de nuclidenkaart waarvan we experimentele informatie hebben. Pas na 1990, toen het mogelijk werd om bundels van radioactieve kernen te produceren (RNB) met deeltjesversnellers, werden grote gebieden van de "Terra Incognita" van de nuclidenkaart bereikbaar. Dit zijn gebieden van de nuclidenkaart met superzware en zeer kortlevende kernen (op dit moment is men gekomen tot isotopen met Z=115), of kernen met een extreme neutron-proton verhouding. Extrapolaties van de voorspellingen van de bestaande theoretische modellen naar deze "exotische" gebieden van de nuclidenkaart, leveren niet steeds betrouwbare resultaten. Wat de massa van deze atoomkernen betreft treden vaak grote afwijkingen op in vergelijking met de meest recente experimentele gegevens, en vertonen de verschillende theorieën geen convergentie voor wat betreft de voorspelde kernmassa's. Dit wijst op een duidelijk gebrek in onze kennis van de kernkracht in atoomkernen met extreem groot aantal neutronen en/of protonen in vergelijking met de kernen in de onmiddelijke omgeving van de stabiliteitslijn.t

De studie van de atoomkern draagt bij tot het algemene begrip van diverse vakgebieden in de fysica, zoals bijvoorbeeld de dynamica van veeldeeltjessystemen, waar de atoomkern een specifiek voorbeeld van is. In de atoomkern is (afgezien van de heel lichte atoomkernen tot masse A=12) het niet mogelijk om met hedendaagste technieken een exacte wiskundige oplossing van het eigenwaardeprobleem te bekomen. Anderzijds bevat de gemiddelde atoomkern te weinig deeltjes om op een betrouwbare manier statistische methodes toe te passen. De verschillende benaderingen die gebruikt worden bij de studie van de atoomkern (macroscopisch, microscopisch, symmetrieën, ...) kunnen ook toegepast worden in an-

dere gebieden van de fysica. De interacties die een rol spelen in de studie van de samenhang en de stabilititeit van de atoomkern zoals de sterke kernkracht, de electromagnetische en zwakke wisselwerkingen) vormen drie van de vier fundamentele krachten van de Natuur. Een studie van hoe deze fundamentele krachten zich gedragen in de atoomkern, kan ons leren hoe de lichte elementen zoals D, ^{3}He,^{4}He,^{7}Li ontstaan zijn uit de "hete soep" van subatomaire deeltjes tijdens de eerste momenten van de vorming van het heelal. Alle zwaardere elementen zijn geproduceerd (en worden nog steeds geproduceerd) in sterren of in supernovae. In deze synthese-processen spelen exotische kernen, die op aarde niet bestaan, vaak een cruciale rol. Het artificieel produceren van deze exotische kernen, hun experimentele studie en de ontwikkeling van aangepaste theoretische modellen, draagt dus rechtstreeks bij tot het vakgebied van de Nucleaire Astrofysica, en tot een beter begrip van hoe alle materie onstaan is.

Het hier beschreven theoretische onderzoekswerk is sterk geïnspireerd door een aantal belangrijke recente resultaten in de experimentele kernfysica:

- A. Andreyev *et al.* publiceerden recent in Nature resultaten over het bestaan van drie co-existerende kernvormen in de $^{186}_{82}$Pb atoomkern [14], en brachten zo het fenomeen van kernvorm coëxistentie weer volop in de experimentele en theoretische belangstelling. Het blijkt namelijk dat een beperkte herschikking van protonen doorheen de proton gesloten schil bij Z=82 in staat is om aanleiding te geven tot de vorming van collectieve banden. In het specifieke geval van de $^{186}_{82}$Pb isotoop vormen de grondtoestand en de eerste twee aangeslagen toestanden (een triplet van 0^{+} toestanden) vermoedelijk drie fundamenteel verschillende configuraties in de atoomkern In een beschrijving die gebruik maakt van van macroscopische kernmodellen worden verschillende configuraties geassocieerd met drie verschillende kernvormen (zie fig. 1.9). Deze experimentele resultaten vormden een van de aanleidingen teneinde een theoretische beschrijving te geven van deze fenomenen die toepasbaar zou zijn voor het volledige $Z \sim 82$ gebied, waarvan bekend is dat verschillende isotopenreeksen (o.a. de Pt,Hg en Po isotopen) gelijkaardige kernvorm coëxistentie verschijnselen vertonen. Dit theoretische model wordt uitgebreid beschreven in hoofdstuk 2.

- Kernmassa metingen met een zeer hoge resolutie zijn recent uitgevoerd voor het $Z \sim 82$ gebied, voornamelijk aan de ISOLTRAP opstelling (CERN), gebruik makend van de Penning-trap techniek. De ongeëvenaarde precisie van 10^{-5} maakt het mogelijk om kernmassa's te bepalen zodat het mogelijk wordt om lokale onregelmatighenden in het voor de rest zeer globaal verloop te bestuderen (men noemt dit ook lokale correlaties). Deze lokale correlaties leveren dan ook extra informatie over het verschijnsel van kernvorm coëxistentie dat optreedt in dit massagebied van de nuclidenkaart [15]. Een theoretische

beschrijving van de kernmassa, waarin het globale aandeel en het lokale aandeel op een consistente manier beschreven worden, is dan wel noodzakelijk. Strutinsky was de eerste om een dergelijke consistente beschrijving te realiseren. In diezelfde geest stellen wij in hoofstuk 3 een consistente kernmassa beschrijving voor.

In de volgende paragrafen worden de onderzoeksresultaten van dit werk beknopt samnengevat in het licht van de bovengenoemde twee type experimenten.

Kernvormcoëxistentie in de neutron-arme loodisotopen

Een reden voor de grote interesse in kernen die co-existerende vormen vertonen, is dat het fenomeen ontstaat door inhomogeniteiten in de energieverdeling van de orbitalen die de nucleonen beschrijven in hun beweging in de atoomkern. De orbitalen vertonen een zogenaamde schillenstructuur met een aantal "shell gaps" daartussen. Het is mogelijk deze schillenstructuur te beschrijven aan de hand van een centrale potentiaal (fenomenologische potentialen of gebruik maken van Hartree-Fock technieken). Het aandeel van de effectieve nucleon-nucleon interacties, dat niet inbegrepen is in dit gemiddelde veld, wordt veelal beschreven met behulp van schematische residuele interacties (zoals een paarkracht en de kwadrupool-kwadrupoolwisselwerking, of vertrekkend van meer realistische effectieve interacties). Theoretische voorspellingen of beschrijvingen van kernvorm coëxistentie fenomenen vormen daarom een goede test van de bestaande modellen. Kernvorm coëxistentie is waargenomen in verschillende gebieden van de nuclidenkaart, voornamelijk dichtbij de "magische" proton- en neutronaantallen. De neutron-arme loodisotopen vertonen bijzonder interessante eigenschappen: in de meest neutron-arme kernen (in de buurt van N=104) werden drie verschillende families van ge$'$exciteerde toestanden (collectieve bandenstructuren) in hetzelfde energiegebied waargenomen wat op het bestaan van co-existerende toestanden kan wijzen. Verschillende theoretische modellen kunnen gebruikt worden om deze energiespectra te begrijpen.

In de **gemiddelde veld** benadering, worden de energiespectra van de loodisotopen beshreven als de excitaties geassocieerd met verschillende minima in een axiaal-symmetrisch kwadrupool gedeformeerd energielandschap. Deze minima corresponderen respectievelijk met een sferische, oblate (frisbee-vormig) en prolate (sigaar-vormig) deformaties (zie fig. 1.9). Het is echter niet mogelijk (ref. M. Bender *et al.*) de waargenomen eigenschappen van de neutronarme loodisotopen te beschrijven enkel op basis van de statische eigenschappen van het gedeformeerde gemiddelde veld. De minima die bekomen worden als een functie van de deformatie zijn veelal ondiep, en het is niet *a priori* duidelijk of deze minima dynamische effecten zoals kwadrupoolvibraties,paarexcitaties,... zullen overleven. Er werd eveneens gebruikt gemaakt van zuiver **fenomenologische kernvorm-menging** als een

methode om de experimentele resultaten te beschrijven. In deze benadering worden de fysisch geobserveerde toestanden geïnterpreteerd als de resultaten van een menging tussen de verschillende zuivere configuraties. Elke geëxciteerde toestand van de kern wordt dus beschreven als een superpositie van de sferische, oblate en prolate configuraties, waarin de relatieve gewichten bepaald worden door een fit aan de experimentele gegevens. Het is echter ook mogelijk om, startend van het kernschillenmodel, het onstaan de drie verschillende families te beschrijven indien men ook toelaat dat de Z=82 romp kan opgebroken worden. Daarbij laat men toe dat zowel proton twee-deeltje twee-gat (2p-2h) las proton en vier-deeltje vier-gat (4p-4h) excitaties optreden, excitaties die in eerste instantie kunnen coexisteren met de "reguliere" configuratie met een afgesloten protonschil. De excitatie-energie van de proton veel-deeltje veel-gat ($\mathfrak{m}$mp-$\mathfrak{m}$h) toestanden neemt sterk af als gevolg van de residuele proton-neutron kwadrupoolinteractie. Vanuit dit gezichtspunt is het mogelijk het gemiddelde-veld oblate minimum (met een kleinere evenwichtsvervorming in vergelijk met de prolate kernvorm) te associeren met de proton 2p-2h configuratie en het prolate minimum met de proton 4p-4h configuratie. Veel-deeltje veel-gat excitaties kunnen niet eenvoudig behandeld worden in het raamwerk van het kernschillenmodel, voornamelijk omdat een bijzonder grote basisruimte vereist is om kernen met open proton en neutron schil en tevens met een groot aantal valentienucleonen te beschrijven en berekeningen numeriek onhaalbaar worden. Zulke berekeningen, vanuit een analoog microscopisch gezichtspunt, kunnen wel behandeld worden met algebraïsche modellen zoals het **Interagerende Bosonmodel** (IBM) waarin een truncatie van de uitgebreide modelruimte uitgevoerd wordt op basis van interagerende s en de boson (kunnen geassocieerd worden met de $J^\pi = 0^+$ en $J^\pi = 2^+$ nucleonen paren in de atoomkern) (symmetrie-truncatie).

In dit onderzoekswerk hebben we daarom gebruik gemaakt van de mogelijkheden van het Interagerend Bosonmodel om enorme modelruimtes te trunceren met behoud van de meest belangrijke vrijheidsgraden. Hierdoor is het mogelijk om de reguliere aangeslagen toestanden, de proton twee-deeltje twee-gat toestanden, en de proton vier-deeltje vier-gat toestanden te associeren met configuraties in het IBM-model met N, $N + 2$ en $N + 4$ bosonen, respectievelijk. De parameters voor de proton veeldeeltje-veelgat geassocieerde excitaties hebben we gefit aan de hand van de nabijliggende Pt en W isotopenreeksen. Daarvoor hebben we gebruik gemaakt van een specifieke symmetrie die in een uitgebreide versie van het IBM aanwezig is nl. Indringerspin symmetrie (I-spin). Het opleggen van deze symmetrie leidt tot een grote restrictie in het aantal parameters. Deze benadering is veelbelovend om het fenomeen van kernvorm coëxistentie doorheen het volledige $Z \sim 82$ gebied te beschrijven binnenin eenzelfde theoretisch raamwerk, en kan een vruchtbaar onderzoeksgebied vormen voor de nabije toekomst. Ook vanuit een puur theoretisch gezichtspunt vormt de I-spin een interessant studieonderwerp. Een volledige algebraïsche uitwerking leidt tot de niet-compacte $U(6,6)$ groep, die

in zijn nucleaire context al verkend is, maar die een meer diepgaand onderzoek vereist. Het uiteindelijke resultaat van de IBM berekeningen levert een behoorlijk goede beschrijving van de geobserveerde bandstructuur, en van het verloop in energie van de verschillende aangeslagen toestanden als functie van het neutron aantal N (zie fig. 2.4 voor een vergelijking van de experimentele gegevens en de theoretische beschrijving).

De parameterkeuze binnen de hier uitgevoerde IBM-benadering lijkt te worden bevestigd door een recente theoretische studie van C. Vargas *et al.* waarbij gebruikt gemaakt wordt van boson coherente toestanden voor de ^{186}Pb isotoop. Startend van de IBM parameters die we afgeleid hebben in hoofdstuk 2, wordt een energieoppervlak verkregen dat een zeer grote gelijkenis vertoont met de energieoppervlaken verkregen binnen een gemiddeld-veld benadering (vergelijk fig. 5.1 met fig. 1.9). De sterkte van de menging tussen de verschillende co-existerende configuraties blijft evenwel onduidelijk, maar dit is een theoretisch vraagstuk dat in andere massagebieden evenmin opgeklaard is. In de benadering van de boson coherente toestanden, blijkt het dat met de mengingsterkte zoals wij die oorspronkelijk bepaald hebben, maar twee (sferisch en prolaat) van de oorspronkelijke drie minima overleven. Een reductie van de mengingsterkte leidt opnieuw tot drie coexisterende minima. De reden voor deze reductie zijn niet duidelijk op dit moment.

We reeds gestart met verder onderzoek naar de precieze rol van de opmenging in de neutronarme loodisotopen tussen de verschillende waargenomen collectieve banden die werden waargenomen. We concentreren ons vooral op de ^{188}Pb isotoop aangezien recente experimenten erin geslaagd zijn om meer spectroscopische informatie te bepalen, en vooral informatie over de E2 en E0 overgangswaarschijnlijkheden tussen de verschillende geëexciteerde toestanden te bepalen van dit zeer onstabiele isotoop. Overgangswaarschijnlijkheden, voornamelijk B(E2) informatie, waren nog niet in overweging genomen in hoofdstuk 2, maar zullen ongetwijfeld een beter inzicht geven over de waargenomen banden in dit isotoop (met name in welke mate we ze kunnen klasseren volgens een 0p-0h, 2p-2h of 4p-4h configuratie hierarchie). De laagliggende aangeslagen toestanden van de neutron-arme loodisotopen kunnen namelijk zodanig opgemegd worden, dat een eenvoudige labeling bijzonder moeilijk wordt. E2 overgangswaarschijnlijkheden vormen daarbij een interessant criteriumn om aangeslagen toestanden in de 'juiste' band onder te brengen, uitgaande van de overweging dat intra-band overgangen (overgangen tussen toestanden van dezelfde band) altijd groter moeten zijn dan inter-band overgangen (overgangen tussen toestanden van verschillende banden). Een rangschikking van de aangeslagen toestanden van ^{188}Pb volgens dit criterium wordt geillustreerd in fig. 5.2, waar de experimentele informatie vergeleken wordt met de theoretische resultaten. Een verder onderzoek naar deze situatie, en de evolutie van deze toestanden in de andere neutronarme loodisotopen zal een vruchtbaar onderzoeksdomein vormen in de nabije toekomst.

Lokale correlaties in het globale verloop van de kernmassas: naar een consistente theoretische beschrijving

In de studie naar het verloop van de kernmassa doorheen de nuclidenkaart, zijn de gebruikte modellen geëevolueerd van studies binnen het vloeistofdruppelmodel, naar macroscopisch-microscopische modellen, tot - heel recent - Hartree-Fock en Hartree-Fock-Bogoliubov modellen. In de laatste jaren is de precisie waarmee experimentele massametingen uitgevoerd kunnen worden zeer sterk toegenomen. Zelfs voor kernen ver van de stabiliteit, zoals bv. de neutronarme isotopen in het loodgebied, zijn nu kleine lokale variaties zichtbaar van maar enkele honderden keV. Deze experimentele data geven erg waardevolle informatie over specifieke kernstructuureffecten zoals lokale gebieden van kerndeformatie, kernvormcoëxistentie, ...

Een realistische studie van deze lokale correlaties vereist gedetailleerde schillenmodelberekeningen. Zulke berekeningen zijn niet eenvoudig uitvoerbaar voor kernen met een groot aantal valentienucleonen buiten gesloten schillen configuraties (waarbij zowel protonen als neutronen actief zijn), vooral vanwege de enorm grote basisruimten die dan kunnen optreden. Binnen het raamwerk van het schillenmodel zijn echter een aantal schematische interacties geconstrueerd die een adequate beschrijving geven van de belangrijkste eigenschappen van atoomkernen bij lage excitatie-energie, voor nucleonen aantallen in de nabijheid van gesloten schillenconfiguraties blijft. In hoofdstuk 4 hebben we bestudeerd hoe de meest gebruikte schematische interacties bijdragen tot de nucleaire bindingsenergie. In paragraaf 4.1 hebben we de paarkracht en de delta-interactie vergeleken. Alhoewel beide interacties gelijkaardige energiespectra beschrijven, blijkt toch dat deze schematische interacties op een totaal verschillende manier bijdragen tot de nucleaire bindingsenergie. Het is namelijk zo dat de bijdrage tot de bindingsenergie bij gebruik van een paarkracht afhangt van het aantal vrije paren in een orbitaal. Hierdoor maximaliseert de bijdrage tot de bindingsenergie in de nabijheid van een halfgevuld orbitaal (mid-shell), waarna de bijdrage weer afneemt bij het verder opvullenn van de orbitaal. Hieruit kunnen we concluderen dat een paarkracht een minder geschikte keuze is voor een schematische interactie als men de de bindingsenergie wil bestuderen in een gebied waarbij nucleonen opeenvolgende nucleonorbitalen gaan bezetten. Bij het gebruik van een delta-interactie daarentegen neemt de bindingsenergie lineair toe met het totale aantal nucleonen in een gegeven orbitaal. De verschillen tussen beide interacties kunnen belangrijk zijn bij een studie van lange isotopenreeksen. In paragraaf 4.2 hebben we een analoge vergelijkende studie gemaakt voor de paarkracht en de proton-neutron kwadrupoolwisselwerking. Het blijkt dat de bijdrage tot de bindingsenergie als gevolg van de extra proton-neutron kwadrupoolwisselwerking op dezelfde manier afhangt van het aantal valentieparen doorheen een orbitaal als de bijdrage afkomstig van de paarkracht zelf. In een eerste benadering zal de proton-neutron kwadrupoolwis-

selwerking dus aanleiding geven tot een ”renormalisatie” van de sterkte van de paarkracht. In een voortgezette studie zal het interesant zijn na te gaan hoe goed deze ”genormaliseerde” paarkracht bijdraagt tot een beschrijving van paar-excitaties in zware kernen, en ook hoe lokale correlaties in het verloop van experimentele bindingsenergieën kunnen beschreven worden.

Een mogelijke manier om de numerieke problemen bij het uitvoeren van uitgebreide kernschilberekeningen op een zinvolle wijze te benaderen, bestaat in het toepassen van een truncatie van de schillenmodel basisruimte en dit geïnspireerd op de symmetrie eigenschappen die eigen zijn aan het kernsysteem. Een voorbeeld van een elegante truncatie is het Interagerend Bosonmodel (IBM). Het IBM geeft een goede beschrijving van de lage-energie aangeslagen toestanden, ook in die gebieden van de nuclidenkaart waar het aangetoond is dat de kernstructuur zeer snel varieert, zoals bijvoorbeeld in gebieden met kernvormtransities of kernvormcoëxistentie (zie hoofstuk 2). Bij de analyse van een gegeven atoomkern binnen het raamwerk van het IBM, worden de verschillende grondtoestandseigenschappen (zoals bv. de kernmassa (of de bindingsenergie, of de verschillende separatie-energieën, ...)) zeer niet in rekening gebracht. Men beschouwt enkel de specifieke energiespectra, relatief ten opzichte van de grondtoestand. Onlangs heeft men echter opgemerkt dat deze grondtoestandseigenschappen belangrijk zijn bij de bepaling van de meest geschikte Hamiltoniaan, zeker in gevallen waar een zekere parametervrijheid kan optreden (zie bv. de figuren 1.10 en 1.11). In hoofdstuk 3 wordt een procedure voorgesteld en uitgewerkt om, binnen het raamwerk van het IBM, een consistente beschrijving te geven van de aangeslagen toestanden, zowel als van de grondtoestandseigenschappen (vooral de massa) van de kern. Deze beschrijving maakt het ook mogelijk om gelijktijdig de globale evolutie van de bindingsenergie evenals de lokale variaties (afkomstig van specifieke kernstructuureffecten) te beschrijven. Bij de gevolgde benadering treden een aantal technische problemen in atoomkernen waarbij het aantal valentienucleonen precies overeenkomt met een halfgevulde kernschil. Deze problemen zijn afkomstig van de parametrisatie die deeltjes gebruikt in de eerste helft van de schil, maar gaten in het tweede deel van de schil. In het tweede deel van hoofdstuk 3 wordt uitgebreid ingegaan op toepassingen van dit model voor het gebied van de zeldzame aarden. Hierbij hebben we ons vooral geconcentreerd op de beschrijving van de lokale variaties in het voor de rest zeer globale gedrag van de nucleaire bindingsenergieën. Bij deze lokale variaties is veel belang gehecht aan de effecten van kernvormcoëxistentie in het loodgebied (gezien de recente maasametingen uitgevoerd aan de ISOLTRAP (ISOLDE/CERN) meetopstelling). De resultaten van onze IBM berekeningen worden vergeleken met de voorspellingen van een macroscopisch- microscopische benadering waarbij massa's bepaald worden aan de hand van het absolute energieminimum in de potentiële energieoppervlakken (PES). Experimentele kernmassametingen worden hoe langer hoe belangrijker, omdat de bereikte precisie het nu mogelijk maakt om microscopische modellen te

testen op hun betrouwbaarheid bij de beschrijving van kernvormdeformaties, configuratiemenging en kernvormmenging en de effecten ervan voor de grondtoestand van de kern,... Dit zal zeer duidelijk een belangrijke piste worden voor verder onderzoek.

Publications

The results presented in this work have been published and presented in the following papers

- S. Schwarz, F. Ames, G. Audi, D. Beck, G. Bollen, C. De Coster, J. Dilling, O. Engels, R. Fossion, J.-E. Garca-Ramos, S. Henry, F. Herfurth, K. Heyde, A. Kellerbauer, H.-J. Kluge, A. Kohl, E. Lamour, D. Lunney, I. Martel, R. B. Moore, M. Oinonen, H. Raimbault-Hartmann, C. Schneidenberger, G. Sikler, J. Szerypo, C. Weber and the ISOLDE Collaboration, *Accurate masses of neutron-deficient nuclides close to Z=82*, Nucl. Phys. **A693** (2001) 533.

- J.E. Garca-Ramos, C. De Coster, R. Fossion and K. Heyde, *Two-neutron separation energies, binding energies and phase transitions in the interacting boson model*, Nucl. Phys. **A688** (2001) 735.

- R. Fossion, C. De Coster, J.-E. Garca-Ramos, T. Werner and K. Heyde, *Nuclear Binding Energies: Global collective structure and local shell-model correlations*, Nucl. Phys. **A697** (2002) 703.

- R. Fossion, C. De Coster, J.-E. Garca-Ramos and K. Heyde, *Proton-neutron quadrupole interactions: An effective contribution to the paring field*, Phys. Rev. **C65** (2002) 044309.

- K. Heyde, R. Fossion, J.-E. Garca-Ramos, C. De Coster and R. F. Casten, *Differences between pairing and zero-range effective interactions for nuclear binding energies*, Eur. Phys. J. **A13** (2002) 401.

- R. Fossion, C. De Coster, J.-E. Garca-Ramos, T. Werner and K. Heyde, *Nuclear Binding Energies: Global collective structure and local shell-model correlations*, Proc. Of the 3rd International Conference on Exotic Nuclei and Atomic Masses ENAM, Hmeenlinna, Finland, july 2001, eds. J. yst, P. Dendooven, A. Jokinen and M. Leino, Springer-Verlag Berlin Heidelberg (2003), p. 19

- R. Fossion, *Coexistence des formes nuclaires diffrentes dans les isotopes de Pb*, Proc. Of the Journes Jeunes Chercheurs, Aussois, France, december 2002, p. 199

- R. Fossion, K. Heyde, G. Thiamova and P. Van Isacker, *Intruder bands and configuration mixing in the lead isotopes*, Phys. Rev. **C67** (2003) 024306.
- R. Fossion, K. Heyde, G. Thiamova and P. Van Isacker, *Intruder bands and configuration mixing in the lead isotopes*, Proc. Of the 11th International Symposium on Capture Gamma-Ray Spectroscopy and Related Topics, Pruhonice near Prague, Czech Republic, september 2002, eds. J. Kvasil, P. Cejnar and M. Krtika, World Scientific, New Jersey, London, Singapore, Hong Kong (2003), p. 164

Bibliography

[1] K. Heyde, *Basic Ideas and Concepts in Nuclear Physics*, Institute of Physics Publishing, Bristol and Philadelphia, 2nd edition (1994).

[2] R.F. Casten, *Nuclear Structure from a Simple Perspective*, Oxford University Press Inc., New York, second edition (1990,2000).

[3] J. Carlson and R. Sciavilla, Revs. Mod. Phys. **70** (1998) 743.

[4] S.C. Pieper, Eur. Phys. J. **A13** (2002) 75.

[5] K. Heyde, *The nuclear shell-model* (Springer-Verlag, Berlin, Heidelberg, New York, 1994).

[6] A. Bohr and B. Mottelson, *Nuclear Structure*, Vols. I and II (1969, 1975), Benjamin, New York; World Scientific, Singapore (1998).

[7] M. Bender, P.-H. Heenen and P.-G. Reinhard, Rev. Mod. Phys. **75** (2003) 121.

[8] P. Ring, Prog. Part. Nucl. Phys. **37** (1996) 193.

[9] H. Kucharek and P. Ring, Z. Phys. **A339** (1991) 23.

[10] F.Iachello and A.Arima, *The Interacting Boson Model*, (Cambridge University Press, 1987)

[11] V.M. Strutinsky, Nucl. Phys. **A95** (1967) 420.

[12] V.M. Strutinsky, Nucl. Phys. **A122** (1968) 1.

[13] B. Povh, K. Ritz, C. Scholz, F. Zetsche, *Particles and Nuclei*, Springer-Verlag Berlin Heidelberg New York, 2nd edition (1995, 1999).

[14] A. N. Andreyev et al., Nature 405 (2000) 430.

[15] S. Schwarz, F. Ames, G. Audi, D. Beck, G. Bollen, C. De Coster, J. Dilling, O. Engels, R. Fossion, J. E. García Ramos, S. Henry, F. Herfurth, K. Heyde, A. Kellerbauer, H.-J. Kluge, A. Kohl, E. Lamour, D. Lunney, I. Martel, R. B. Moore, M. Oinonen, H. Raimbault-Hartmann, C. Scheidenberger, G. Sikler, J. Szerypo, C. Weber, Nucl. Phys. **A693** (2001) 533.

[16] H. Morinaga, Phys. Rev. 102 (1956) 254.

[17] K. Heyde et al., Phys. Rep. 102 (1983) 291; J.L. Wood et al., Phys. Rep. 215 (1992) 101.

[18] G.D. Dracoulis et al., Phys. Rev. C69 (2004) 054318.

[19] A. Dewald et al., Phys. Rev. **C68** (2003) 034314.

[20] M. Bender et al., Phys. Rev. **C69** (2004) 064303, and references therein.

[21] R.R. Rodríguez-Guzmán, J.L. Egido and L.M. Robledo, Phys. Rev. **C69** (2004) 054319.

[22] J.E. García-Ramos, C. De Coster, R. Fossion, and K. Heyde, Nucl. Phys. **A688** (2001) 735.

[23] G. Bollen *et al.*, Nucl. Instr. and Meth. A **368**, 675 (1996).

[24] S. Schwarz, PhD. Thesis, University of Mainz, (1998), unpublished.

[25] A. Kohl, PhD. Thesis, University of Heidelberg, (1999), unpublished.

[26] S. Schwarz *et al.*, Nucl. Phys. **A693** (2001) 533.

[27] K. Heyde, P. Van Isacker, M. Waroquier, J.L. Wood and R.A. Meyer, Phys. Repts. **102** (1983) 291.

[28] J.L. Wood, K. Heyde, W. Nazarewicz, M. Huyse and P. Van Duppen, Phys. Repts. **215** (1992) 101.

[29] K. Heyde, J. Jolie, J. Moreau, J. Ryckebusch, M. Waroquier, P. Van Duppen, M. Huyse and J.L. Wood, Nucl. Phys. **A446** (1987) 189.

[30] R. Bengtsson, T. Bengtsson, J. Dudek, G. Leander, W. Nazarewicz and Jing-Ye Zhang, Phys. Lett. **B183** (1987) 1.

[31] P. Van Duppen, E. Coenen, K. Deneffe, M. Huyse, K. Heyde and P. Van Isacker, Phys. Rev. Lett. **52** (1984) 1974.

[32] P. Van Duppen, E. Coenen, K. Deneffe, M. Huyse and J.L. Wood, Phys. Lett. **B154** (1985) 354.

[33] P. Van Duppen, E. Coenen, K. Deneffe, M. Huyse and J.L. Wood, Phys. Rev. **C35** (1987) 1861.

[34] P. Dendooven, P. Decrock, M. Huyse, G. Reusen, P. Van Duppen and J. Wauters, Phys. Lett. **B226** (1989) 27.

[35] J. Heese, K.H. Maier, H. Grawe, J. Grebosz, H. Klüge, W. Meczynski, M. Schramm, R. Schubart, K. Spohr and J. Styczen, Phys. Lett. **B302** (1993) 390.

[36] R. Julin, K. Helariutta and M. Muikku, J. Phys. **G27** (2001) R109.

[37] P. Van Duppen and M. Huyse, Hyp. Ints. **129** (2000) 149.

[38] A.N. Andreyev et al., Nature **Vol.405** (2000) 430.

[39] A.N. Andreyev et al., Nucl. Phys. **A682** (2001) 482c.

[40] A.P. Byrne et al., Eur. Phys. J. **A7** (2000) 41.

[41] Y. Le Coz et al., Eur. Phys. J. Direct **A3** (1999) 1.

[42] N. Bijnens et al., Z. Phys. **A356** (1996) 3.

[43] G.D. Dracoulis, A.P. Byrne, A.M. Baxter, P.M. Davidson, T. Kibedi, T.R. McGoran, R.A. Bark and S.M. Mullins, Phys. Rev. **C60** (1998) 014303.

[44] A.M. Baxter et al., Phys. Rev. **C48** (1993) R2140.

[45] A.N. Andreyev et al., Eur. Phys. J. **A6** (1999) 381.

[46] J.F.C. Cocks et al., Eur. Phys. J. **A3** (1998) 17.

[47] D. Jenkins et al., Phys. Rev. **C62** (2000) 021302.

[48] P. Van Duppen, M. Huyse and J.L. Wood, J. Phys. **G16** (1990) 441.

[49] G.D. Dracoulis, Phys. Rev. **C49** (1994) 3324.

[50] G.D. Dracoulis, A.P. Byrne and A.M. Baxter, Phys. Lett. **B432** (1998) 37.

[51] R.G. Allatt et al., Phys. Lett. **B437** (1998) 29.

[52] R.D. Page et al., Proc. Of the 3rd International Conference on Exotic Nuclei and Atomic Masses ENAM, Hmeenlinna, Finland, july 2001, eds. J. yst, P. Dendooven, A. Jokinen and M. Leino, Springer-Verlag Berlin Heidelberg (2003), p. 309.

[53] Y. Xu, K.S. Krane, M.A. Gummin, M. Jarrio, J.L. Wood, E.F. Zganjar and H.K. Carter, Phys. Rev. Lett. **68** (1992) 3853.

[54] D. Seweryniak et al., Phys. Rev. **C58** (1998) 2710.

[55] B. Cederwall et al., Phys. Lett. **B443** (1998) 69.

[56] S.L. King et al., Phys. Lett. **B443** (1998) 82.

[57] F. Soramel et al., Eur. Phys. J. **A4** (1999) 17.

[58] G.D. Dracoulis et al., J. Phys. **G12** (1986) L97.

[59] P.M. Davidson et al., Nucl. Phys. **A657** (1999) 219.

[60] L.A. Bernstein et al., Phys. Rev. **C52** (1995) 621.

[61] W. Younes et al., Phys. Rev. **C52** (1995) R1723.

[62] W. Younes and J.A. Cizewski, Phys. Rev. **C55** (1997) 1218.

[63] N. Fotiades et al., Phys. Rev. **C55** (1997) 1724.

[64] N. Bijnens et al., Phys. Rev. Lett. **75** (1995) 4571.

[65] N. Bijnens et al., Phys. Rev. **C58** (1998) 754.

[66] K. Helariutta et al., Phys. Rev. **C54** (1996) R2799.

[67] K. Helariutta et al., Eur. Phys. J. **A6** (1999) 289

[68] R. Bengtsson and W. Nazarewicz, Z. Phys. **A334** (1989) 269.

[69] W. Nazarewicz, Phys. Lett. **B305** (1993) 195.

[70] R.R. Chasman, J.L. Egido and L.M. Robledo, Phys. Lett. **B513** (2001) 325.

[71] A.M. Oros, K. Heyde, C. De Coster, B. Decroix, R. Wyss, B.R. Barrett and P. Navratil, Nucl. Phys. **A465** (1999) 107.

[72] A. Frank and P. Van Isacker, *Algebraic Methods in Molecular and Nuclear Structure Physics* (Wiley, New York, 1994).

[73] P.D. Duval and B.R. Barrett, Nucl. Phys. **A376** (1982) 213.

[74] A.F. Barfield, B.R. Barrett, K.A. Sage and P.D. Duval, Z. Phys. **A311** (1983) 205.

[75] A.F. Barfield and B.R. Barrett, Phys. Lett. **B149** (1984) 277.

[76] M.K. Harder, K.T. Tang and P. Van Isacker, Phys. Lett. **B405** (1997) 25.

[77] K. Heyde, P. Van Isacker, J. Jolie, J. Moreau and M. Waroquier, Phys. Lett. **B132** (1983) 15.

[78] K. Heyde, J. Jolie, P. Van Isacker, J. Moreau and M. Waroquier, Phys. Rev. **C29** (1984) 1428.

[79] K. Heyde, C. De Coster, J. Jolie and J.L. Wood, Phys. Rev. **C46** (1992) 541.

[80] K.Heyde, P. Van Isacker and J.L. Wood, Phys. Rev. **C49** (1994) 559.

[81] C. De Coster, K. Heyde, B. Decroix, P. Van Isacker, J. Jolie, H. Lehmann and J.L. Wood, Nucl. Phys. **A600** (1996) 251.

[82] H. Lehmann, J. Jolie, C. De Coster, K. Heyde, B. Decroix and J.L. Wood, Nucl. Phys. **A621** (1997) 767.

[83] C. De Coster, K. Heyde, B. Decroix, J.L. Wood, J. Jolie and H. Lehmann, Nucl. Phys. **A621** (1997) 802.

[84] C. De Coster, K. Heyde, B. Decroix, K. Heyde, J. Jolie, H. Lehmann and J.L. Wood, Nucl. Phys. **A651** (1999) 31.

[85] K. Heyde, J. Schietse and C. De Coster, Phys. Rev. **C44** (1991) 2216.

[86] C. De Coster, B. Decroix and K. Heyde, Phys. Rev. **C61** (2000) 067306.

[87] C.M. Baglin, Nucl. Data Sheets **84** (1998) 813.

[88] E. Browne and B. Singh, Nucl. Data Sheets **79** (1996) 347.

[89] B. Singh and R.B. Firestone, Nucl. Data Sheets **74** (1995) 402.

[90] J. Penninga, W.H.A. Hesselink, A. Balanda, A. Stolk, H. Verheul, J. van Klinken, H.J. Riezebos and M.J.A. de Voigt, Nucl. Phys. **A471** (1987) 535.

[91] G.D. Dracoulis et al., Phys. Rev. **C44** (1991) R1246.

[92] B. Cederwall et al., Z. Phys. **337** (1990) 283.

[93] M.J.A. De Voigt et al., Nucl. Phys. **A507** (1990) 472.

[94] D.G. Popescu et al., Phys. Rev. **C55** (1997) 1177.

[95] G. Baldsiefen et al., Nucl. Phys. **A574** (1994) 521.

[96] J. Kantele et al., Phys. Lett. **B171** (1986) 151.

[97] T. Kibedi et al., Nucl. Phys. **A688** (2001) 669.

[98] C.Y. Wu, D. Cline, E.G. Vogt, W.J. Kernan, T. Czosnyka, A. Kavka, R.M. Diamond, Phys. Rev. **C40** (1989) R3.

[99] A. Frank, P. Van Isacker and C. Vargas, Phys. Rev. **C69** (2004) 034323.

[100] P. Ring and P. Schuck, *The nuclear many-body problem* (Springer-Verlag, New York, Heidelberg, Berlin, 1980).

[101] S.G. Nilsson and I. Ragnarson, *Shapes and shells in the nuclear structure*. (Cambridge University Press, Cambridge, 1995).

[102] A.H. Wapstra, *Handbuch der Physik* Vol. 1 (1958).

[103] A.H. Wapstra and N.B. Gove, Nucl. Data Tables **9** (1971) 267.

[104] W.D. Myers and W.J. Swiatecki, Ark. Fys. **36** (1967) 343.

[105] W.D. Myers and W.J. Swiatecki, Ann. Phys. (NY) **55** (1969) 395.

[106] P. Möller and J.R. Nix, Nucl. Phys. **A361** (1981) 117.

[107] R. Bengtsson, P. Möller, J.R. Nix, and J.-Y. Zhang, Phys. Scr. **29** (1984) 402.

[108] P. Möller and J.R. Nix, At. Data Nucl. Data Tables **26** (1981) 165.

[109] P. Möller and J.R. Nix, At. Data Nucl. Data Tables **39** (1988) 213.

[110] P. Möller, J.R. Nix, W.D. Myers, and W.J. Swiatecki, At. Data Nucl. Data Tables **59** (1995) 185.

[111] P. Möller, J.R. Nix, and K.-L. Kratz, At. Data Nucl. Data Tables **66** (1997) 131.

[112] Y. Aboussir, J.M. Pearson, A.K. Dutta, and F. Tondeur, At. Data Nucl. Data Tables **61** (1995) 127.

[113] G.A. Lalazissis, S. Raman, and P. Ring, At. Data Nucl. Data Tables **71** (1999) 1.

[114] S. Goriely, F. Tondeur, and J.M. Pearson, At. Data Nucl. Data Tables **77** (2001) 311.

[115] H. Raimbault-Hartmann *et al.*, Nucl. Instr. and Meth. **B126** (1997) 378.

[116] C.F. von Weizsäcker, Z. Phys. **96** (1935) 431.

[117] H.A. Bethe and R.F. Bacher, Rev. Mod. Phys. **8** (1936) 193.

[118] A.T. Kruppa, M. Bender, W. Nazarewicz, P.-G. Reinhard, T. Vertse, and Ćwiok, Phys. Rev. **C61** (2000) 03413.

[119] A. de Shalit and I. Talmi, *Nuclear shell theory* (Academic Press, New York and London, 1963).

[120] I. Talmi, *Simple models of complex nuclei* (Harwood Academic Publishers, 1993).

[121] I. Talmi, Nucl. Phys. **A172** (1971) 1.

[122] J.L. Wood, private communication and to be published.

[123] M. Dufour and A.P. Zuker, Phys. Rev. **C54** (1996) 1641.

[124] J. Duflo and A.P. Zuker, Phys. Rev. **C59** (1999) R2347.

[125] B.A. Brown and B.H. Wildenthal, Ann. Rev. Nucl. Part. Sci **38** (1988) 29.

[126] E.K. Warburton, J.A. Becker, and B.A. Brown, Phys. Rep. **41** (1990) 1147.

[127] A. Frank and P. Van Isacker, *Algebraic methods in molecular and nuclear structure physics* (Wiley-Interscience, 1994).

[128] R.F. Casten and D.D. Warner, Rev. Mod. Phys. **6 0** (1988) 389.

[129] W.-T. Chou, N.V. Zamfir, and R.F. Casten, Phys. Rev. **C56** (1997) 829.

[130] D.D. Warner and R.F. Casten, Phys. Rev. Lett. **48** (1982) 1385.

[131] V.M. Strutinsky, Nucl. Phys. **A95** (1967) 420.

[132] V.M. Strutinsky, Nucl. Phys. **A122** (1968) 1.

[133] P.J. Brussaard and P.W.M. Glaudemans, *Shell-model applications in nuclear spectroscopy* (North-Holland, Amsterdam, 1977).

[134] G. Audi and A.H. Wapstra, Nucl. Phys. **A565** (1993) 193.

[135] G. Audi and A.H. Wapstra, Nucl. Phys. **A595** (1995) 409.

[136] G. Audi, D. Bersillon, J. Blachot, and A.H. Wapstra Nucl. Phys. **A624** (1997) 1. Database http://csn.www.in2p3.fr/amdc.

[137] B. Beck, *et al.*, Eur. Phys. J. **A8** (2000) 307.

[138] K. Heyde, P. Van Isacker, M. Waroquier, J.L. Wood, and R.A. Meyer, Phys. Rep. **102** (1983) 292.

[139] P.D. Duval and B.R. Barrett, Phys. Lett. **B100** (1981) 223.

[140] P.D. Duval and B.R. Barrett, Nucl. Phys. **A376** (1982) 213.

[141] A.F. Barfield, B.R. Barrett, K.A. Sage, and P.D. Duval, Z. Phys. **A311** (1983) 205.

[142] M.K. Harder, K.T. Tang, and P. Van Isacker, Phys. Lett. **B405** (1997) 25.

[143] A. Oros, K. Heyde, C. De Coster, B. Decroix, R. Wyss, B.R. Barrett, and P. Navratil, Nucl. Phys. **A645** (1999) 107.

[144] C. De Coster, K. Heyde, B. Decroix, J.L. Wood, J. Jolie, and H. Lehmann, Nucl. Phys. **A651** (1999) 31.

[145] M. Délèze, S. Drissi, J. Kern, P.A. Tercier, J.P. Vorlet, J. Rikovska, T. Otsuka, S. Judge, and A. Williams, Nucl. Phys. **A551** (1993) 269.

[146] M. Délèze, S. Drissi, J. Jolie, J. Kern, and J.P. Vorlet, Nucl. Phys. **A554** (1993) 1.

[147] H. Lehmann, J. Jolie, C. De Coster, K. Heyde, B. Decroix, and J.L. Wood, Nucl. Phys. **A621** (1997) 767.

[148] K. Heyde, J. Jolie, J. Moreau, J. Ryckebusch, M. Waroquier, P. Van Duppen, M. Huyse, and J.L. Wood, Nucl. Phys. **A621** (1997) 767.

[149] Y. Utsuno, T. Otsuka, T. Mizusaki, and M. Honma, Phys. Rev. **C60** (1999) 054315.

[150] F. Azaiez, Phys. Scr. **88** (2000) 118.

[151] E. Caurier, F. Nowacki, A. Poves, and J. Retamosa, Phys. Rev. **C58** (1998) 2033.

[152] R.R. Rodríguez-Guzmán, J.L. Egido, and L.M. Robledo, Phys. Rev. **C62** (2000) 054319.

[153] C. De Coster, B. Decroix, and K. Heyde, Phys. Rev. **C61** (2000) 067306.

[154] T. Kibédi, G.D. Dracoulis, A.P. Byrne, P.M. Davidson, and S. Kuyucak, Nucl. Phys. **A567** (1994) 183.

[155] P. Van Duppen, E. Coenen, K. Deneffe, M. Huyse, and J.L. Wood, Phys. Rev. **C35** (1987) 1861.

[156] P. Van Duppen, M. Huyse, and J.L. Wood, J. Phys. **G16** (1990) 441.

[157] M. Brack, J. Damgaard, A.S. Jensen, H.C. Pauli, V.M. Strutinsky, and Wong C.Y, Rev. Mod. Phys. **44** (1972) 320.

[158] R. Bengtsson and W. Nazarewicz, Z. Phys. **A334** (1989) 269.

[159] S. Ćwiok, J. Dudek, W. Nazarewicz, J. Skalski, T.R. Werner, Comp. Phys. Comm. **46** (1987) 379.

[160] J. Dudek, Z. Szymański, T.R. Werner, A. Faessler, C. Lima, Phys. Rev. **C26** (1982) 1712.

[161] J. Dudek, Z. Szymański, T.R. Werner, Phys. Rev. **C23** (1981) 920.

[162] R. Bengtsson, T. Bengtsson, J. Dudek, G. Leander, W. Nazarewicz, and J.-Y. Zhang, Phys. Lett. **B183** (1987) 1.

[163] W. Satula, S. Ćwiok, W. Nazarewicz, R. Wyss and A. Johnson, Nucl. Phys. **A529** (1991) 289.

[164] W. Nazarewicz, Phys. Lett. **B305** (1993) 195.

[165] F.R. May, V.V. Pashkevich, and S. Frauendorf, Phys. Lett. **B68** (1977) 113.

[166] J. Dudek, A. Majhofer, J. Skalski, J. Phys. **G6** (1980) 447.

[167] H.J. Lipkin, Ann. Phys. (NY) **31** (1976) 525.

[168] H.C. Pradhan, Y. Nogami, and J. Law, Nucl. Phys. **A201** (1973) 357.

[169] W. Nazarewicz, M.A. Riley, and J.D. Garrett, Nucl. Phys. **A512** (1990) 61.

[170] R. Wyss, private communication.

[171] W. Nazarewicz, T.R. Werner, J. Dobaczewski, Phys. Rev. **C50** (1994) 2860.

[172] D.L. Hill and J.A. Wheeler, Phys. Rev. **89** (1953) 1102.

[173] J.J. Griffin and J.A. Wheeler, Phys. Rev. **108** (1957) 311.

[174] S. Pèru, M. Girod, and J.F. Berger, Eur. Phys. J. **A9** (2000) 35, and references therein.

[175] A. Valor, P.-H. Heenen, and P. Bonche, Nucl. Phys. **A671** (2000) 145, and references therein.

[176] M. Honma, T. Mizusaki, and T. Otsuka, Phys. Rev. Lett. **75** (1995) 1284.

[177] N. Shimizu, T. Otsuka, T. Mizusaki, and M. Honma, Phys. Rev. Lett. **86** (2001) 1171.

[178] A. M. Lane, *Nuclear Theory - Pairing Correlations and Collective Motion* (W.A.Benjamin, Inc., New-York, Amsterdam, 1964)

[179] J.L.Wood, priv.comm.

[180] J.E. García-Ramos, C. De Coster, R. Fossion, and K. Heyde, Nucl. Phys. **A688** (2001) 735.

[181] R. Fossion, J.E. García-Ramos, C. De Coster, and K. Heyde, Nucl. Phys. **A697** (2002) 703.

[182] A.Bohr and B.Mottelson, *Nuclear Structure*, vol.2 (Benjamin, New-York, 1975)

[183] A.Poves and J.Retamosa, Nucl.Phys. **A571** (1994) 221.

[184] E.Caurier, F.Nowacki, A.Poves and J.Retamosa, Phys. Rev. **C58** (1998) 2033.

[185] T.Otsuka, T.Mizusaki, Y.Utsuno and M.Honma,*ENAM98, Exotic Nuclei and Atomic Masses*, eds. B.M.Sherill, D.J.Morrissey and C.N.Davids, 1998, Am. Inst. of Physics.

[186] D.J.Dean, M.T.Ressell, M.Hjorth-Jensen, S.E.Koonin, K.Langanke and A.P.Zuker, Phys. Rev. **C59** 2474.

[187] K.Heyde, J.Jolie, J.Moreau, J.Ryckebusch, M.Waroquier, P.Van Duppen, M.Huyse and J.L.Wood, Nucl.Phys.**A446** (1987) 189.

[188] D.Rowe, *Nuclear Collective Motion*, (Methuen, London, 1970)

[189] L.S. Kisslinger and R.A. Sorensen, Mat. Fys. Medd. Dan. Vid. Selsk. **32**, n° 9 (1960).

[190] K.Heyde and J.Sau, Phys. Rev. **C33** (1986) 1050.

[191] A. Frank and P. Van Isacker, *Algebraic Methods in Molecular and Nuclear Structure Physics*, (Wiley, New-York,1994).

[192] V. Hellemans, R. Fossion, S. De Baerdemacker and K. Heyde, to be published.